



**HAL**  
open science

# Study of the nanostructured active cavities with photonic bandgaps

Abdallah El Soussi

► **To cite this version:**

Abdallah El Soussi. Study of the nanostructured active cavities with photonic bandgaps. Electronics. Université de Valenciennes et du Hainaut-Cambrésis, 2019. English. NNT: 2019VALE0019 . tel-03367019

**HAL Id: tel-03367019**

**<https://uphf.hal.science/tel-03367019v1>**

Submitted on 5 Nov 2021

**HAL** is a multi-disciplinary open access archive for the deposit and dissemination of scientific research documents, whether they are published or not. The documents may come from teaching and research institutions in France or abroad, or from public or private research centers.

L'archive ouverte pluridisciplinaire **HAL**, est destinée au dépôt et à la diffusion de documents scientifiques de niveau recherche, publiés ou non, émanant des établissements d'enseignement et de recherche français ou étrangers, des laboratoires publics ou privés.

**N° ORDRE : 19/18**

**Thèse de doctorat**

**Pour obtenir le grade de Docteur de**

**l'UNIVERSITÉ POLYTECHNIQUE HAUTS-DE-FRANCE**

Discipline, spécialité selon la liste des spécialités pour lesquelles l'Ecole Doctorale est accréditée :

**Electronique**

**Présentée et soutenue par Abdallah, EL SOUSSI.**

**Le 09/07/2019, à Valenciennes**

**Ecole doctorale :**

Sciences Pour l'Ingénieur (ED SPI 072)

**Equipe de recherche, Laboratoire :**

Institut d'Electronique de Microélectronique et de Nanotechnologie - Département Opto-Acousto-  
Electronique (IEMN DOAE – UMR 8520)

**Etude des Cavités Actives dans les Nanostructures Périodiques à Gap de Photons**

Study of the Nanostructured Active Cavities with Photonic Bandgaps

## **JURY**

- Mme Frédérique GADOT, Professeure à l'Université de Paris Nanterre, Rapporteur
- Mr Ramon ALCUBILLA, Professeur à l'Universitat Politècnica de Catalunya, Rapporteur
- Mr Nico F. DECLERCQ, Professeur à The Georgia Institute of Technology (USA), President
- Mr Joseph GAZALET, Professeur à l'UPHF, Directeur de Thèse
- Mr Rafic HAGE CHEHADE, Professeur à l'Université Libanaise, Co-Directeur
- Mr Samuel DUPONT, Professeur à l'UPHF, Co-Encadrant
- Mme Samia BAHLAK, Maître de Conférences à l'Université Libanaise, Membre Invitée
- Mr Bahram DJAFARI-ROUHANI, Professeur à l'Université de Lille, Membre Invité

# Acknowledgements

This thesis is an account of research undertaken between March 2016 and July 2019 in the IEMN laboratory, within the “Composants et Systèmes Acousto-Optoélectronique” team of the OAE Department of Université Polytechnique Hauts-de-France. I received a grant from Hariri Foundation for Sustainable Human Developments.

Obtaining a doctoral thesis is not a one-person work, but the fruit of the teamwork that makes it real and possible to achieve. First and foremost, I would like to render my warmest thanks to my Ph.D. supervisor Professor Joseph GAZALET, for accepting me as part of his research group and introducing me to this research field which made my Ph.D. work a memorable experience. His contributions of time, ideas, and expert advices have been invaluable throughout all stages of the work. I am also highly grateful to Professor Samuel DUPONT for his precious help to make my Ph.D. experience productive and stimulating. I am indebted for his valuable contributions and suggestions when they were sorely needed, that shaped this thesis and helped to make it better. I would like to show my deepest gratitude to Professor Rafic HAJJ CHEHADE for his availability, collaboration, and wise advices. I would also like to thank Dr. Samia BAHLAK for her time and her valuable contributions. I gratefully acknowledge the Hariri Foundation for Sustainable Human Developments for its funding sources that made my Ph.D. work possible. I would like to express my sincere thanks to all my friends for the wonderful moments and memories that made us a family during these three years. Lastly, I would like to thank my family for all their love and encouragement. Their regular support, advices, and friendship throughout my research work have been a very vital factor in seeing this day. And most of all for my loving, supportive, encouraging, and patient wife Mayssane whose faithful supports during the final stages of this Ph.D. is appreciated.

# Publications

## **Journal Article:**

A. El Soussi, J. Gazalet, S. Dupont, and J.C. Kastelik, “Evaluation of second order optomechanical coupling strength in photonic crystal cavities including the case of degenerated modes,” *Journal of Optics*, vol. 21, no. 4, p. 045103, Mar. 2019.

## **Workshop:**

A. E. Soussi, J. Gazalet, S. Dupont, & J. C. Kastelik. (2018, October). Second order optomechanical coupling strength in photonic crystal cavities. *Word Press Gradient – IEMN – Lille*

# General Introduction

This thesis presents the development and applications of a semi-analytic study of the properties of active cavities in periodically nanostructured materials. The analysis of wave propagation in periodic media leads to the concept of bandgaps, a well-known concept to whom are familiar with topics such as photonic crystals or phononic crystals. Those concepts are inspired by the quantum mechanical description of electronic waves propagating in a periodic potential: a natural conducting crystal. The transcription was made possible by the universal nature of the concept of “wave”.

Optical waves are described by the spatio-temporal variations of electric and magnetic field vectors in space, including vacuum. They are governed by Maxwell equations. Acoustic waves are described by the strain spatio-temporal fluctuations in material media. They are governed by Newton’s and Hook’s law. Even though the nature of the waves is different, the scattering properties of periodic structures can be evidenced in both scientific areas. Hence, the idea of developing artificial periodic structures with desired properties to control photons and phonons propagation has appeared in the respectively concerned scientific communities. The emergence of a joint effort to develop such structures can be found in literature under the overarching concept of phoXonic crystals, combining forbidden bands for both waves. The motivation underneath these efforts is the expectation of developing functional devices with improved performance.

The concept of active cavities takes part to that research concern. “Active” here means that the cavities present modulation properties for the optical waves, thanks to the acoustic waves. Improvement of the modulation properties are expected due to the strong confinement of waves, therefore a better overlapping of photonic and phononic modes is made possible. But, owing to the wave nature of photons and phonons and to the generalized concept of scalar product underlying the “overlapping” concept, one understands that the symmetry of the eigenmodes for both waves can affect drastically the modulation behavior. The efforts made to develop the semi-analytic method to assess modulation characteristics and performances derive from these issues.

Actually, this thesis presents the study of active cavities in periodic structures and the understanding of their modulation properties which deals with opto-mechanical coupling mechanisms. The aim of this work is more practically to present how the 2<sup>nd</sup> order perturbation theory assorted with symmetry considerations can help to predict the different modulation behaviours. This provides a systematic approach leading to physical interpretations of opto-mechanical coupling in phoXonic crystal cavities. In order to fulfil the principal goal of this thesis, we study the acousto-optical coupling mechanisms in  $L_1$  point defect cavity, case of one missing hole in a two-dimensional array of air holes drilled in silicon. PhoXonic structures are pragmatically designed by a numerical modelling technique using the Finite Element Method (FEM), a practical way to obtain the cavity eigenmodes exploited to evaluate the opto-mechanical coupling factors.

The manuscript is organized in four chapters. In chapter one, we present the problematic and a state of the art on photonic, phononic, and phoXonic crystals. In the second chapter, some

theoretical reminders are developed about waves and periodic media. The third chapter presents the concepts enabling the design of phoXonic crystals and the identification of suitable cavity modes for our study. In chapter four, the development of the semi-analytical approach is presented, starting from the generalization of the perturbation method to opto-mechanical coupling, extended to the degenerated modes and including the second order perturbations. The method ends with semi-analytical expressions for the first and second order correction terms. Its ability to analyse acousto-optical coupling efficiency, to predict, and explain the behaviour of the modulation is justified.

# List of Figures

**Figure 1:** Illustration of one-dimensional, two-dimensional, and three-dimensional structures [1].

**Figure 2:** Illustrative example of two-dimensional Centered Rectangular lattice.

(Left) Different choices of basis vectors and their associated unit-cell defined as the area inside the parallelogram determined by the basis vectors. 3 Primitive lattices and unit-cells (lower row) and non-primitive ones (upper row).

(Right) The Wigner-Seitz (down) cell and the non-primitive conventional Centered Rectangular cell (up).

**Figure 3:** The five Bravais lattices in two dimensions (2-D) [2].

**Figure 4:** Hexagonal lattice and corresponding reciprocal lattice with highlighted Brillouin zone (blue). The yellow area is an irreducible first Brillouin zone with the corners M, K and  $\Gamma$ .

**Figure 5:** Square lattice and corresponding reciprocal lattice with highlighted Brillouin zone (blue). The yellow area is an irreducible first Brillouin zone with the corners M, X and  $\Gamma$ .

**Figure 6:** Representation of the band structure. The periodic band scheme representation (a), the reduced band structure scheme to the 1<sup>st</sup> Brillouin zone (b), the extended band scheme (c). The dashed lines represent the dispersion relation ( $\omega = v_\varphi k$ ) of a photon propagating in the non-dispersive bulk material of phase velocity  $v_\varphi$ .

**Figure 7:** Dispersion diagram of a square 2-D TM (transverse magnetic) photonic crystal consisting of silicon ( $Si$ ) and air hole of radius  $r = 0.48a$  along the high-symmetry axis  $\Gamma X$ ,



XM, and  $\Gamma$ M of the first Brillouin zone. The yellow rectangle represents the bandgap between the normalized angular frequency  $\omega_N \approx 0.46$  and  $\omega_N \approx 0.52$ . The blue square represents the reciprocal lattice while the green triangle represents the irreducible Brillouin zone.

**Figure 8:** Structure of the electromagnetic wave in a homogeneous isotropic medium (Transverse Electro-Magnetic).

**Figure 9:** Structure of the electromagnetic wave in a homogeneous anisotropic medium (Electric field has a longitudinal component).

**Figure 10:** Representation of photonic crystal Square and Triangular lattices. The blue region represents silicon (*Si*) the material used for the host medium, while the white circles represent the voids drilled in the host medium with radius  $r = 0.48a$  where  $a = 650 \text{ nm}$  and are composed of *air*.

**Figure 11:** Representation of the Geometry, TE, TM, and Phononic Unit-Cell Dispersion Curve. Dispersion diagram of Photonic and Phononic Crystals Along the high-symmetry axis  $\Gamma$ X, XM, M  $\Gamma$  of the First Brillouin zone.

**Figure 12:** Sketch of a square 2-D phoXonic crystal  $L_I$  Nano-cavity.

**Figure 13:** Representation of the Geometry, TE, TM, and Phononic Supercell Dispersion Diagram. Dispersion diagram of Photonic and Phononic Crystals Along the high-symmetry axis  $\Gamma$ X of the first Brillouin zone.

**Figure 14:** Illustration of the refractive index variation corresponding to an interface shifting caused by acoustic displacements.

**Figure 15:** Modes profiles of the elastic and electromagnetic fields in the  $(x, y)$  plane. TM photonic modes profiles  $H_z$  ( $\alpha, \beta, \gamma, \delta$ , and  $\varepsilon$ ) the arrows indicate the polarization vector

(electric field); Phononic modes profiles of the modes  $C$  and  $F$  the colored scale stands for the displacement magnitude  $|\vec{U}|$  the arrows specify the displacement vector field. The values of the normalized angular eigenfrequencies are given under the corresponding cavity mode profiles.

**Figure 16:** Profiles of the new modes obtained subsequently to degeneracy lifting, as a result of the perturbation introduced by the presence of the acoustic mode  $C$ , during the 1<sup>st</sup> order treatment. The corresponding new eigenfrequencies are presented in Figure 15.

**Figure 17:** Modulation of the 5 photonic modes eigenfrequencies induced by the acoustic mode  $C$  during one acoustic cycle:  $0 \leq \Omega t \leq 2\pi$ . First and second rows give respectively the 1<sup>st</sup> and 2<sup>nd</sup> order corrections, the 3<sup>rd</sup> row represents the 1<sup>st</sup> and 2<sup>nd</sup> order combined effects. The singlet mode  $\alpha$  is disposed in the 1<sup>st</sup> column and the two doublet modes  $(\beta, \gamma)$  and  $(\delta, \varepsilon)$  are piled in the 2<sup>nd</sup> and 3<sup>rd</sup> columns respectively. Each one of the dot dashed and the continuous lines stands for one of the split angular frequencies of the new doublet modes after degeneracy is lifted.

**Figure 18:** Modulation of the 5 photonic cavity modes eigenfrequencies induced by the acoustic mode  $F$  during one acoustic cycle:  $0 \leq \Omega t \leq 2\pi$ . First and second rows give respectively the 1<sup>st</sup> and 2<sup>nd</sup> order corrections the 3<sup>rd</sup> row represents the 1<sup>st</sup> and 2<sup>nd</sup> order combined effects. The singlet mode  $\alpha$  is disposed in the 1<sup>st</sup> column and the two doublet modes  $(\beta, \gamma)$  and  $(\delta, \varepsilon)$  are piled in the 2<sup>nd</sup> and 3<sup>rd</sup> columns respectively. The breathing mode  $F$  does not introduce degeneracy lifting.

# List of Tables

**Table 1:** The fourteen Bravais lattices in three dimensions (3-D) [3].

**Table 2:** 2-D direct and reciprocal lattice vectors correspondence expressed in a rectangular framework. Case of hexagonal and square lattices,  $\hat{x}$  and  $\hat{y}$  are unit-vectors of the rectangular framework used and  $a$  is the lattice constant.

**Table 3:** Electromagnetic and elastic waves similarities and differences.

**Table 4:** Photo-elastic coefficients for *Si* [4] [5].

**Table 5:** Opto-mechanical coupling rate between TM photonic Eigen-modes  $\alpha, \beta, \gamma, \delta,$  and  $\varepsilon$  and phononic Eigen-modes  $C$  and  $F$  for first and second order perturbations. The symbol  $\ll$  means that the value is below the numerical errors.

**Table 6:** Coefficients  $c_1^\pm$  and  $c_2^\pm$  for the new zero-order modes (after the degeneracy have been lifted) for TM degenerated photonic eigenmodes  $\beta$  &  $\gamma, \delta$  and  $\varepsilon$  with phononic perturbation induced by the eigenmode  $C$ .

# Table of Contents

<b>General Introduction</b>	<b>3</b>
<b>Chapter I</b>	
<b>State of the Art</b>	<b>13</b>
1.1 Introduction .....	13
1.2 A Short Introduction to Waves in Artificial Periodic Media .....	16
1.2.1 From Diffraction to Photonic Crystals .....	16
1.2.2 Generalization to Phononic Crystals .....	20
1.2.3 The Emergence of PhoXonic Crystals .....	22
1.3 Active PhoXonic Cavities .....	28
1.4 Conclusion .....	30
<b>Chapter II</b>	
<b>Introduction to Periodic Media Theory</b>	<b>31</b>
2.1 Introduction .....	31
2.2 Description of a Crystal: Lattice and Unit-Cell .....	32
2.3 Primitive, Conventional, and Wigner-Seitz Cells .....	34
2.4 3-D Analytic Expression of the Lattice and Unit-Cell .....	35
2.5 Bravais Lattices .....	36
2.5.1 2-D Bravais Lattice.....	37
2.5.2 3-D Bravais Lattice .....	39
2.6 Crystal Structure : Lattice + Unit-Cell .....	40
2.7 Reciprocal Space and Brillouin Zones .....	41

2.7.1 Reciprocal Space Basis Vectors.....	41
2.7.2 Brillouin Zones .....	43
2.8 Irreducible Brillouin Zones .....	44
2.8.1 Hexagonal Lattice .....	44
2.8.2 Square Lattice .....	45
2.8.3 Transformation of the Reciprocal Lattice Vectors .....	45
2.9 The Band Diagram .....	46
2.9.1 Bloch Propagating Modes .....	47
2.9.2 Bloch Waves in the Reciprocal Domain .....	48
2.9.3 Periodicity of the Dispersion Relation .....	49
2.9.4 Bandgap: From a Perturbation Point of View .....	51
2.9.5 Bandgap: From a Scattering Point of View .....	51
2.9.6 Band Structures in 2-D Crystals .....	52
2.10 Conclusion .....	54

### **Chapter III**

<b>PhoXonic Crystals</b> .....	<b>55</b>
3.1 Introduction .....	55
3.2 Wave Propagations in Homogeneous Media .....	56
3.2.1 Electromagnetic Wave in Homogeneous Dielectric .....	58
3.2.2 Acoustic Wave in Homogeneous Media.....	66
3.3 Wave Propagations in Periodic Media .....	69
3.3.1 Eigenproblems and Generalized Eigenproblems .....	70
3.3.2 Solving the Wave Equation .....	71
3.3.3 The Unit-Cell Concept .....	72

3.4 Specific Features of Wave Propagations in 2-D Periodic Structures .....	72
3.5 Principle Parameters of 2-D Crystals Design .....	74
3.5.1 Periodic Structure Parameters of the Studied Structure .....	75
3.5.2 Dispersion Diagrams of the Periodic Structure Considered .....	75
3.6 Photonic Crystals Cavities .....	78
3.6.1 Cavity Confinement and Quality Factor .....	79
3.6.2 Concept of Supercell .....	80
3.7 Mechanisms Behind Photon-Phonon Interaction .....	85
3.7.1 Photo-Elastic Effect .....	86
3.7.2 Opto-Mechanical Effect .....	86
3.8 Conclusion .....	88
<b>Chapter IV</b>	
<b>Evaluation of the Opto-Mechanical Coupling</b> .....	<b>89</b>
4.1 Introduction .....	89
4.2 Perturbation Approach of Opto-Mechanical Coupling .....	91
4.3 Opto-Mechanical Cavity Characteristics.....	99
4.4 Perturbative Modulation Induced by Acoustical Perturbation .....	102
4.5 Potentialities of the Perturbation Approach .....	104
4.6 Conclusion .....	114
<b>General Conclusion</b> .....	<b>115</b>
<b>Appendix A</b> .....	<b>117</b>
<b>TM and TE Polarizations</b> .....	<b>117</b>
<b>References</b> .....	<b>118</b>

# Chapter I

## State of the Art

### 1.1 Introduction

Nowadays, technologies are shaping the world and its evolutions. Electronics, micro/nanotechnologies are fast moving fields, they offer new paths for rising applications in engineering that in turn play a role in society evolutions thanks to communication technologies, safety systems, production plants, health and leisure techs, etc....

In 1959, the physicist Richard Feynman started a lecture by: *“There’s plenty of room at the bottom”*, hence he introduced the principle of micro/nanotechnologies. Shrinking our dimensions into nanometer scale, a lot of new phenomena open in front of us and become available for studying and exploring, causing quantum physics to roll in and ignite the sparkle of nanoscience revolution. In this context, the control of waves at the micro/nanometer scale became a scientific and technological issue.

*“If only were possible to make materials in which electromagnetically waves cannot propagate at certain frequencies, all kinds of almost-magical things would happen”* Sir John Maddox, *Nature* (1990).

New fields of application have consequently emerged with the manufacture of artificially structured materials which aim to control wave propagation. Advances in micro and nanotechnologies have made it possible to design structures called: PhoXonic crystals. That is,

crystals exhibiting both photonic and phononic crystals properties; the  $(X)$  taking the place of the  $(t)$  and  $(n)$ . Explicitly, these crystals are designed so that their spatial period reaches the order of magnitude of both wavelengths: photonic and phononic. The design and fabrication of these periodic structures open up bandgaps; that is frequency bands where wave's propagation is forbidden regardless of the propagation direction. These crystals have thus the ability to confine both electromagnetic and elastic waves in judiciously built cavities. An easy way for producing cavities in periodic structures is by creating defects that are similar to impurities in semiconductors in solid state physics. It's then possible to create localized photonic or phononic states such as electronic localized states. These concurrent confinements provide a way to the realization of strong interactions between high frequency mechanical resonators and near infrared light. The interest in light-sound interaction on recent years was mainly driven by the so-called "Cavity Opto-Mechanics" topic, leading to fundamental and technological developments [6].

The properties of wave propagation in periodic media can be expressed by the band diagram: a plot of the angular frequency as a function of the wavevector in different directions. This diagram helps to visualize the photonic and phononic frequency bandgaps. A 1-D illustrative example, in case of photonic crystals, is the well-known dielectric mirror where the periodicity resides in an alternate stack of two layers of distinct dielectric materials. The reflected wave amplitude, at a given point in the incident medium, results from the superposition of the multiple partial reflections on the successive dielectric interfaces. For certain frequency ranges, all the reflected waves are in phase resulting in a constructive interference, and thus an overall 100% reflection occurs. In crystallography, the phase matching condition required to obtain this 100% reflection is named after Bragg: "Bragg Condition" and the dielectric mirror: a Bragg mirror. In the optical terminology, the frequency band where the incident wave is totally reflected is called the stop-band while in the photonic



crystal terminology this phenomenon of total reflection “Zero Transmission” is referred to as the “Bandgap”: the frequency band where the wave cannot propagate having in mind the analogy with the electronic bandgap phenomenon.

The concept of cavity in periodic media relies on structural defects: one or some missing patterns in the periodic structure. These defects will cause deviations in periodicity in which the discrete translation symmetry is broken, leading to localized modes inside the bandgap. Hence, the effect of a defect can also be seen on the band diagram: discrete eigenfrequencies appear within the forbidden bandgaps. They correspond to the so-called “Cavity Modes” that correspond to confined energy within the vicinity of the cavity. Such modes can be coupled to propagating modes. As in the 1-D case of Fabry-Perot resonant cavities using dielectric mirrors, the eigenmodes of the cavity can be evidenced experimentally by the appearance of transmission peaks in the forbidden band.

We can then imagine structures that simultaneously confine electromagnetic and mechanical waves. Such structures are of particular interest as they could enhance the opto-mechanical interaction. The acousto-optical coupling strength in opto-mechanical crystal cavity is the result of different mechanisms that are behind the photon-phonon interaction: The photo-elastic effect, the opto-mechanical effect (also called the “moving boundary” effect), and the piezoelectric effect in specific materials.

We introduce in this chapter a state of the art as synthetic as possible of photonic, phononic, and phoXonic crystals. Finally, we introduce the study of the photon-phonon interaction in these structures.

## 1.2 A Short Introduction to Waves in Artificial Periodic Media

### 1.2.1 From Diffraction to Photonic Crystals

Light is an electromagnetic wave, this notion has emerged of centuries of cautious observations, among with diffraction phenomenon by periodic structures. We present hereafter a selection of pioneer works thanks to which the concepts we use have emerged.

Recalling history, a year after Newton's prism experiments displaying sunlight spectral content, James Gregory discovered the principles of diffraction grating by using a bird feather to create diffraction [7].

In 1785, an American astronomer David Rittenhouse made the first diffraction grating, where he strung hairs between two finely threaded screws [8] [9]. A diffraction grating is used to separate light composed of different wavelengths with high resolution, it is constituted of a number of closely parallel spaced slits. The condition to get a maximum diffracted intensity is to increase the number of slits, since with a large number of slits the maximum intensity becomes narrow and very sharp. This provides high resolution useful for spectroscopic applications for example.

*"A Dynamical Theory of the Electromagnetic Field"* was published in 1865 by scientist James Clerk Maxwell, taking advantage of the observations of Faraday and Thompson (Lord Kelvin), Ampere, Ohm, and Gauss. In his paper Maxwell derives a mathematical description of light and thus deduces that light is an electromagnetic wave [10].

In 1887, Lord Rayleigh was the first to theoretically study the electromagnetic wave propagation in one-dimensional periodic structures, his work was related to the peculiar reflective properties of a crystalline mineral with periodic planes. Due to different periodicities experienced by light propagating at non-normal incidences, he realized a narrow angle dependent band gap preventing light propagation through the planes and producing iridescent reflected color patterns that vary sharply with angle. This effect is responsible for many other iridescent colors in nature, such as butterfly wings, and natural opals (hydrated amorphous forms of silica, where its internal structure causes the diffraction of light and results in pseudo-chromatic optical effects). These are some of the most prominent examples of naturally occurring photonic crystals. This type of structure can be reduced to an arrangement consisting of periodic dielectric layers having different refractive indices, which is typically an arrangement of alternating layers of high and low refractive indices with sufficient contrast. It thus emerged the hypothesis that the bandgap effect in these systems would make it possible to obtain mirrors with high reflection coefficients, the so-called Bragg mirrors.

Another milestone was effectively reached in 1913. Bragg formulation of X-ray diffraction was first proposed by William Lawrence Bragg and William Henry Bragg [11]. William Lawrence Bragg modeled the crystal as a set of discrete parallel planes separated by a constant parameter ( $d$ ). He suggested that the incident X-ray radiation would produce a diffraction peak if their reflections from the various planes interfered constructively.

About a decade later, the concept of Bloch wave was first introduced by the Swiss physicist Felix Bloch in 1928. The ideas he introduced are of prime interest in the study of waves in periodic structures and are expressed by the so-called “Bloch’s Theorem” [12] [13]. This theorem states that electrons in a periodic media have energies that are described by periodic functions in wave vector space. Or likewise in the real domain, monochromatic wave functions

are given as the product of periodic function multiplied by a phase factor  $e^{(-ik \cdot r)}$ . This is an application of works by the mathematician Gaston Floquet about differential equations with periodic coefficients in 1883. Bloch generalized Floquet's results to three dimensional systems and obtained the description of the wave function associated with an electron traveling through a periodic crystal lattice [14].

In the fifties, Brillouin made a major contribution to the understanding of wave propagation in periodic media, whatever the wave nature is. Following an exhaustive study based on the two-domain correspondence: the real and the reciprocal space (k-vector space), he established the so called "Brillouin zones". He showed that the first Brillouin zone contains all information about propagating modes. In 1976, Amnon Yariv and Pochi Yeh studied dielectric multilayer stacks, waveguides and Bragg fibers [15] [16]. In their paper "*Bragg Reflection Waveguides*" they proposed and analyzed the possibility of using Bragg reflection to obtain lossless confined propagation in slabs with a dielectric constant that is lower than the surrounding media [17]. In addition, they employed the concepts of Bloch waves and band structures to study periodically layered media in "*Electromagnetic propagation in periodic stratified media. I. General theory*"[18].

In 1987, the research interest on more than one dimensional optical periodic structures led to the prediction of photonic crystals [19] [20]; this is when the propagation of optical waves in periodic structures was first thought to produce complete 3-D bandgaps. This recalls the work of Brillouin [21] considering the elastic waves in periodic strings, electrons in crystals, and electromagnetic waves in electrical circuits. The notion of 3-D photonic crystals lead to the generalization of important concepts of the Brillouin zone, bandgap, etc.... that are applied on different types of waves like electromagnetic waves (such as optical waves), or elastic waves.

The field of photonic crystals was opened by Yablonovitch [19]. with the aim of reducing spontaneous emission. He suggested to generalize the concept of Fabry-Perot resonator to three dimensions using the well-known concept of dielectric mirror. This enables one to reduce the laser cavity dimension not only along the laser axis but also in all the three dimensions. He observed that losses won't occur in a medium preventing light to propagate in certain frequency bands.

Yablonovitch proposed some ways to implement 3-D periodic structures based on creating voids in transparent materials. The large difference between the refractive indices of air and transparent material ensures the opening of large gaps, limiting the electromagnetic density of states and thus reduce the losses. In the same year Sajeev John used the idea of photonic crystals to affect localization and control of light [20]. In 1990, the plane wave method [22] was applied to Maxwell's equations from a theoretical point of view in periodic dielectric media [23] [24].

In 1991, Yablonovitch did two experiments; the first one was done on samples of centimeter scale with drilled holes in stycast low-temperature glue. The measurements evidenced experimentally the first photonic band gap (in the microwave frequency band). In the second experiment, due to intended crystal defects, Yablonovitch found localized states (case of high  $Q$ -cavities) in the band gap [25]. In 1994, experiments were done at microwave frequencies on a series of alumina rods by Ozbay et al. [26], where they confirmed the existence of forbidden bands. High transmission defect modes were reported a few years later [27], with a possible evolution towards controllable structures [28].

In 1995, the group of V. N. Astratov from the A.F. Ioffe Physical-Technical Institute of St.-Petersburg, Russia, realized that natural and synthetic opals are photonic crystals with an incomplete bandgap [29].

A few years after, in 1997, thanks to the evolution of technology, Miguez et al. [30] created silica spheres with diameters ranging from  $200nm$  to  $700nm$ . In 1998, Judith [31] did a similar work to that of Miguez et al. on inverted titanium spheres with diameters of  $500nm$ .

In 2002, and in the continuity of pioneering work on 3-D lattices, Florencio et al. [32] fabricated a diamond structure with  $0.9\mu m$  silica spheres by means of nano-robotic manipulation of microspheres. But studies on 3-D lattices are still not evolving in the way studies on 2-D lattices do either theoretical or experimental, and that is because of the technological difficulty of implementing opals in photonic circuits. However, these studies show that 3-D lattices provide band gaps wider than that of 2-D lattices.

## 1.2.2 Generalization to Phononic Crystals

In the same way as the studies of electromagnetic waves propagation in periodic structures lead to the photonic crystal concept; the study of elastic waves in periodic structures lead to the theme of phononic crystals. In other words, phononic crystals are the elastic counterparts of photonic crystals. Usually they are classified into several categories according to their useful frequency range:

- Sonic crystals between 1 Hz and 20 kHz, that is relative to the audible sound [33].
- Ultrasonic crystals between 20 kHz and 1 GHz, where this frequency range is used for non-destructive imaging and control [34].
- Hypersonic crystals more than 1 GHz, where the frequency range is used for acousto-optics, signal processing and thermoelectricity [35].

Remark that, historically, for practical reasons, the first experimental studies were made on sonic crystals [33] , that allowed by the use of the scaling law to design crystals of small dimensions, in particular for the frequencies of the order of GHz.

In 1972, the study of A.H. Fahmy and E.L. Adler on the propagation of elastic waves in artificial periodic structures, established a formalism to describe the propagation of surface waves in a multilayer system which was a 1-D system [36].

In 1987, Lakhtaki did the first theoretical work on two-dimensional crystals. He studied the coefficients of reflection and transmission of elastic waves on circular elastic cylinders arranged periodically in an elastic slab for low frequencies [37].

The concept of phonon in periodic structures was introduced by J. Liu in 1990, who experimentally studied the propagation of sound wave through a composite medium of fluid and solid spheres [38]. Later on, J.Liu and X.Jing conducted a theoretical study to establish the dispersion pattern of an acoustic wave in fluid and link it with the measured band gaps [39] [40].

In 1991, the attenuation of elastic waves in non-homogeneous liquids was studied by Anthony A. Ruffa in the liquid phase [41].

The first calculations of acoustic bandgaps were published in 1993 [42], the similarities of electronic, optical, and elastic waves were also stated. A survey of electronic, photonic, and phononic wave propagation in periodic media is presented in [43]. In addition, studies have been done and scattering diagrams of phononic crystals have been deduced [44] [45] [46] [47]. These studies gave birth to the theme of phononic crystals, and the number of articles on this subject increased gradually [48]. Then, until now, the studies of photonic and phononic crystals have been continuously inspired from one another.

### 1.2.3 The Emergence of PhoXonic Crystals

Following the studies on photonic and phononic crystals, a new field of study was born, that is the phoXonic crystals which are periodic structures behaving as both photonic and phononic crystals. In early 2002, the first studies done on phoXonic crystals concerned 1-D crystals [49], for they are simple to study theoretically and experimentally. After 4 years, the study of 2-D crystals started and became the hugest field of study till our present days. While studies concerning 3-D crystals are rising slowly.

The great interest dragged by phoXonic crystals is due to their capacity to allow the simultaneous confinement of an electromagnetic wave and an acoustic wave in the same device. The possible enhancement of the interaction between these two types of waves has opened a new field of study: acousto-optical interaction in structures with high confinement. More specifically, the aim behind phoXonic crystals research area is to exploit the phenomena of confinement, guidance and slow wave in favor of acousto-optical coupling.

PhoXonic crystals studies focused first on the theoretical developments to obtain simultaneous acoustic and optical band gaps in the same structure. Indeed, simultaneous acoustic and optical bandgaps existence constitute the necessary preliminary condition for obtaining simultaneous confinement of electromagnetic and elastic modes in the same cavity. Due to this simultaneous confinement, the acousto-optical coupling is expected to be magnified. Several mechanisms can be involved in these interactions: the photo-elastic effect, the moving interface effect, and the piezoelectric effect in specific material. The coupling coefficients relative to those effects will be presented at the end of Chapter III.

First studies about coupling rely on a multilayer system with a cavity, constituted of a gap between two highly reflecting dielectric mirrors (1-D crystal). The Fabry-Perot cavity



simultaneously confines acoustic and optical waves; from this setup, coupling between the waves is experimentally measured. In order to induce positive gain with acoustic signal amplification, acousto-optical parametric oscillatory instabilities in light-sound Fabry-Perot resonators [50] were proposed. Here the acoustic modes of the resonator are excited when light is coupled through an optical cavity mode and is confined within the resonator's walls.

The work on 1-D crystals has followed two distinct axes in recent years. The first is the creation of a phonon by the strong confinement of an electromagnetic wave in a cavity [49] [51]. This led to the idea of generating a monochromatic acoustic wave, like lasers in the field of optics. The second corresponds to the opposite case, where the acoustic wave modifies the propagation of the optical wave [52].

The modulation of the transmission and reflection of an optical wave in a multilayer thin film due to an acoustic wave generated by a picosecond optical pulse was described by Matsuba et al. in 2002 [49]. After that, Trigo et al. introduced a cavity into a multilayer system [51]. Then this principle was generalized in 2003 by Worlock et al., by proposing the generation of a monochromatic acoustic wave by an optical wave [52].

Trigo's work [51] was taken up by Lacharmoise et al. [53] in 2004, who proposed the optimization of the geometric dimensions of the cavities to increase the acousto-optical interaction by a factor of 5. Gérard et al. [54] then proposed a periodic structure on a piezoelectric substrate excited by interdigital transducers in 2007, where the incident optical wave perpendicular to the plane of the grating is modulated by the elasto-optical effect. Then the transmission intensity of the wave is modulated by the change in the extraordinary refractive index generated by the acoustic wave.

The modulation of the optical field in a periodic lattice by an acoustic pulse in a cavity, was studied experimentally by Bestermann et al. [55] in 2010. In this system, it is possible to create a picosecond modulator where the optical wave is reflected on a very short time when the acoustic wave is confined. In the same year, Papanikolaou et al. [56] [57] theoretically demonstrated the possibility of modulating the optical resonance frequency of a cavity in an equivalent system. Due to the opto-mechanical and elasto-optical effect, the transmission of an optical wave is modulated according to the acoustic period.

Another approach based on the phonon generation by an optical pulse was experimentally performed in 2011 [58]. The idea was close to that of Worlock [52], but this time it was to use non-resonance modes of the cavity to improve the generation and detection of acoustic waves.

In 2012, studies conducted by Piliposian et al. [59] showed the impact of a piezoelectric material on the forbidden bands of a photonic and phononic crystal.

While 1-D networks are limited to the angle of incidence of the waves, which forces the use of a parallel beam in a single direction, 2-D crystals help overcome this limitation when they present complete forbidden bands. Studies on 2-D crystals focused then a growing interest in the following years.

Studies done on 2-D photonic and phononic crystals began in 2006, when Maldovan and Thomas theoretically demonstrated the simultaneous existence of acoustic and optical forbidden bands in silicon [60]. This work showed that lattices constituted of drilled holes were able to obtain simultaneous forbidden bands like other lattices constituted of pillars. Hence, thanks to the use of the supercell method [61], the existence of localized modes was demonstrated allowing to confine acoustical and optical waves in a unique cavity.

The study by Maldovan was extended by Sadat Saleh et al. in 2009 to different lattices other than the square ones, such as triangular and honeycomb lattices [62]. Hence, it was found that it is possible to obtain larger bandgaps by the addition of inclusions of different radii and materials in silicon. More studies emerged, but they based their studies on materials other than silicon, like the use of lithium niobate (a piezoelectric material) by Sadat Saleh et al. [63], or the use of sapphire by Bria et al. [64].

Between 2010 and 2011 a large number of publications were published concerning the research of bandgaps in photonic crystals. Most of the publications were extended to 2-D crystals with an additional finite thickness according to the third dimension (which sometimes is referred to as 2.5-D case, particularly membranes between two air layers [65] also called “Slabs” or “Photonic Membranes”), or on semi-infinite substrates (in the latter the finite thickness refers to the penetration depth of the drilled holes constituting the 2-D periodic structure). The different geometrical parameters are no longer limited to radius inclusion (or even its shape) but also to the thickness of the membrane. As a result, the width of the simultaneous band gaps then depends on  $(h, r, a)$ , where  $(h)$  is the membrane thickness,  $(r)$  is the hole radius, and  $(a)$  is the lattice parameter.

Different periodic structures constituted of air inclusions [66] [67] were analyzed. The study of periodic structures constituted of pillars was also carried out, which allow the existence of bandgaps as well. Similar to 2-D studies, different lattices (such as honeycomb or triangular lattices) result in different bandgaps, each having different geometric parameters  $(h, r)$ , which differ from one configuration to another [68] [69].

Moreover, the possibility of guiding the wave in periodic structures in membranes has recently been studied [65] [68]. Indeed, the wave must not only be confined between two layers of air but also guided along the crystal. The study of the dispersion diagram is then necessary

where the choice of the resonance mode of the guide must be carefully chosen in order to confine and guide at the same time without propagating loss.

Concerning the study of phoXonic crystals on a semi-infinite structure, which consists of two layers: a layer where the wave is guided and a substrate on which it is laid; a particular attention must be paid to the latter since its dielectric and mechanical properties must allow confinement in the layer comprising the periodic network. In this perspective, the dielectric constant of the substrate must be lower than that of the layer. For example, a photonic crystal machined in silicon of index  $n = 3.5$  will be placed on silica of index  $n = 1.5$  smaller than that in silicon. The optical wave is 50% slower in silica than in air, which makes it possible to confine the wave in silicon, in a manner equivalent to a membrane between two air layers. The same precautions must be taken in order to insure the confinement of the acoustic wave in the membrane. Whatever the nature of the propagating wave is, in order to insure the total internal reflection, the phase velocity must be lower (higher wavevector) in the membrane material than it is in the substrate material.

The impact of geometric imperfections has been also studied because in practice a perfect cylinder is not technologically realizable, it will turn to be somehow conical more or less pronounced for semi-infinite substrates. These, according to their angle and their depth, will have an impact on the confinement of the optical [70] and acoustical waves [71] in the photonic and phononic crystals respectively. For example, some patterns having no sufficient depth in the layer will generate losses to the substrate. Similarly, cones with an angle too steep can diffract the wave to the substrate.

Different patterns are envisaged to allow a better confinement, like the cross-shaped or star-shaped patterns. Yan Pennec et al. proposed the use of "strip waveguides" with a suspended membrane consisting of a beam attached at both ends with a single row of holes in a square

lattice pattern [72]. The idea is to implement two sidebars, where the two "stubs" are of dimensions equivalent to the lattice parameter at the ends of each pattern. The advantages of introducing these stubs is that it enables to get a parameter for tuning the elastic resonance, resulting in the possibility to obtain wider phononic bandgaps, while the holes parameters allow the tuning of the photonic bandgaps. Such a device, with optimized parameters, present wide simultaneous bandgaps. Moreover, the actual values of the geometrical parameters compatible with technological fabrication techniques have been discussed, so that the photonic cavity mode could be found in the range of telecommunication wavelengths while the acoustic frequencies are falling in the gigahertz range. An equivalent structure created by Hsiao et al. used a micro-beam consisting of a row of circular inclusions [73]. The acousto-optical interaction with the elasto-optical and opto-mechanical effect makes it possible to modulate the optical transmission of the device theoretically.

Tian-Xue Ma et al. investigated theoretically the properties of photonic and phononic bandgaps in phoXonic crystals with veins for wide range of geometry parameters, where square, triangular, and honeycomb lattices were taken [74]. It ended up with favorable results for the concurrent generation of the photonic and phononic band gaps in the phoXonic square and honeycomb lattices, but not in the triangular lattice since it can't generate large dual bandgaps. Hence, the maximum photonic-phononic bandgap was achieved in the honeycomb lattice but for a square lattice it is more favorable since it is easier and cheaper when it comes to fabrication [75].

Moreover, the snowflake 2-D opto-mechanical coupling structure was presented by Amir H. Safavi-Naeini et al., providing the foundation for developing planar circuits for the optical and acoustical wave's interaction [76]. These circuits will allow for the realization of coupled arrays of devices for advanced photonic or phononic signal processing, such as dynamic

trapping and storage of optical pulses or the tunable filtering and routing of microwave over optical signals.

The acousto-optical coupling in periodic structures with simultaneous photonic and phononic band gaps, based on photo-elastic and opto-mechanical mechanisms, was investigated by Rolland et al. using a fully numeric Finite Element Method [77]. They evaluated the impact of the perturbation introduced by an acoustic mode confined in a cavity on the optical modes localized in this same cavity. They compared the strength of the photo-elastic and opto-mechanical effects in different cases. Both mechanisms can be in phase or out of phase and produce additive or subtractive effects in the total acousto-optical coupling strength.

### 1.3 Active PhoXonic Cavities

A cavity, built in periodic structures with simultaneous photonic and phononic band gaps for modulation purpose, as proposed by Rolland et al. [77], is an emblematic case of active cavity in a phoXonic crystal. As just recalled, the modulation behaviour can be quite different when considering various couples of photonic / phononic modes, different qualitatively and quantitatively. Also, as a result of a full numeric *FEM* approach, the calculation time can rapidly become a limiting factor to who wants to develop an algorithm for device optimization that requires numerous iterations before converging towards an optimized design.

When the developments presented in this thesis have started, following the results from [77], two questions were still opened:

- Is it possible to understand the reasons explaining the different coupling behaviours as observed by the numerical experiments?

- Is it possible to predict the coupling efficiency by a physical approach rather than by a computational approach?

Of course, as a side problem of the numerical approach, the possibility to gain time on evaluation procedure would be a serious advantage.

Hence, the starting point of the following developments was motivated by the will to adapt the perturbation theory. This theory is an approximation scheme well adapted to describe the evolution of a “mode”, case of solution of an eigenvalue problem, when considering a “small difference” to the problem: a perturbation. The evolution of the eigenvalue, i.e. energy (or frequency) of the mode is also perfectly described in the frame of such concept. Usually, developments up to the first order are sufficient and the corrections (or “evolutions”) of the eigenvalues are given by projections of the unperturbed modes over the operator (or function) describing the perturbation.

More precisely, we seek for developments of the perturbation method to provide physical interpretations of opto-mechanical coupling in simultaneous photonic and phononic crystal cavities. Starting from the classical perturbation method, we intend to extend it to the degenerated modes including second order terms; with the aim to identify design rules applicable to active phoXonic cavities design.

For the sake of simplicity and for purpose of expediency when comparison with previously published results is required [77], we focus on  $L_1$  point defect cavities in two dimensional square array phoXonic crystals. The host material considered is silicon, as it is widely used in the microelectronics industry for the maturity of manufacturing techniques and as it also presents good optical qualities.

## 1.4 Conclusion

In this chapter we have introduced the general concepts that have led to the emergence of the concept of photonic crystals, phononic crystals, and later to phoXonic crystals. We have highlighted the fact that such structures have drawn a lot of attention due to the possibility they offer to promote the design of active devices, for modulation purpose as an example, with improved efficiency.

Full numeric studies of active phoXonic cavities have revealed their ability to promote the development of opto-mechanical modulators, but also have raised questions about the physical reasons explaining the different behaviours observed. This thesis is a step toward the development of semi-analytical tools to predict the coupling behaviours in active phoXonic cavities.



# Chapter II

## Introduction to Periodic Media Theory

### 2.1 Introduction

From the early centuries, humans were always fascinated by crystals. Of course, the understanding of the mystery of diamond brightness was very challenging. But also, the regular cleavage properties of natural crystals were at the origin of the very first theories about the intimate constituents of materials. However, beyond any doubt, it is the introduction of X-ray diffraction as a tool of crystal analysis that is at the root of the modern crystallography.

It is now well established that depending on the cooling process conditions, that is: the pressure, the temperature, as well as the rate of the decrease of the temperature, materials solidify in two main forms: crystalline or amorphous. In the former state the atoms are arranged in a regular periodically repeated pattern while in the latter the atoms are randomly distributed. An intermediate state exists; the so-called polycrystalline state where the long-term periodicity is broken while it is locally preserved; i.e. the crystal appears in the form of a set of single crystals juxtaposed next to each other. The resulting crystal structure type depends on the chemical nature of its constituents and the inherent nature of atomic bounding forces.

A crystal structure is usually described using the concept of a lattice associated to a unit-cell. The lattice is defined as a system of points, referred to as "nodes", arranged periodically where each of these nodes faces an identical surrounding. According to the considered space dimensions, the lattice is said to be 1-D, 2-D or 3-D. The unit-cell contains all the material's

constituents in the neighborhood of a given lattice node. Successive translations of the unit-cell from a lattice node to its nearest neighbors will reconstruct the crystal. The same concepts apply to artificial periodic structures as studied in this thesis.

This chapter introduces the basic principles of photonic crystals structures, starting from the description of a crystal, moving onto the type of lattices, explaining the real and reciprocal space representations, and ending up with the presentation of the band diagram.

## 2.2 Description of a Crystal: Lattice and Unit-Cell

Beside the natural crystals, thanks to the advent of semiconductor technologies, man-made nano-structured materials may be fabricated with different dimensionalities. Modulating the physical parameters of a homogeneous material "in only one" dimension leads to the so-called 1-D materials. A typical example is the stratified media illustrated in Figure 1-(a) by two layers of different materials alternatively stacked on top of each other. In the same way Figure 1-(b) show an example of 2-D inhomogeneity designed by modulating the material parameter in two directions (say  $x$  and  $y$ ) while the material still homogeneous in the third direction  $z$ . In this example, pillars arranged in air (or holes drilled in a bulk material), the 2-D material description may be limited to any cross section parallel to the  $(x, y)$  plane. Figure (1-c) gives an example of a 3-D structure formed by spheres stacked on top of each other.

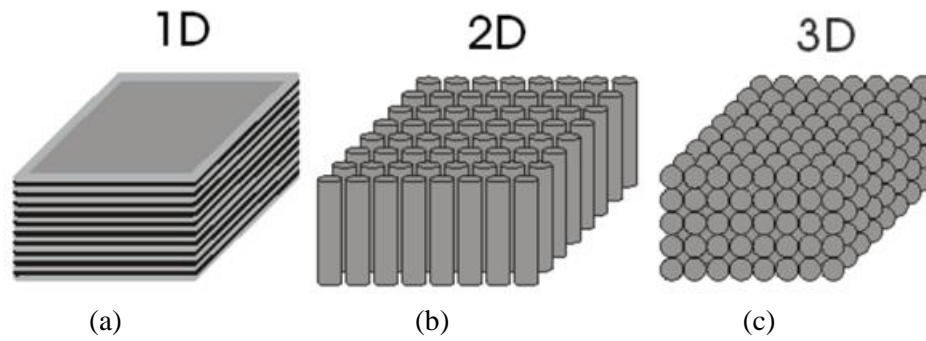


Figure 1: Illustration of one-dimensional, two-dimensional, and three-dimensional structures [1].

Whatever the crystal dimensionality and/or symmetry is, it may be described using a lattice associated to a unit-cell. The choice of the lattice is not unique. An illustrative example is shown in Figure 2-(a) for the special case of a 2-D centered rectangular lattice. The red dots represent the nodes, the black arrows stand for the basis vectors. The associated unit-cells are colored in yellow. Any of these unit-cells if successively translated by any linear combination of the associated basis vectors will reconstitute the 2-D lattice. While, the three lower row unit-cells cover the same area and comprise only one node (4 nodes shared by 4 neighbor unit-cells), the upper row unit-cells exhibit twice this area and contain two nodes. Another difference resides in the fact that the basis vectors of the upper row will not address all the nodes by successive translation. Finally, as illustrated at the right of the upper row in Figure 2-(a). The unit-cell is not necessarily included in the basis vectors parallelogram, but it may be shifted to embrace the nodes it owns.

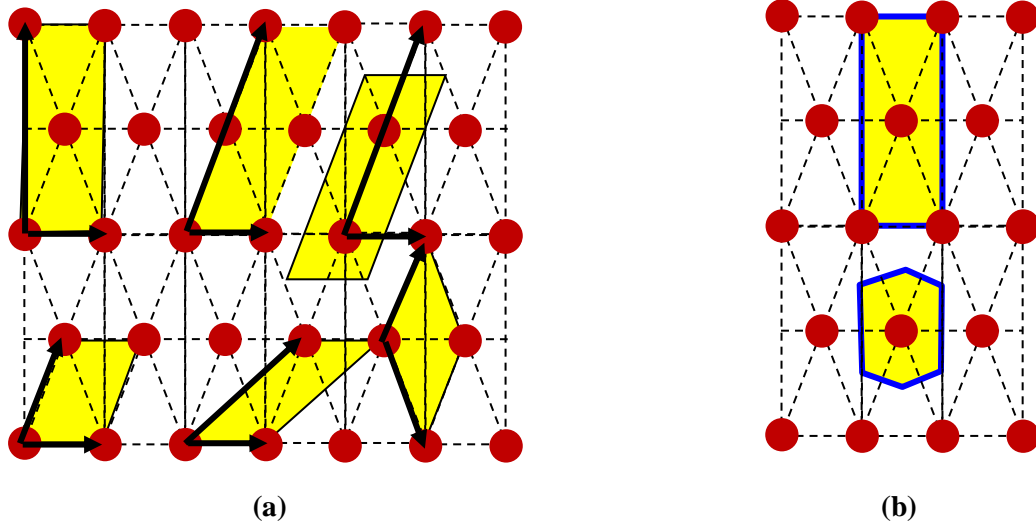


Figure 2: Illustrative example of two-dimensional Centered Rectangular lattice.

(a) (Left) Different choices of basis vectors and their associated unit-cell defined as the area inside the parallelogram determined by the basis vectors. 3 Primitive lattices and unit-cells (lower row) and non-primitive ones (upper row).

(b) (Right) The Wigner-Seitz cell (down) and the non-primitive conventional Centered Rectangular cell (up).

## 2.3 Primitive, Conventional, and Wigner-Seitz Cells

A lattice and its associated unit-cell are said to be primitive if the latter encloses a unique node and represents the smallest volume of unit-cell. It is worth noting that a unit-cell contains all the structural and symmetry information to build up the macroscopic structure of the lattice by successive translations without neither blanks nor overlaps.

Continuing the preceding example of Figure 2-(a), all the unit-cells have been chosen as the area defined by the parallelogram delimited by the basis vectors. But these chosen unit-cells may not explicitly exhibit the inherent symmetry properties of the lattice. So, in the field of crystallography, one usually defines a conventional unit-cell which is not necessarily primitive for lattice classification. In the above example only, the Centered Rectangle shaped

unit-cell (on the left of the upper row) exhibit the overall symmetry properties. This is the reason why it is this "basis vectors / unit-cell" combination that has been selected as the conventional one and that the representation and this lattice symmetry is named after it.

In the field of symmetry group analysis, it is not too troublesome to use a non-primitive unit-cell. But, in the field of wave propagation and its special case X-ray diffraction, the use of a non-primitive unit-cell will lead to band folding effects and complicates the interpretation of the theoretical obtain results. So, when wave propagation in periodic media is addressed, one prefers the use of primitive cells.

In Figure 2-(b), we redraw the conventional centered rectangular cell in the upper row. In the lower row, we represent the Wigner-Seitz cell defined as the inner area delimited by the planes which perpendicularly bisect the straight lines joining the nearest neighbors of the lattice node. The Wigner-Seitz offers the advantage to be a primitive cell and to exhibit the lattice symmetries as well.

## 2.4 3-D Analytic Expression of the Lattice and Unit-Cell

Given a three dimensional lattice, we can adequately express the node positions of a primitive lattice using a set of 3 primitive basis vectors  $\vec{a}_1, \vec{a}_2, \vec{a}_3$ , i.e. chosen as the translation vectors between nearest neighbors 3-D nodes. Indeed, starting from one node, designated by its position vector  $\vec{r}_0$ , all the other nodal points will be addressed by the vector  $\vec{r} = \vec{r}_0 + \vec{R}_{n_1, n_2, n_3}$ ; where  $\vec{R}_{n_1, n_2, n_3}$  is the translation vector given by:

$$\vec{R}_{n_1, n_2, n_3} = n_1 \vec{a}_1 + n_2 \vec{a}_2 + n_3 \vec{a}_3 \quad \dots (1)$$

Where  $n_1, n_2, n_3 = 0, \pm 1, \pm 2, \dots$

In the same way, starting from any other point different from a nodal one i.e.  $\vec{r}' \neq \vec{r}_0$  all the points addressed by:  $\vec{r} = \vec{r}' + \vec{R}_{n_1, n_2, n_3} = \vec{r}' + n_1 \vec{a}_1 + n_2 \vec{a}_2 + n_3 \vec{a}_3$  will have an identical surrounding as that around the initial point  $\vec{r}'$ . This explain the arbitral position and virtual characters of the lattice i.e. the origin or the lattice can be shifted anywhere within the unit-cell.

The primitive unit-cell is often chosen as the volume inside the parallelepiped defined by the primitive basis vectors. Its volume is simply given by the vector triple product:

$$V_{U\_cell} = \vec{a}_1 \cdot \vec{a}_2 \times \vec{a}_3 \quad \dots (2)$$

Again, the unit-cell will fill the whole space and reconstructs the crystal when shifted by the lattice vectors  $\vec{R}_{n_1, n_2, n_3}$  for all the infinite sets of triplet integers  $(n_1, n_2, n_3)$

As in 2-D, the 3-D Wigner-Seitz cell is defined as the inner volume delimited by the planes which perpendicularly bisect the straight lines joining the nearest neighbors of the lattice node. Its volume is equal to the one given by equation (2).

## 2.5 Bravais Lattices

In the middle of the nineteen century, in a geometrical approach, Bravais has enumerated and classified the different symmetries that are compatible with lattice structures. Briefly, by simply varying the relative length of the basis vectors and the angle between them, Bravais enumerated the geometrical figures (quadrilaterals in 2-D and hexahedron in 3-D) that can be used as lattice unit-cells (parallelograms in 2-D and parallelepiped in 3-D), and he classified them according to the geometrical symmetries that can be encountered. The number of 2-D

Bravais lattices is limited to five and are classified in 4 classes, while in 3-D there are fourteen Bravais lattices classified in seven classes. These classes are also called Lattice Systems.

## 2.5.1 2-D Bravais Lattice

Let us start with the Oblique System which is the most general case. As shown in Figure 3, its unit-cell consists of a parallelogram characterized by unequal basis vectors length  $|\vec{a}_1| \neq |\vec{a}_2|$  with an arbitrary angle between them  $\varphi \neq 90^\circ$ . Let the  $\vec{a}_1$  parallel to the horizontal  $x$ -axis so  $\varphi$  is view as the angle of  $\vec{a}_2$  with respect to the horizontal axis. Consider the angle  $\varphi$  increasing from tiny angles up to approaching  $180^\circ$ . Only two specific angles leading to additional symmetric elements can be found. The most evident one match the orthogonality condition  $\varphi = 90^\circ$  which leads to the Rectangular Bravais lattice. This situation introduces two planes of mirror symmetry (perpendicular bisector planes) and/or equivalently a 2-fold rotational axis (the mutual intersection of the mirror planes). The second situation, a bit less evident, is the angle making the horizontal projection of  $\vec{a}_2$  exactly coincide with one half of the length of the vector  $\vec{a}_1$  i.e.  $\cos \varphi = |\vec{a}_1| / (2|\vec{a}_2|)$ . This leads to the centered rectangular lattice we introduce in section 2.2. Since they exhibit the same symmetry elements, we say that these two Bravais lattices: the Primitive Rectangular and the Centered Rectangular (not primitive) belong to the same symmetry class. Usually the class is labeled with the name of primitive lattice. In other words: the Rectangular Class contains two Bravais lattices: the Primitive Rectangular and the Centered Rectangular ones. Other symmetries can be introduced if we consider the case of two basis vectors with equal lengths. One can identify two classes each comprising a unique Bravais lattice the Square one if  $\varphi = 90^\circ$  and the Hexagonal one if  $\varphi = 120^\circ$  as shown in Figure 3.





## 2.5.2 3-D Bravais Lattice

Proceeding in the same way for the case of 3-D lattices, i.e. beginning with the Triclinic Bravais lattice and varying the angles  $\alpha_{ij}$  between the 3 basis vectors  $\{\vec{a}_i, \vec{a}_j, \vec{a}_k\}$  and their relative length, fourteen different lattices are identified which pertain to seven classes (or Systems):

- Triclinic: all the 3 pairs of faces are parallelograms.
- Monoclinic: 1 pair of faces is a parallelogram the other 2 pairs are rectangles.
- Orthorhombic: all the 3 pairs of faces are rectangles.
- Tetragonal: 1 pair of faces is a square (the base) the other 2 pairs are rectangles.
- Cubic: all the 3 pairs of faces are squares.
- Hexagonal: 1 pair of faces is a lozenge ( $\varphi = 120^\circ$ ) and 2 pairs are rectangles.
- Trigonal: all the 3 pairs of faces are lozenges.

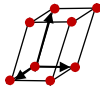
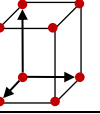
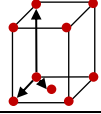
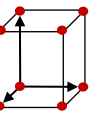
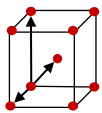
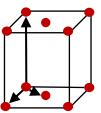
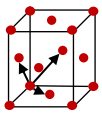
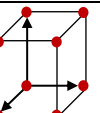
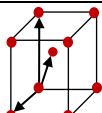
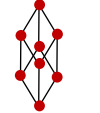
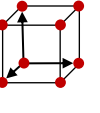
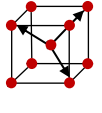
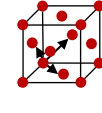
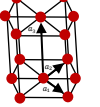
Bravais Lattice	Parameters	Simple (P)	Volume Centered (I)	Base Centered (C)	Face Centered (F)
Crystal Systems					
Triclinic	$a_1 \neq a_2 \neq a_3$ $\alpha_{12} \neq \alpha_{23} \neq \alpha_{31}$				
Monoclinic	$a_1 \neq a_2 \neq a_3$ $\alpha_{23} = \alpha_{31} = 90^\circ$ $\alpha_{12} \neq 90^\circ$				
Orthorhombic	$a_1 \neq a_2 \neq a_3$ $\alpha_{12} = \alpha_{23} = \alpha_{31} = 90^\circ$				
Tetragonal	$a_1 = a_2 \neq a_3$ $\alpha_{12} = \alpha_{23} = \alpha_{31} = 90^\circ$				
Trigonal	$a_1 = a_2 = a_3$ $\alpha_{12} = \alpha_{23} = \alpha_{31} < 120^\circ \neq 90^\circ$				
Cubic	$a_1 = a_2 = a_3$ $\alpha_{12} = \alpha_{23} = \alpha_{31} = 90^\circ$				
Hexagonal	$a_1 = a_2 \neq a_3$ $\alpha_{12} = 120^\circ$ $\alpha_{23} = \alpha_{31} = 90^\circ$				

Table 1: The fourteen Bravais lattices in three dimensions (3-D) [3].

## 2.6 Crystal Structure: Lattice + Unit-Cell

The addition of the unit-cell material may affect the lattice symmetry elements. The group theory states that only 32 between the 230 space groups are compatible with the periodicity of the lattice. The 32 groups are classified in the seven classes following their symmetries. The

parameter of the bulk material depends drastically on its individual symmetry group: extinction of tensor elements as stiffness constant, refractive indices.... We will return to this point in the following chapter.

## 2.7 Reciprocal Space and Brillouin Zones

Initially the reciprocal space, more specifically, its reciprocal basis vectors have been introduced in geometrical crystallography. They appear to be a very useful tool to handle non-orthogonal basis. Indeed, they are introduced as a set of three vectors in such a way that each one of them is orthogonal to the plane sustained by two of the basis vectors of the direct lattice. So, their use facilitates the dot product and thus makes easier the writing of the analytical expression of lattice planes. The reciprocal lattice vectors are direct measures of the spacing distance between 2 planes of the same family; an essential parameter for X-ray analysis in modern crystallography. Here we will introduce the reciprocal lattice following another approach based on wave propagation in periodic material which is concerned in the present thesis. We also present the concept of Brillouin zones.

### 2.7.1 Reciprocal Space Basis Vectors

The Bloch-Floquet theorem states that if  $\varphi(\vec{r})$  stands for the spatial part of a monochromatic wave propagating in a periodic media it will display a special kind of discrete translation symmetry expressed as:

$$\varphi(\vec{r} + \vec{R}) = e^{i\vec{k}\cdot\vec{R}}\varphi(\vec{r}) \quad \dots (3)$$

Where,  $\vec{k}$  is an arbitrary chosen wavevector pointing towards the propagation direction and  $\vec{R} = \vec{R}_{n_1, n_2, n_3}$  stands for any of the lattice translation vectors as defined in equation (1).

It is worth noting that once the arbitrary wavevector  $\vec{k}$  have been chosen, it will come with an infinite series of wavevectors. Indeed, the Bloch-Floquet condition (3) is simultaneously verified by an infinite series of the wavevectors  $(\vec{k} + \vec{G})$ . Provided that:

$$e^{i(\vec{k} + \vec{G}) \cdot \vec{R}} = e^{i\vec{k} \cdot \vec{R}}. \quad \dots (4)$$

Thus,  $\vec{G}$  is a solution of:

$$e^{i\vec{G} \cdot \vec{R}} = 1 \Leftrightarrow \vec{G} \cdot \vec{R} = 2\pi N; \quad \dots (5)$$

Where N is an integer and  $\vec{R} = \vec{R}_{n_1, n_2, n_3} = n_1 \vec{a}_1 + n_2 \vec{a}_2 + n_3 \vec{a}_3$

In order to facilitate the dot product in equation (5), it is convenient to expand  $\vec{G}$  on the so-called reciprocal basis vectors  $\vec{b}_1, \vec{b}_2, \vec{b}_3$ . That is,  $\vec{G}$  writes:

$$\vec{G} = m_1 \vec{b}_1 + m_2 \vec{b}_2 + m_3 \vec{b}_3 \quad \dots (6)$$

Where  $m_1, m_2, m_3 = 0, \pm 1, \pm 2, \dots$

The reciprocal basis vectors  $b_i$  are introduced so that they satisfy the condition:

$$a_i \cdot b_j = 2\pi \delta_{ij} \quad \dots (7)$$

Where  $\delta_{ij}$  is the Kronecker delta:  $\delta_{ij} = 1$  if  $(i = j)$  and  $\delta_{ij} = 0$  if  $(i \neq j)$ .

This definition insures that the cross terms of the dot product in equation (5) will cancel despite the fact that both the basis  $\{\vec{a}_1, \vec{a}_2, \vec{a}_3\}$  and  $\{\vec{b}_1, \vec{b}_2, \vec{b}_3\}$  are not orthogonal. Equation (5) reduces to:

$$\vec{G} \cdot \vec{R} = 2\pi(n_1m_1 + n_2m_2 + n_3m_3) = 2N\pi \quad \dots (8)$$

The end-result is that equation (4) is implicitly verified for all the reciprocal lattice vectors  $G$  i.e. whatever is the triplet of integers  $(m_1, m_2, m_3)$  is. An equivalent definition of the reciprocal lattice basis vectors writes:

$$b_i = 2\pi (a_j \times a_k) / a_i \cdot (a_j \times a_k); \quad i, j, k = 1, 2, 3 \quad \text{and cyclic permutations} \quad \dots (7')$$

## 2.7.2 Brillouin Zones

Brillouin has showed that, the information concerning wave propagation in periodic media also exhibits a certain type of periodicity in the reciprocal domain i.e. the  $k$ -space. Thus, the reciprocal domain may be divided into consecutive equivalent zones named after him the Brillouin zones. Here is the reason why, without loss of generality, the studies in the reciprocal domain may be restricted to only one of these zones: the 1<sup>st</sup> Brillouin zone. The 1<sup>st</sup> Brillouin zone is delimited by the planes that perpendicularly bisect straight lines joining the nearest neighbors of the lattice node [78]. Its construction is analogue to the construction of the Wigner-Seitz cell but in the reciprocal domain.

## 2.8 Irreducible Brillouin Zones

The first Brillouin zone exhibits the same symmetry as that of the lattice. So, to limit the calculation time one restricts the study to the so-called irreducible Brillouin zone. That is, the portion of the first Brillouin zone that avoids any redundancy due to symmetry. Then, if needed, one can deduce the results to the whole first Brillouin zone using the same symmetry criteria. In the following sub-sections, we give some typical examples of 2-D lattices.

### 2.8.1 Hexagonal Lattice:

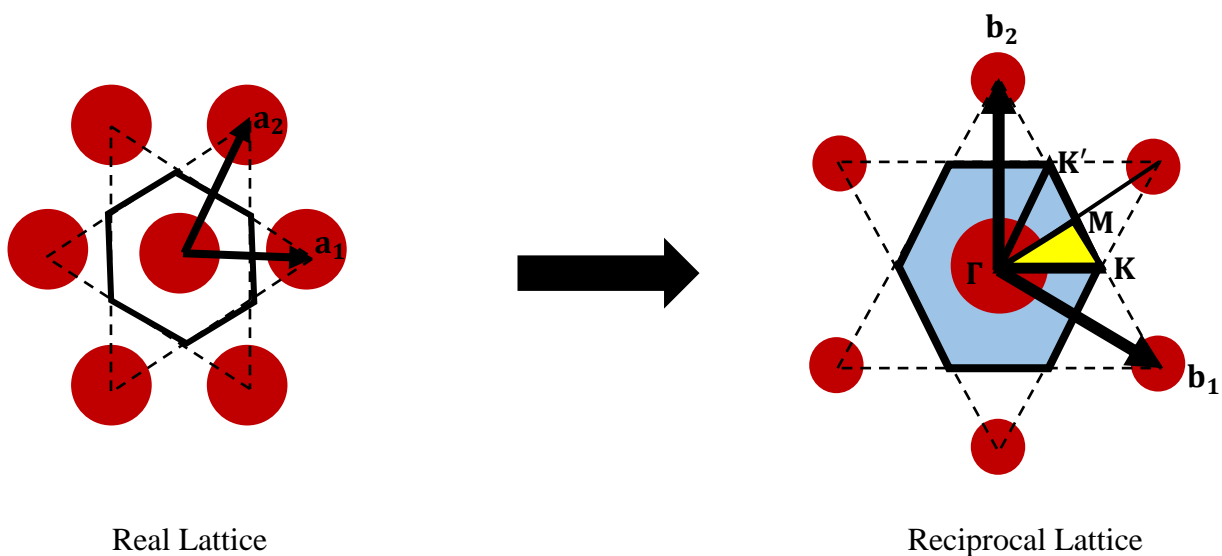


Figure 4: Hexagonal lattice and corresponding reciprocal lattice with highlighted Brillouin zone (blue). The yellow area is an irreducible first Brillouin zone with the corners  $M$ ,  $K$  and  $\Gamma$ .

## 2.8.2 Square Lattice:

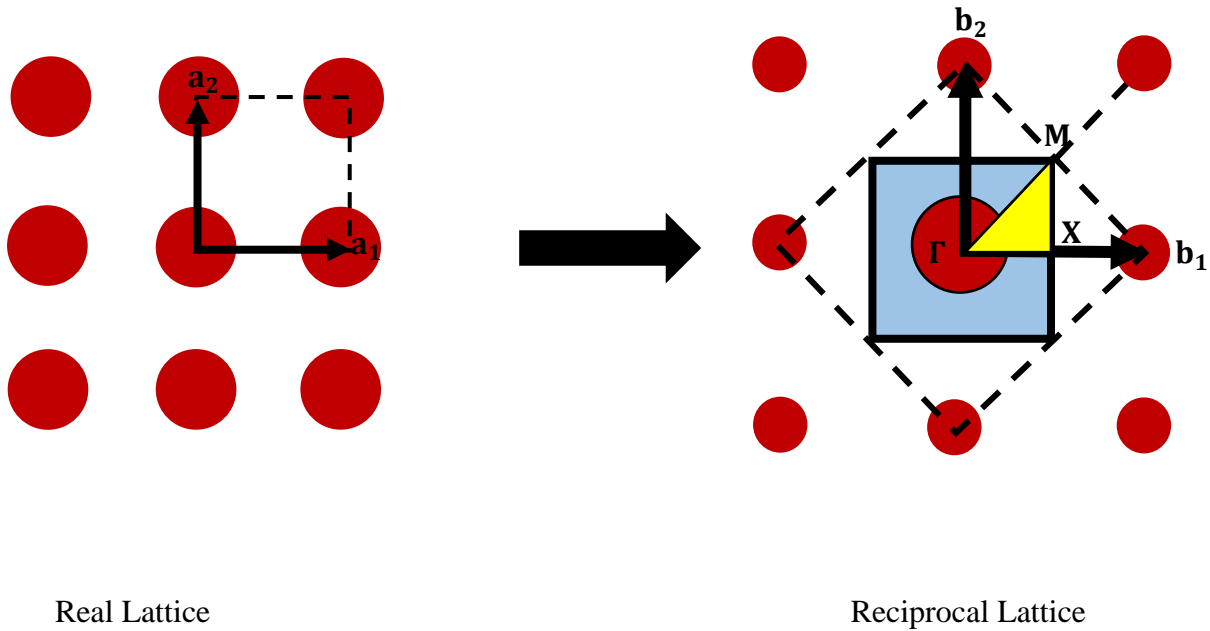


Figure 5: Square lattice and corresponding reciprocal lattice with highlighted Brillouin zone (blue). The yellow area is an irreducible first Brillouin zone with the corners M, X and  $\Gamma$ .

## 2.8.3 Transformation of The Reciprocal Lattice Vectors

	Real Lattice	Reciprocal Lattice	Angle $\alpha$ between $\vec{a}_1$ and $\vec{b}_1$ & reciprocal basis vector magnitude
Hexagonal Lattice	$\vec{a}_1 = a\hat{x}$ $\vec{a}_2 = \frac{a}{2}(\hat{x} + \hat{y}\sqrt{3})$	$\vec{b}_1 = \left(\frac{2\pi}{a}\right)\left(\hat{x} - \frac{\sqrt{3}}{3}\hat{y}\right)$ $\vec{b}_2 = \left(\frac{4\pi}{a}\right)\left(\frac{\sqrt{3}}{3}\hat{y}\right)$	$\alpha = 30^\circ$ $ b  = \frac{4\pi}{a\sqrt{3}}$
Square Lattice	$\vec{a}_1 = a\hat{x}$ $\vec{a}_2 = a\hat{y}$	$\vec{b}_1 = \left(\frac{2\pi}{a}\right)\hat{x}$ $\vec{b}_2 = \left(\frac{2\pi}{a}\right)\hat{y}$	$\alpha = 90^\circ$ $ b  = \frac{2\pi}{a}$

Table 2: 2-D direct and reciprocal lattice vectors correspondence expressed in a rectangular framework. Case of hexagonal and square lattices,  $\hat{x}$  and  $\hat{y}$  are unit-vectors of the rectangular framework used and  $a$  is the lattice constant.

## 2.9 The Band Diagram

Solid crystals are good propagating media for different wave fields such as light wave in dielectric media, electron wave functions, and crystal lattice vibrations. These phenomena may be addressed either from a microscopic or macroscopic point of view. If the propagating fields' wavelength is much larger than the interatomic distance, a macroscopic treatment is sufficient, and the medium may be considered as a continuum described by some effective material parameters. So, at these wavelength ranges, the consequences of the 3-D periodic nature of the crystal resume to the appearance of some anisotropic behaviors in an overall homogeneous bulk material. But, at higher frequencies, where the wavelengths decrease approaching the spatial period of the crystal, the microscopic aspect cannot be neglected. The concept of wave propagation turns into a problem of scattering of the incident wave by the atomic array. The periodicity of the propagating medium manifests itself by the appearance of the well-known phenomenon of bandgaps in the dispersion relation  $\omega(k)$ . That is, the existence of some angular frequency intervals where wave propagation is forbidden.

The phononic and photonic crystals are nano-scale man-made periodic structures. To be specific, we focus here on the particular case where the non-homogeneity is restricted to an abrupt transition between two materials. In particular, the case where one of the materials takes over the structure and becomes the host material providing mechanical support while the other material fills in the voids drilled into the host.

Similarly to the case of electronic wavefunctions in natural solid crystals, the dispersion relation curves of photonic and phononic crystals, respectively  $\omega(k)$  and  $\Omega(k)$ , present periodic band structures in the wave-vector domain which contains bandgaps i.e. frequency intervals where optical/elastic waves propagation is forbidden. The dispersion relation is



controlled by the photonic/phononic crystal geometry and its constitutive materials that is: the type of lattice, the basis vectors, the shape and the dimension of the inclusion, and obviously the host material itself by means of the parameters they involve. For conciseness, we restrict the presentation to the 1-D case. The extension to other dimensionalities is straightforward [78].

## 2.9.1 Bloch Propagating Modes

Using the Bloch-Floquet theorem given in equation (3), we can find the structure of a Bloch wave, i.e. the general shape of the propagating waves in periodic media. If we divide both sides of equation (3) by  $e^{i\vec{k}\cdot(\vec{r}+\vec{R})}$ , we get for the one-dimension case  $\vec{R} \rightarrow a \equiv$  the 1-D lattice constant and  $\vec{k} \rightarrow k_x \equiv k$  the 1-D scalar wavevector:

$$\frac{\varphi(x+a)}{e^{ik\cdot(x+a)}} = \frac{\varphi(x)}{e^{ik\cdot x}} \quad \dots (9)$$

Now, we define a new function  $\mu(x) = \varphi(x)/e^{ik\cdot x}$ . Equation (9) tells us that:  $\mu(x+a) = \mu(x)$  i.e. the function  $\mu(x)$  is necessarily periodic at the lattice period ( $a$ ). Finally, we can write:

$$\varphi(x) = e^{ik\cdot x} \mu(x) \quad \dots (10)$$

The structure of a Bloch wave is thus a travelling wave  $e^{i\vec{k}\cdot\vec{r}}$  modulated by a function exhibiting the periodicity of the lattice  $\mu(\vec{r})$ . Equation (10) is another expression of the Bloch-Floquet theorem.

## 2.9.2 Bloch Wave in the Reciprocal Domain

Again, for the one-dimensional problem of lattice period  $a$ , the periodic part  $\mu(x)$  of the Bloch wave in equation (10) can be expanded in a Fourier series:

$$\mu(x) = \sum_m U_m \cdot e^{j \cdot m \frac{2\pi}{a} x} = \sum_m U_m \cdot e^{j \cdot m b x} \quad \dots (11)$$

Thus equation (10), for a given value of  $k$  writes:

$$\varphi(x) = \sum_m U_m \cdot e^{j \cdot (k + m b) x} \quad \dots (12)$$

Equation (12) shows that, if an arbitrary wavevector  $k$  appears in the summation, then all the wavevectors are equally spaced from  $k$  by reciprocal lattice vectors  $b$  (and only those) will also appear in the summation. Thus, in the reciprocal domain, the coefficient  $U_m$  corresponds the spatial Fourier component  $k + m b$  where,  $m = \text{integer}$ . In order to emphasize this correspondence, we can label the Fourier components  $U_m$  as  $U_{k+m b}$  in equation (12) without the risk of confusion.

Using this new notation, equation (12) for a given wave vector  $k = k' + n \cdot b$  writes:

$$\begin{aligned} \varphi_k(x) &\equiv \sum_m U_{k+m b} \cdot e^{j \cdot (k+m b) x} \xrightarrow[\text{Substituting: } k=k'+n \cdot b]{} \sum_m U_{k'+(m+n)b} \cdot e^{j \cdot (k'+(m+n)b) x} \\ &= \sum_{m'} U_{k'+m' b} \cdot e^{j \cdot (k'+m' b) x} = \varphi_{k'}(x) \quad \dots (13) \end{aligned}$$

### **Equivalence of labelling $\varphi_k$ with wavevectors spaced by reciprocal lattice vectors.**

Since the summation is done on all the integers of  $m' = m + n$ , we notice that the function is another expression of  $\varphi_k(x) \Leftrightarrow \varphi_{k'}(x)$ . This equivalence shows that we can identify indifferently a mode given by any vector of the series:  $k' = k + n \cdot b$ . Thus, writing  $\varphi_{k'}(x)$  is

completely equivalent to writing  $\varphi_k(x)$ . But, as suggested by Brillouin it is preferable to identify the mode by its principal value  $\tilde{k}$  such that:  $-\frac{\pi}{a} < \tilde{k} < \frac{\pi}{a}$  [43].

### 2.9.3 Periodicity of the Dispersion Relation

In periodic media the angular frequency ( $\omega$ ) of an electron and its wave vector ( $k$ ) are related to each other by the dispersion relation  $\omega(k)$  and its graphical representation provides the dispersion curve. In his analysis of wave propagation in periodic media Brillouin (following a different but equivalent approach to the Bloch-Floquet theorem, tackled in the foregoing section) established the periodicity of the dispersion relation  $\omega(k)$  in the wavevector domain. He also suggested to restrict the study of the dispersion relation to the first period nowadays named after him the 1<sup>st</sup> Brillouin zone.

The set of 1-D dispersion curves  $\omega(k)$  are known as the band diagram. It shows the different frequency bands as well as the forbidden ones called “bandgaps” which open at the limit of the Brillouin zones.

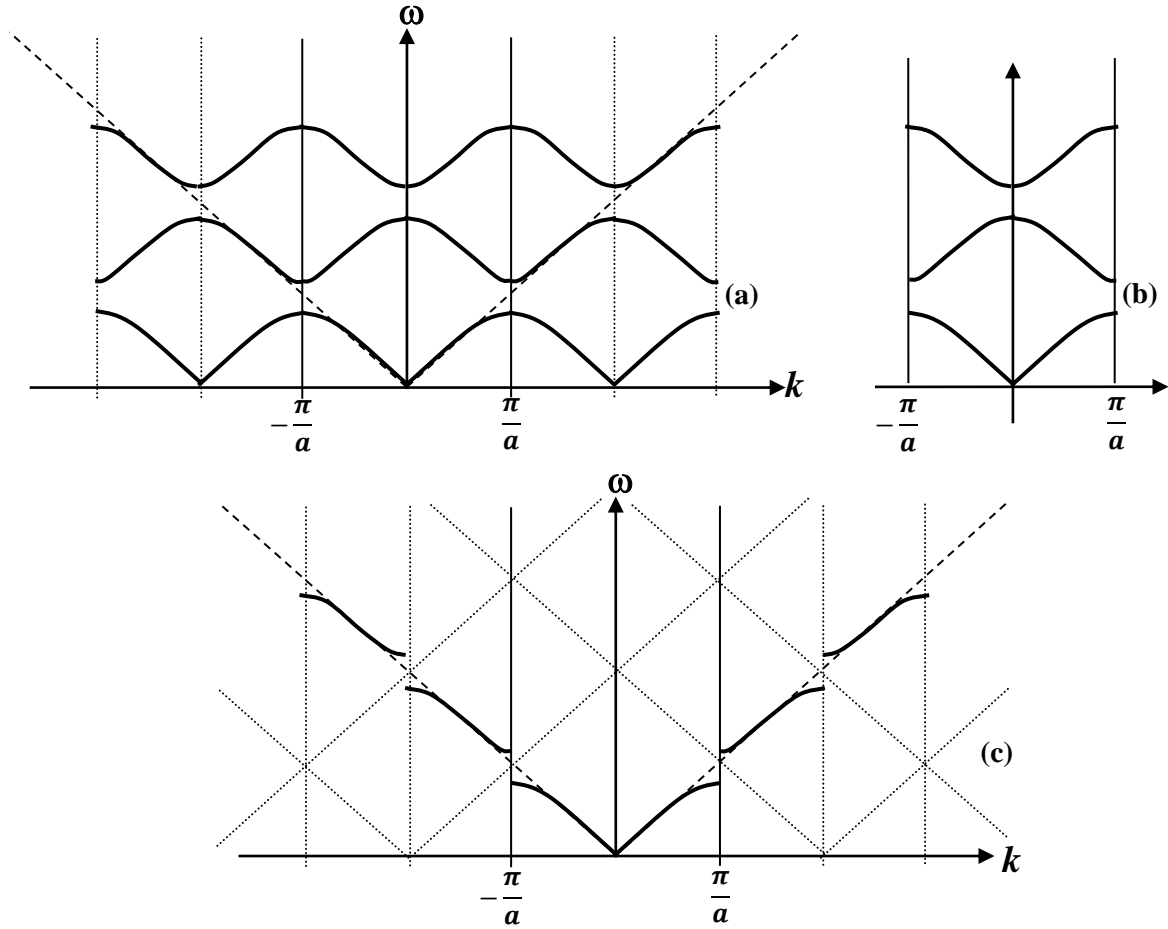


Figure 6: Representation of the band structure. The periodic band scheme representation (a), the reduced band structure scheme to the 1<sup>st</sup> Brillouin zone (b), the extended band scheme (c). The dashed lines represent the dispersion relation ( $\omega = v_\phi k$ ) of a photon propagating in the non-dispersive bulk material of phase velocity  $v_\phi$ .

We present in Figure 6 various representations of the band diagram in the case of 1-D periodic material: (a) the complete periodic band structure centered, as suggested by Brillouin, around  $k = 0$ ; (b) the reduced scheme of the band structure of the 1<sup>st</sup> Brillouin zone, and (c) the extended zone scheme to the successive Brillouin zones. One can simply go from extended zone scheme to the reduced first Brillouin zone scheme or even to the periodic scheme, following translations involving reciprocal lattice vectors. In the extended zone scheme, the first band pertains to the 1<sup>st</sup> Brillouin zone, second band to the 2<sup>nd</sup> Brillouin zone and so on. Each band is separated for the following one by a frequency bandgap. These band gaps are located at the Brillouin zone edges.

The dashed lines correspond to the dispersion relation of a wave propagating in an effective homogeneous medium where the periodic inclusions are omitted, resulting in the non-dispersive bulk wave governed by the dispersion relation:  $\omega = v_\varphi k$ . Where  $v_\varphi$  stands for the phase's velocity of the wave in the bulk medium. The extended zone scheme in Figure 6 (c), clearly illustrates the departure of the dispersion curves from their straight-line aspect in case of homogeneous host material.

## 2.9.4 Bandgap: From a Perturbation Point of View

Also illustrated on the extended zone scheme in Figure 6 (c), are the band folding (dotted lines) introduced by the structure periodicity. This band folding creates a two-fold degeneracy (i.e. two modes share the same frequency) at the Brillouin zone edges  $= \pm n\pi/a$ ; ( $n$  integer). The frequency gaps opening and the departure of the dispersion relation from its straight line behavior near the Brillouin zone limits are direct results of the lifting of the two-fold degeneracy [21]. The perturbation responsible of this degeneracy lifting is the periodic modulation of the material parameter around its mean value. We will return on the perturbation theory in Chapter IV.

## 2.9.5 Bandgap: From a Scattering Point of View

The frequency gaps correspond to the Bragg reflections condition. In other words, if the wave attempts to travel in a given direction, it will be nearly totally reflected in the opposite direction. The Bragg mirror is based on the principle that all the reflected waves from the successive periods fulfill the phase matching condition. That is, they are in phase and so interface constructively with the end result that the reflection coefficient rapidly grows. The counter part of this high reflection is that the transmitted amplitude of the wave gradually

decreases each time the wave undergoes a new reflection on the successive unit-cells along its incident propagation direction. At the matching conditions, the amplitude damping is so important that the penetration depth is usually limited to few periods. The bandgap corresponds to the frequency range where the Bragg condition is satisfied. The resulting damping effect in the incident direction implies complex or imaginary  $k$  values.

## 2.9.6 Band Structures in 2-D Crystals

In 2-D, thanks to symmetry criteria, the calculation domain of dispersion diagrams is limited to the irreducible Brillouin zone. Usually, the  $(\omega, k)$  surface have its extreme values on the direction of high symmetry. Therefore, it is often sufficient to plot the dispersion relation on the edges of the irreducible Brillouin zone.

Figure 7 illustrates the dispersion curves in case of a square lattice photonic crystal plotted along the high symmetry directions ( $\Gamma$ X, $\Gamma$ M, $\Gamma$ M) [79] [80]. In the presented 2-D crystal dispersion diagram, the path starts from the origin  $\Gamma$ , continuing towards of X, then to the direction of M, and finally returns back to the origin  $\Gamma$ . This dispersion diagram shown is obtained for a square 2-D TM (transverse magnetic) Silicon photonic crystal. It shows a bandgap (yellow rectangle) between the normalized angular frequency  $\omega_N \approx 0.46$  and  $\omega_N \approx 0.52$ . Similar band diagram exists for TE polarization.

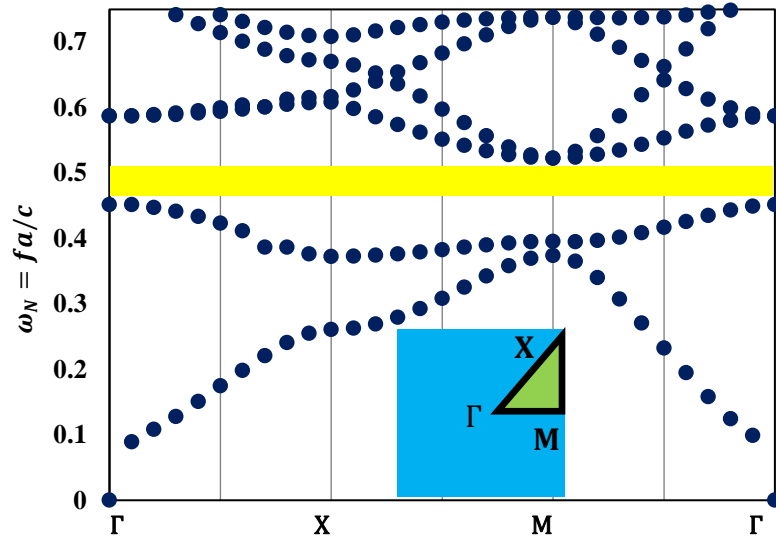


Figure 7: Dispersion diagram of a square 2-D TM (transverse magnetic) photonic crystal consisting of silicon (*Si*) and air hole of radius  $r = 0.48a$  along the high-symmetry axis  $\Gamma X$ ,  $XM$ , and  $\Gamma M$  of the first Brillouin zone. The yellow rectangle represents the bandgap between the normalized angular frequency  $\omega_N \approx 0.46$  and  $\omega_N \approx 0.52$ . The blue square represents the reciprocal lattice while the green triangle represents the irreducible Brillouin zone.

The concept of the band diagram is universal, whatever the nature of the wave considered is. Hence, the band diagram of the same structure as in Figure 7 but for photons can be determined for phonons (as presented in next chapters).

Considering the terminology used in band diagrams, a bandgap where the wave propagation is forbidden whatever the direction of propagation is, are called omnidirectional bandgaps. In the case of vector fields, an omnidirectional bandgap can exist for a given polarization but not for the others. In the case where an omnidirectional bandgap exists for all the polarizations, it's designated as a complete bandgap.

## 2.10 Conclusion

In this chapter we have presented periodic structures, either natural or artificial. We then have introduced the theoretical basis of direct and reciprocal lattices, the general form of Bloch waves in periodic media, the phenomena of bandgap, and diffraction. The case of photonic and phononic crystals have been highlighted.



## Chapter III

# PhoXonic Crystals

### 3.1 Introduction

Scientists have been interested with the photonic and phononic crystals ability to filter, guide, and confine a wave. Recently, researchers have concentrated on the simultaneous photonic and phononic band crystals, advancing with their early work which was done separately on photonic and phononic crystals. The early researches focused on multilayer systems, and acousto-optical coupling based on photo-elastic and opto-mechanical effects [49].

The study in 2-D crystals has then emerged. These crystals have also been the subject of research on acousto-optical interactions. The first work done related to these structures, concerned mainly the existence of simultaneous forbidden bands [60]. The interest of 2-D crystals is to have 2-D band gaps. However, they require a more complicated design and preliminary optimization work. PhoXonic crystals are nanostructures built on a bulk material, in such a way that the non-homogeneity introduced may be considered as a juxtaposition of piecewise homogenous media.

In this chapter, we first recall the properties of electromagnetic and elastic waves propagation in homogenous materials, then in periodic media, and we end-up with insights about opto-mechanical coupling mechanisms.

## 3.2 Wave Propagations in Homogeneous Media

A moving disturbance with energy transported from one place to another without transporting matter is called a wave. In this section, our interest is in the propagation of electromagnetic and mechanical waves in homogeneous media where the parameters don't depend on space coordinates. For determining the structure of a propagating wave while avoiding reflection and refraction; the effect of the interfaces, we take the ideal case of an infinite medium, where we can also ignore the techniques of introducing the wave to the propagation medium. For a lossless medium the wave equation is reduced to a linear differential equation of the second order with constant coefficients both spatially and temporally.

For the simplest case of a scalar wave, the general solution  $f$  is a plane propagating wave in a given direction of unit-vector  $\vec{l}$ , which can be progressive for  $f(t, \vec{r}) = f\left(t - \frac{\vec{r} \cdot \vec{l}}{v_{\phi l}}\right)$ , contra-propagative for  $f(t, \vec{r}) = f\left(t + \frac{\vec{r} \cdot \vec{l}}{v_{\phi l}}\right)$ , or a combination of the two functions. The spatiotemporal variable  $\left(t - \frac{\vec{r} \cdot \vec{l}}{v_{\phi l}}\right)$  for the function  $f$  shows that it propagates without deformation in the direction of the unit-vector  $\vec{l}$  at the phase velocity  $v_{\phi l}$ ; stated as invariant by continuous translations. The scalar product  $\vec{r} \cdot \vec{l}$  shows that all points, belonging to the same plane wavefront normal to unit-vector  $\vec{l}$  are included in the same rectilinear propagation motion; stated that they are in phase and that the wave front is an equiphasic plane. Usually, the problem is treated in harmonic regime: to decompose the functions in terms of their spatiotemporal harmonics:  $F_{\omega, \vec{k}} e^{i(\omega t - \vec{k} \cdot \vec{r})}$  where  $\vec{k} = \left(\frac{\omega}{v_{\phi}}\right) \vec{l}$  and the exponential  $e^{i(\omega t - \vec{k} \cdot \vec{r})}$  is the phase factor.

In the case of crystals, with vector fields  $\vec{V}$ , the problem of propagation is more complex. Crystals are naturally anisotropic so, an action in a given direction doesn't have to give a parallel response to that action: the "action/response" interrelations are expressed using tensor relations. This introduces coupling between the field vector components:  $V_1, V_2$ , and  $V_3$ . The problem turns into a system of coupled partial differential equations. For a given propagation direction, the solution is found by determining the spatiotemporal expressions of the components  $V_i(t, \vec{r})$  for  $i = 1, 2, 3$ . The coupling between the three components implies what can be expressed as solutions in the form of a linear superposition:  $\sum_{j=1} m_j V_j(t, \vec{r})$  where  $m_j$  are constants. In the general case, the translation invariance of the components  $V_i$ :  $V_i(t, \vec{r}) \neq V_i\left(t - \frac{\vec{r} \cdot \vec{l}}{v_{\phi l}}\right)$  cannot be asserted. Traditionally, this difficulty is overcome by using the method of searching the eigenvalues and eigenfunctions of the system. Generally, we reduce the problem of finding functions specific to a system of equations to eigenvalues and eigenvectors. It is well known that, for each propagation direction, a unique orthonormal coordinate system  $(\hat{x}_1, \hat{x}_2, \hat{x}_3)$  in which the three  $\vec{V}$  components propagate independently of each other with a phase velocity  $v_{\phi}$ . In this particular frame the three  $\vec{V}$  components are not coupled. They are expressed in the form of  $V_i(t, \vec{r}) = V_i\left(t - \frac{\vec{r} \cdot \vec{l}}{v_{\phi l}}\right)$ , thus stated as invariant by continuous translation. These solutions are called the eigenfunctions or eigensolutions, and the corresponding speeds  $v_{\phi l}$  are called eigenspeeds. By this we mean specific solutions propagating without deforming. Differently stated, three plane vector waves  $(\hat{x}_1, \hat{x}_2, \hat{x}_3)$  orthogonal to each other can propagate in a given direction  $\vec{l}$ , each with a speed  $v_{\phi l}$  of its own. In general, the directions of polarization are distinct from the direction of propagation  $\vec{l}$  and the orientation of the polarization trihedron is a function of the direction  $\vec{l}$ .

Electromagnetic waves consist of oscillating electromagnetic fields. While mechanical waves are displacement of the material particles from their equilibrium positions, these particles will return to equilibrium positions when the wave is passed.

The propagation of electromagnetic and elastic waves in composite periodic materials [44] [81] [82] [83], have attracted scientists attention, for the dielectric or elastic properties are functions of the position and have a period proportionate to the wavelength.

<b>Electromagnetic Waves</b>	<b>Elastic Waves</b>
<b>Similarities</b>	
Transfers energy	
Don't transfer matter	
<b>Differences</b>	
Can travel with or without a medium	Needs a medium
Fastest in space	Fastest in solids
Can travel in vacuum	Can't travel in vacuum
Radiant energy	Mechanical Energy
Always transverse waves (Travelling perpendicular to wave motion)	Transverse or longitudinal waves (Travelling perpendicular or parallel to wave motion)

Table 3: Electromagnetic and elastic waves similarities and differences.

### 3.2.1 Electromagnetic Wave in Homogeneous Dielectric

In a macroscopic treatment, the electromagnetic (E.M.) wave equation is easily derived starting from Maxwell's equations [84]. In the international unit-system (S.I.) Maxwell's equations write in a set of coupled partial differential equations together with constitutive relations:

$$\left. \begin{aligned} \nabla \cdot B &= 0 \\ \nabla \cdot D &= \rho \\ \nabla \times E + \frac{\partial B}{\partial t} &= 0 \\ \nabla \times H - \frac{\partial D}{\partial t} &= J \end{aligned} \right\} \dots (14)$$

Maxwell's equations

$$\left. \begin{aligned} D(\mathbf{r}) &= \epsilon_0 \epsilon_r(\mathbf{r}) E(\mathbf{r}) \\ B(\mathbf{r}) &= \mu_0 \mu_r(\mathbf{r}) H(\mathbf{r}) \end{aligned} \right\} \dots (15)$$

Constitutive relations

Where, the operators  $\nabla \times ( )$  and  $\nabla \cdot ( )$  stand respectively for the rotational and divergence operators and E and H are the macroscopic electric and magnetic fields in the propagation medium and measured respectively in units of Volt and Ampere by meter (V/m and A/m), while D is the electric field displacement in Coulomb/m<sup>2</sup> (C/m<sup>2</sup>) and B is the magnetic induction field in Tesla (T). The E.M. sources in the equations are the free current density J in A/ m<sup>2</sup> and the free electric charge density  $\rho$  in Coulomb/m<sup>3</sup> (C/m<sup>3</sup>).  $\epsilon_0$  and  $\epsilon_r(\mathbf{r})$  stand for the free-space and relative dielectric permittivities, in Farad by meter (F/m). In case of homogeneous media, the relative permittivity is not a function of coordinates:  $\epsilon_r(\mathbf{r}) = \epsilon_r$ , but may be a tensor in case of an anisotropic media. For shortness in what follows, unless otherwise specified, we will omit the index  $r$  and denote respectively the relative and absolute permittivity as  $\epsilon(\mathbf{r})$  and  $\epsilon_0 \epsilon(\mathbf{r})$ . In nondispersive dielectrics  $\epsilon$  is not a function of frequency. For nonmagnetic material considered here, the relative magnetic permeability  $\mu_r(\mathbf{r})$  is equal to unity so, the absolute permeability  $\mu = \mu_0 \mu_r(\mathbf{r})$  reduces to the free space permeability:  $\mu = \mu_0$  in T·m/A.

In case of a medium free of charges and current densities, substituting equations (15) in (14) we get:

$$\left. \begin{aligned} \nabla \cdot \mathbf{H}(\mathbf{r}, t) &= 0 \\ \nabla \cdot [\varepsilon(\mathbf{r})\mathbf{E}(\mathbf{r}, t)] &= 0 \\ \nabla \times \mathbf{E}(\mathbf{r}, t) + \mu_0 \frac{\partial \mathbf{H}(\mathbf{r}, t)}{\partial t} &= 0 \\ \nabla \times \mathbf{H}(\mathbf{r}, t) - \varepsilon_0 \varepsilon(\mathbf{r}) \frac{\partial \mathbf{E}(\mathbf{r}, t)}{\partial t} &= 0 \end{aligned} \right\} \quad \dots (16)$$

Both E and H are time and space dependent functions. Since Maxwell equations are linear, we can separate time and space dependence expanding the fields in a set of harmonic modes.

Thus, for one harmonic mode of angular frequency  $\omega$  the fields can be written as:

$$\left. \begin{aligned} \mathbf{H}(\mathbf{r}, t) &= \mathbf{H}(\mathbf{r})e^{i\omega t} \\ \mathbf{E}(\mathbf{r}, t) &= \mathbf{E}(\mathbf{r})e^{i\omega t} \end{aligned} \right\} \quad \dots (17)$$

Substituting equation (17) in equations (16) the curl equations of E(r) and H(r) become:

$$\left. \begin{aligned} \nabla \times \mathbf{E}(\mathbf{r}) + i\omega\mu_0\mathbf{H}(\mathbf{r}) &= 0 \\ \nabla \times \mathbf{H}(\mathbf{r}) - i\omega\varepsilon_0\varepsilon(\mathbf{r})\mathbf{E}(\mathbf{r}) &= 0 \end{aligned} \right\} \quad \dots (18)$$

Dividing the second equation of (18) by  $\varepsilon(\mathbf{r})$  and applying the curl operation on its right- and left-hand sides straightforwardly gives us:

$$\nabla \times \left( \frac{1}{\varepsilon(\mathbf{r})} \nabla \times \mathbf{H}(\mathbf{r}) \right) = \omega^2 \varepsilon_0 \mu_0 \mathbf{H}(\mathbf{r}) \quad \dots (19)$$

Where we have used the expression  $\nabla \times \mathbf{E}(\mathbf{r})$  from the 1<sup>st</sup> equation of (18).

Equation (19) is the master equation of electromagnetic wave propagation through a dielectric medium. It is also called the H-formulation of the wave equation as it must be satisfied by the magnetic field of any propagating electromagnetic wave. This formulation is not unique; an equivalent master equation can be derived following the same procedure but this time eliminating the H vector in the system of equations (18), leading to the so-called E-formulation:

$$\nabla \times \nabla \times \mathbf{E}(\mathbf{r}) = \omega^2 \mu_0 \epsilon_0 \epsilon(\mathbf{r}) \mathbf{E}(\mathbf{r}) \quad \dots (20)$$

In the above derivation of the master equation, we have not yet imposed restrictions concerning neither the homogeneity nor the isotropy of the dielectric material. So, equations (19) and (20) are quite general: in case of inhomogeneous media,  $\epsilon(\mathbf{r})$  is a function of the coordinates and in case of an anisotropic material,  $\epsilon(\mathbf{r})$  will be a second rank tensor.

### *Case of homogeneous isotropic dielectric.*

Equation (19) further simplifies in case of homogeneous media. The permittivity is a scalar constant i.e.  $\epsilon(\mathbf{r}) = \epsilon_r$ . Using the differential operator identity,  $\nabla \times (\nabla \times ( \ )) = \nabla(\nabla \cdot ( \ )) - \nabla^2( \ ))$ , it reduces to the Helmholtz equation  $\nabla^2 \mathbf{H}(\mathbf{r}) + \omega^2 \mu_0 \epsilon_0 \epsilon_r \mathbf{H}(\mathbf{r}) = 0$ .

Beside the collinearity of electric displacement  $\vec{D}$  and the electric field  $\vec{E}$ , the electromagnetic field propagating in a homogeneous isotropic medium is said to be Transverse Electro-Magnetic (TEM). Its structural aspect is illustrated in Figure 8. The Poynting vector  $\vec{S} = \vec{E} \times \vec{H}$  is colinear with the wavevector  $\vec{k}$  as shown on the figure.

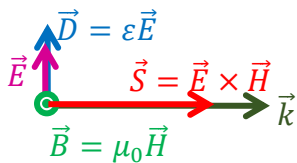


Figure 8: Structure of the electromagnetic wave in a homogeneous isotropic medium (Transverse Electro-Magnetic).

Both the electric and magnetic field vectors are orthogonal to each other and propagate with a phase velocity  $v_\phi$  independent of the frequency, in the direction perpendicular to the plane containing  $E, D$  and  $B, H$  (in the wavevector direction). Thus, these four vectors lie in the wavefront equiphase plane. The plane containing  $E, D$  and  $k$  is referred to the plane of polarization ( $B$  and  $H$  are normal to the polarization plane). The description of wave structure

appears easily if we place ourselves in the context of harmonic plane waves expansion with the spatiotemporal dependence:

$$\vec{E}_0 e^{j(\omega \cdot t - \vec{k} \cdot \vec{r})} \quad ; \quad \vec{H}_0 e^{j(\omega \cdot t - \vec{k} \cdot \vec{r})} \quad \dots (21)$$

Which are the monochromatic propagation modes at an angular frequency  $\omega$  and a wavevector  $\vec{k}$  (the 3-D angular spatial-frequency) pointing towards the propagation direction.

First, substituting of (21) in Maxwell's equations gives us:

$$\left. \begin{aligned} \vec{k} \cdot \vec{H}_0(\vec{k}, \omega) &= 0 \\ \vec{k} \cdot [\epsilon_r \vec{E}_0(\vec{k}, \omega)] &= 0 \\ -i\vec{k} \times \vec{E}_0(\vec{k}, \omega) + i\omega\mu_0 \vec{H}_0(\vec{k}, \omega) &= 0 \\ -i\vec{k} \times \vec{H}_0(\vec{k}, \omega) - i\omega\epsilon_0 \epsilon_r \vec{E}_0(\vec{k}, \omega) &= 0 \end{aligned} \right\} \dots (22)$$

The zero dot products in the first two equations express the transverse nature of both magnetic and electric fields ( $\epsilon_r$  is a scalar) i.e.  $\vec{E}$  and  $\vec{H}$  are perpendicular to the wavevector  $\vec{k}$ . The cross products in last two equations express the mutual orthogonality of  $\vec{E}$  and  $\vec{H}$ . Ultimately, the vectors  $(\vec{E}, \vec{H}, \vec{k})$  form a direct trihedron.

Second, substituting in the Helmholtz equation gives the well-known homogeneous isotropic media dispersion relation  $v_\varphi \equiv \omega/k = 1/\sqrt{\mu_0 \epsilon_0 \epsilon_r} = c/\sqrt{\epsilon_r}$ , where  $c = 1/\sqrt{\mu_0 \epsilon_0}$  is the vacuum speed of the light. The phase velocity can also be written as  $v_\varphi = c/n$ , where we introduce the definition of the refractive index  $n = \sqrt{\epsilon_r \mu_r}$ , with the assumption that the medium is a nonmagnetic material  $n = \sqrt{\epsilon(\mathbf{r})}$  since  $\mu_r \approx 1$ . Finally, under the assumption that in purely dielectric media, the refractive index does not depend on the frequency (condition usually verified far from any resonant peak absorption), the homogeneous isotropic material is dispersionless: the phase velocity is not frequency dependent.



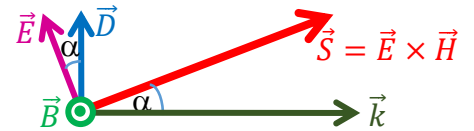
### *Case of homogeneous anisotropic dielectric.*

Usually in crystalline materials, the permittivity is now a second-rank tensor:

$$\begin{pmatrix} D_1 \\ D_2 \\ D_3 \end{pmatrix} = \begin{pmatrix} \epsilon_{11} & \epsilon_{12} & \epsilon_{13} \\ \epsilon_{21} & \epsilon_{22} & \epsilon_{23} \\ \epsilon_{31} & \epsilon_{32} & \epsilon_{33} \end{pmatrix} \begin{pmatrix} E_1 \\ E_2 \\ E_3 \end{pmatrix} \quad \dots (23)$$

The electric field is no longer transverse: it can have a longitudinal component. The structural aspect is modified as illustrated in Figure 9.

Figure 9: Structure of the electromagnetic wave in a homogeneous anisotropic medium (Electric field has a longitudinal component).



The electric displacement  $\vec{D}$  and magnetic field  $\vec{H}$  vectors are still orthogonal to each other and propagate in the direction of  $\vec{k}$  i.e. perpendicular to the plane containing  $\vec{D}$ ,  $\vec{B}$  and  $\vec{H}$ . But the electric field  $\vec{E}$ , though still lies in the polarization plane ( $\vec{E}$ ,  $\vec{D}$ ,  $\vec{k}$ ) may have a longitudinal component parallel to the wavevector  $\vec{k}$ . The Poynting vector also defined by the cross-product  $\vec{E} \times \vec{H}$ , as shown in Figure 9, deviates from the wave vector  $\vec{k}$  by the same angle separating the vectors  $\vec{E}$ , and  $\vec{D}$  and remains in the polarization plane.

The most remarkable effect, for anisotropic materials, is that the translation invariance is only verified for two specific orientations of the polarization planes each of them have its own phase velocity. This effect is known as the birefringence or birefraction phenomenon referring to the two distinct phase velocities  $v_{\phi i} = c/n_i; i = 1,2$  described by two different refractive indices. The orientation of these polarization planes and their corresponding velocities depend on the wave propagation direction and on the material symmetries as well.

One exception for the birefringent phenomenon is for the materials pertaining to cubic lattice system, like Silicon. They have no privileged polarization planes and so, can be chosen arbitrarily: all the polarization directions propagate with the same phase velocity whatever the propagation direction is. For this reason, they are said to be optically isotropic [85].

The other six crystalline systems are catalogued in two classes owing to their optical birefringent properties: the crystals belonging to the trigonal, tetragonal and hexagonal systems possess a unique propagation direction for which the optical wave exhibit an isotropic behavior. For this reason, these systems are known as uniaxial crystals. All other propagation directions have birefringent behaviors. Finally, the triclinic, monoclinic or orthorhombic systems are biaxial crystals since they own two such propagation directions that exhibit isotropic behaviors.

Again, if we place ourselves in the context of harmonic plane waves expansion but this time substituting in the E formulation (20) of the wave equation gives us:

$$\vec{k} \times \vec{k} \times \vec{E}_0 = -\frac{\omega^2}{c^2} [\epsilon_r] \vec{E}_0 \quad \dots (24)$$

Where,  $[\epsilon_r]$  stands for the tensor notation of permittivity. It is more convenient to use the electric displacement vector  $\vec{D}(\vec{r}, t) = \vec{D}_0 e^{-j(\omega t - \vec{k} \cdot \vec{r})}$  rather than the electric field  $\vec{E}(\vec{r}, t)$  hence using the double vector product identity:  $X \times (Y \times Z) = (Z \cdot X)Y - (X \cdot Y)Z$  the equation (24) is written as:

$$(\vec{k} \cdot \vec{k})[\eta_r] \vec{D}_0 - ([\eta_r] \vec{D}_0 \cdot \vec{k}) \vec{k} = \frac{\omega^2}{c^2} \vec{D}_0 \quad \dots (25)$$

Where the impermittivity tensor  $[\eta]$  is the inverse of the relative permittivity  $[\eta] = [\epsilon_r]^{-1}$ . When expressing the wavevector  $\vec{k} = \frac{\omega}{c} n_l \vec{l}$  where  $n_l = \frac{c}{v_{\phi l}}$  is the refractive index we are

seeking for, i.e. the one corresponding to the chosen propagation direction pointed by the unit-vector  $\vec{l}$ , we get:

$$[\eta_r]\vec{D}_0 - ([\eta_r]\vec{D}_0 \cdot \vec{l})\vec{l} = -\frac{1}{n_l^2}\vec{D}_0 \quad \dots (26)$$

Taking advantage of the transverse nature of the vector  $\vec{D}_0$  (with respect to  $\vec{l}$ ), we choose the system of axes (with the adequate tensor elements) such that one of its basis vectors, say  $x_3 \equiv z$ , to coincide with  $\vec{l}$ . Hence the equation (26) reduces to a two-dimension vector “eigenequation” in the  $(x_1, x_2)$  plane  $x_1 \equiv x$  and  $x_2 \equiv y$  of the new system frame and writes:

$$\begin{pmatrix} \eta_{11} & \eta_{12} \\ \eta_{21} & \eta_{22} \end{pmatrix} \begin{pmatrix} D_1 \\ D_2 \end{pmatrix} = \frac{1}{n_l^2} \begin{pmatrix} D_1 \\ D_2 \end{pmatrix} \quad \dots (27)$$

Where,  $D_1$  and  $D_2$  are the components of  $\vec{D}_0$  in the  $(x_1, x_2)$  plane. The eigensolutions of equation (27) gives two eigenvalues for the seeking eigen-refractive indices  $n_l^2$  sought for the considered propagation direction  $\vec{l}$ , and the two corresponding eigendirections of the electric displacement. Since the impermeittivity tensors are real and symmetrical, the eigenvalues  $\frac{1}{n_l^2}$  are real and positive and the eigendirections of the electric displacement are orthogonal [86]. In this case, the two eigendirections of the electric displacement together with the propagation direction  $\vec{l}$  form an orthogonal trihedron.

Finally, as in the case of isotropic media, there are only two eigenmodes of optical polarization and the eigenvectors  $\vec{D}$  are always in the plane normal to the wave vector. But, this time, each of the two modes has its own velocity and an imposed direction for the displacement electric field. In contrast with the case of isotropic materials where the waves are degenerated, i.e. they have the same velocity and their polarizations are arbitrary in the plane normal to the wave vector. Furthermore, the electric field may have a longitudinal component.

### 3.2.2 Acoustic Wave in Homogeneous Media

An elastic wave is a mechanical disturbance propagating through materials, causing the constituting particles to oscillate about their equilibrium positions [87] [88]. They are described by the displacement field:  $\vec{u}(\vec{r}, t)$ . The displacements are considered to be small enough so that the elastic phenomenon can be treated by a linear approach. The strain is a measure of the relative change of the displacement field: it is related to the deformation or change in shape of the material rather than the change in position. The local deformations arise from the spatial variation of the displacements; hence the strain is dimensionless and is usually expressed as:

$$S_{ij}(r, t) = \frac{1}{2} \left( \frac{\partial u_i}{\partial x_j} + \frac{\partial u_j}{\partial x_i} \right) \quad \dots (28)$$

Thus, the strain tensor may be represented by a unit-less  $3 \times 3$  matrix written as:

$$S = \begin{bmatrix} \frac{\partial u_1}{\partial x_1} & \frac{1}{2} \left( \frac{\partial u_1}{\partial x_2} + \frac{\partial u_2}{\partial x_1} \right) & \frac{1}{2} \left( \frac{\partial u_1}{\partial x_3} + \frac{\partial u_3}{\partial x_1} \right) \\ \frac{1}{2} \left( \frac{\partial u_1}{\partial x_2} + \frac{\partial u_2}{\partial x_1} \right) & \frac{\partial u_2}{\partial x_2} & \frac{1}{2} \left( \frac{\partial u_2}{\partial x_3} + \frac{\partial u_3}{\partial x_2} \right) \\ \frac{1}{2} \left( \frac{\partial u_1}{\partial x_3} + \frac{\partial u_3}{\partial x_1} \right) & \frac{1}{2} \left( \frac{\partial u_2}{\partial x_3} + \frac{\partial u_3}{\partial x_2} \right) & \frac{\partial u_3}{\partial x_3} \end{bmatrix} \quad \dots (29)$$

Due to the definition of equation (28) the strain tensor  $S$  is symmetric, then it will have only six independent elements, where the normal strains are in the diagonal components and the shear strains are in the off-diagonal components.

After an external force is applied and removed, an elastic material returns to its equilibrium position thanks to internal forces. These forces are referred to as strain, which are also expressed by a second rank tensor:  $T_{ij}$ . In elastic media theory, stress and strain are linked by the Hook's law, a constructive relationship that writes:

$$T_{ij} = C_{ijkl} S_{kl} \quad \dots (30)$$

Where  $C_{ijkl}$  are the components of the elasticity (or stiffness) tensor, which is a fourth rank tensor. The strain tensor is symmetric, the stress tensor is also symmetric due to the absence of external torques, and accordingly the stiffness tensor will be symmetric.

Hence the stiffness tensor can be written with different components to satisfy the relation:

$$C_{ijkl} = C_{jikl} = C_{ijlk} = C_{jilk} \quad \dots (31)$$

The Voigt notation can be used instead of the double indices' notation, where:

$$\begin{bmatrix} xx \\ yy \\ zz \\ yz, zy \\ xz, zx \\ xy, yx \end{bmatrix} \rightarrow \begin{bmatrix} 1 \\ 2 \\ 3 \\ 4 \\ 5 \\ 6 \end{bmatrix} \quad \dots (32)$$

Thus, a six elements column can replace a  $3 \times 3$  matrix, the strain tensor (the same convention is applied for stress tensor) becomes:

$$S \rightarrow \begin{bmatrix} S_1 \\ S_2 \\ S_3 \\ S_4 \\ S_5 \\ S_6 \end{bmatrix} \quad \dots (33)$$

Consequently, we can index the stiffness tensor elements by two numbers instead of four letters, and thus the stiffness tensor matrix is read as  $6 \times 6$  matrix.

Waves in elastic, homogeneous, isotropic, and anisotropic mediums have their fundamental dynamical equation of motion written as:

$$\rho \frac{\partial^2 u_i}{\partial t^2} = \frac{\partial T_{ij}}{\partial x_j} \quad \dots (34)$$

Introducing Hook's law, equation (34) can be written as:

$$\rho \frac{\partial^2 u_i}{\partial t^2} = C_{ijkl} \frac{\partial^2 u_l}{\partial x_j \partial x_k} \quad \dots (35)$$

Within the materials' medium, any particle displacement follows the wave equation as expressed by (35). Hence, for a given material of known stiffness tensor and mass density, we can obtain the elastic wave solutions by solving equation (35) with specific boundary conditions.

In an unlimited bulk material considering the simplest elastic wave solution, the plane-wave solution, propagating with an elastic wave velocity  $v_{\phi l}$  along the direction of the unit-vector  $\vec{l}$ , may be written as:

$$u_i = u_{0_i} F \left( t - \frac{\vec{l} \cdot \vec{x}}{v_{\phi l}} \right) \quad \dots (36)$$

Where  $u_i$  and  $u_{0_i}$  stand respectively for the displacement component  $i$  and its amplitude.

Substituting in the wave equation leads to the Christoffel equation [5]:

$$\begin{pmatrix} \Gamma_{11} & \Gamma_{12} & \Gamma_{13} \\ \Gamma_{21} & \Gamma_{22} & \Gamma_{23} \\ \Gamma_{31} & \Gamma_{32} & \Gamma_{33} \end{pmatrix} \begin{pmatrix} u_{0_1} \\ u_{0_2} \\ u_{0_3} \end{pmatrix} = \rho v_{\phi l}^2 \begin{pmatrix} u_{0_1} \\ u_{0_2} \\ u_{0_3} \end{pmatrix} \quad \dots (37)$$

$$\text{Or in tensor notation } \Gamma_{il} u_{0_l} = \rho v_{\phi l}^2 u_{0_i} \text{ where } \Gamma_{il} = C_{ijkl} n_j n_k \quad \dots (38)$$

In other words, we are in the presence of an eigenproblem: the eigenvalues  $\rho v_{\phi l}^2$  give the three possible mode velocities and the eigenvectors give three possible mode polarizations.

This system of equations will have solutions if and only if the proceeding characteristic equation is satisfied:

$$\begin{vmatrix} \Gamma_{11} - \rho v_{\phi l}^2 & \Gamma_{12} & \Gamma_{13} \\ \Gamma_{21} & \Gamma_{22} - \rho v_{\phi l}^2 & \Gamma_{23} \\ \Gamma_{31} & \Gamma_{32} & \Gamma_{33} - \rho v_{\phi l}^2 \end{vmatrix} = 0 \quad \dots (39)$$

Equation (57) is an equation of the third degree, where its three solutions provide the three phase velocities  $v_{\phi l}$  as function of the propagation direction  $\vec{l}$ . The polarization directions are defined by the eigenvectors corresponding to these speeds. Based on symmetry properties of the stiffness tensor,  $\Gamma_{il}$  is symmetric, the eigenvalues of the Christoffel equation  $\rho v_{\phi l}^2$  are consequently real and its eigenvectors are orthogonal [86]. Three plane waves can generally propagate in the same direction; they are classified into a so-called quasi-longitudinal wave whose polarization is the closest to the wave vector and two quasi-transverse waves. Quasi-longitudinal waves are usually faster than transverse waves. According to their respective speeds, the two quasi-transverse waves are called slow or fast. In the case of isotropic materials, it is shown that the Christoffel equation decouples the three polarizations. The directions of polarization  $u_{0l}$  will be related to the direction of propagation  $\vec{l}$ . We find a longitudinal wave and two transverse waves that is to say polarizations respectively parallel and normal to  $\vec{l}$  [86]. The transverse waves are degenerated; they have the same speed and their polarizations are arbitrary; and their velocity is less than that of the longitudinal wave.

### 3.3 Wave Propagations in Periodic Media

Whatever the nature of the propagating waves, they are governed by a second order coupled partial differential equation with periodic coefficients. These periodic coefficients stand for the material parameters characterizing the crystal under consideration; for example, electric permittivity for photonic crystals as it is the case in equations (19 or 20), mass density, and stiffness coefficient for phononic crystals as expressed in equation (35). As mentioned in

Section 3.2.1 these equations held for inhomogeneous media provided that the spatial period of the varying parameters is large compared to the interatomic scale of the constituent materials.

It is convenient to express these equations in the form of an eigenproblem of Hermitian operators for the spatial part  $U(r)$  of time harmonic solutions of the form  $U(r)e^{i\omega t}$ . This is fortunately the case of both the H and E formulations of electromagnetic wave equation (19, 20) and for the acoustic wave equation (35). The Hermitian nature of the operator ensures real and positive eigenvalues and orthogonal non-degenerated eigenfunctions; i.e., pertaining to different eigenvalues. These properties are very helpful as it will be illustrated in Chapter IV. For now, let us introduce the main difference with the case of homogeneous media.

### 3.3.1 Eigenproblems and Generalized Eigenproblems

The master equation of the H-formulation of the electromagnetic wave equation (20) is on the form of an Eigenproblem. Its left-hand side tells us that the action of the operator  $\nabla \times \left( \frac{1}{\varepsilon(r)} \nabla \times ( \ ) \right)$  on the wavefunction  $H(r)$  we are seeking for, restitutes in the right-hand side the wave function itself multiplied by a characteristic constant representative of the solution. The eigenvalue is a constant, in this example  $\left(\frac{\omega}{c}\right)^2$  for a given wavevector  $\vec{k}$ , verifying the wave equation and the corresponding solution is called the eigenfunction or the eigensolution. The term eigen means “appropriate” in the sense it is the natural function pertaining to the operator, since its overall shape is conserved. This operator  $\nabla \times \frac{1}{\varepsilon(r)} \nabla \times ( \ )$  is proved to be a Hermitian operator [89]. So, the eigenvalues  $\left(\frac{\omega}{c}\right)^2$  are real and positive, and the eigenfunctions corresponding to different eigenvalues are orthogonal.



Considering the E-formulation, in the case of inhomogeneous media, the operator  $\nabla \times \nabla \times ( \ )$  does not reconstitute the electric field multiplied by a constant but by a function of the coordinates. Indeed, the right-hand side is proportional to  $\epsilon(r)E(r)$  and the permittivity depends on the coordinates. But, the operator  $\nabla \times \nabla \times ( \ )$  and the multiplication by  $\epsilon(r)$  are both Hermitian so, equation (23) is referred to as a “generalized” Hermitian eigenproblem, denoting the existence of Hermitian operators on both sides. As we will see in the next chapter, the E-formulation is well suited for perturbation theory calculations.

### 3.3.2 Solving the Wave Equation

The general solutions are not anymore harmonic plane waves with spatiotemporal dependence as in the homogeneous case. Now, whatever the nature of the propagating wave is: photonic or phononic or the particular distribution of the periodic parameters inside a given period, the general form of the eigensolutions are Bloch functions (Bloch modes). As introduced in Chapter II, it is a direct consequence of the discrete translation symmetry. Taking advantage of the periodicity of the modulation part  $\mu(r)$  of the Bloch mode, one expands them in a Fourier series in the form of equation (12). The fields being vectorial  $\mu(r) \rightarrow \vec{Y}(r)$ , each component owns its Fourier components. Then, substituting the Bloch mode  $\vec{Y}(r)e^{i(\omega t - \vec{k} \cdot \vec{r})}$  in the wave equations, the coupled partial differential equations turns into an eigenproblem system of coupled algebraic equations: the unknown variables being the Fourier components of the solution we seek for. Thus, the eigenvalues provide the angular frequencies as function of the wavevector that is, "the dispersion relation", while the eigenvectors provide the Fourier components of the mode.

### 3.3.3 The Unit-Cell Concept

In case of numerical solution, it is convenient to restrict the calculation domain to save computation time. Thanks to the discrete translation property of Bloch waves, one can solve the wave equation limited to the unit-cell spatial domain subject to the Bloch-Floquet boundary condition:

$$\varphi(\vec{r} + \vec{a}) = \varphi(\vec{r})e^{i\vec{k}\cdot\vec{a}}$$

Where,  $\vec{a}$  is a direct lattice basis vector and  $\vec{k}$  is the selected wavevector for which the solution of the wave equation is looked for. Then the procedure is repeated for different values of the wavevector  $\vec{k}$  to cover the desired path in the reciprocal space: usually the irreducible Brillouin zone.

In fact, the unit-cell concept stands for the entire periodic media of infinite extend, since the associated Bloch-Floquet boundary condition models the periodic repetition of the layout of the unit-cell pattern in all directions.

## 3.4 Specific Features of Wave Propagations in 2-D Periodic Structures

In 2-D structures, the continuous translation in the 3<sup>rd</sup> dimension, say  $z - axis$  is this direction, the solutions don't depend on  $z$ . This translation symmetry may decouple the polarizations. For example, in 2-D photonic crystals, TE and TM Polarizations waves decouple (as described in Appendix A). Consider the case of cylindrical holes whose central axes are parallel to the  $z - direction$ , the six field components (three for the electric and three for the

magnetic fields) split into two uncoupled polarizations sets: one in which has  $H_z$  field component with  $E_x$  and  $E_y$  in the plane and that triplet is the transverse magnetic (TM) polarization. The other polarization is the transverse electric (TE) polarization in which it has  $E_z$  field component with  $H_x$  and  $H_y$  in the plane. The equations of the two polarizations decouple and each polarization propagates independent of the other. The TE and TM polarization band structures are thus distinct and treated separately.

In contrast, due to the more pronounced anisotropic effect of acoustic constants, the  $z$  invariance of the structure does not necessarily decouple the phononic wave's polarizations in 2-D phononic crystals.

Figure 10 presents examples of phoXonic crystal uniform and infinite in the  $z - direction$ . On the left side of Figure 10 we present a square array in the  $(x, y) - plane$  while on the right side we present a triangular array. In both arrays the blue region represents silicon ( $Si$ ) the material used for the host medium, while the white circles represent the voids drilled in the host medium.

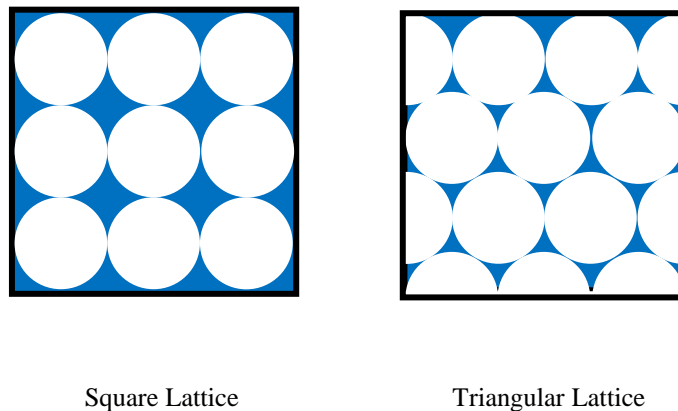


Figure 10: Representation of the photonic crystal Square and Triangular lattices. The blue region represents silicon ( $Si$ ) the material used for the host medium, while the white circles represent the voids drilled in the host medium with radius  $r = 0.48a$  where  $a = 650 \text{ nm}$  and are composed of *air*.

### 3.5 Principle Parameters of 2-D Crystals Design

The first parameter affecting the photonic crystal properties is the chosen Bravais lattice i.e its symmetry properties. The two most studied lattices in 2-D photonic crystals are the square and triangular lattices, but researches also concern honeycomb (or graphene) lattice which belongs to the hexagonal Bravais lattice with two identical (different) inclusions. Once the lattice has been adopted one focuses on the inclusion shape and dimensions to completely define the crystal.

In addition, the filling factor (or packing factor in solid state physics [90]) which is defined as the fraction of the scattering object compared to the total unit-cell volume [91], is a design parameter. In most cases the hole size in a photonic crystal is scaled by  $(r/a)$  ratio and is related to the filling factor. It was found that by increasing the hole radius both the mid-gap position and gap size increases. Also, the refractive step-index ( $\Delta n$ ) is defined as an abrupt transition between the high and low refractive index materials of the periodic structure. The width of the band gap increases as the step-index of the slab increases [92]. The lattice constant i.e. the module of the basis-vector of the lattice determines the order of magnitude of the wavelengths around which the Bragg effect is expected. Finally, the lattice constant and the hole radius (assuming cylindrical drilled holes) are the mostly used parameters to tune the photonic band gaps. A parametric study of the crystal, scanning the design parameters, enables to identify the conditions of emergence of photonic bands within telecom wavelength and phononic bands lying in the ultrasonic range, as showed hereafter.

### 3.5.1 Periodic Structure Parameters of the Studied Structure

We use a commercial *Finite Element Method (FEM)* software in order to determine the band diagram of a perfect crystal: i.e. defect free infinitely extend crystal. The band structures are obtained using the unit-cell technique: solving the wave equation on a unique cell associated to the appropriate Bloch-Floquet boundary conditions. We seek conditions for the existence of simultaneous photonic and phononic bandgaps on a square lattice composed of air holes in silicon (*Si*).

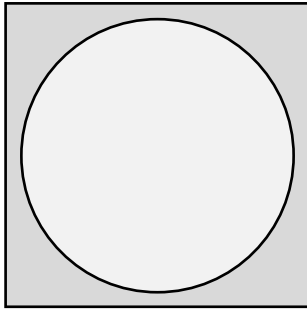
In our calculations, the air hole radius was taken  $r = 0.48a$ , and the lattice parameter has been chosen  $a = 650[nm]$ , which corresponds to filling factor  $f = \frac{\pi r^2}{a^2} = 0.72$ . These values realize a good compromise with wide bandgaps in the optical wavelength telecom range and also in the ultrasonic range.

### 3.5.2 Dispersion Diagrams of the Periodic Structure Considered

In Figure 11, we show the acoustic and optical dispersion diagrams obtained for the square lattice. The calculation of the dispersion diagram was made in the 2-D nanostructured plane. The normalization of the lengths was taken with respect to the constant  $a$  and consequently, the wavevectors and frequency normalizations are with respect to  $2\pi/a$  and  $2\pi c/a$ .

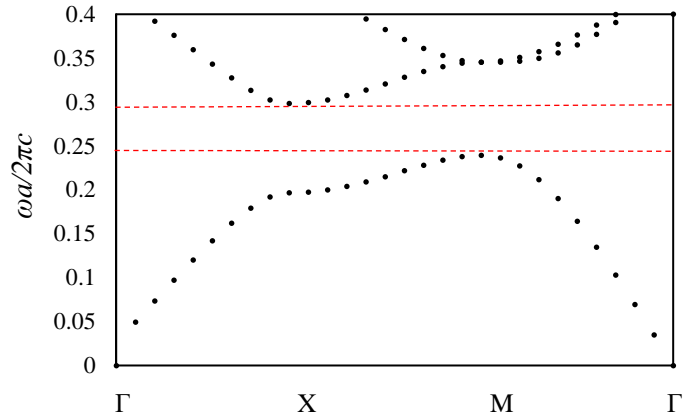
Figure 11 (a) represents the geometry of the unit-cell. The dashed red lines in Figure 11 (b & c) represent the optical bandgap for transverse electric (TE) and transverse magnetic (TM)

polarization respectively. The dotted black lines represent the optical modes band diagram in TE and TM polarization respectively. Similarly, the acoustic modes for phononic crystals are represented in Figure 11 (d), the dashed red lines represent the acoustical bandgap of the structure.



(a)

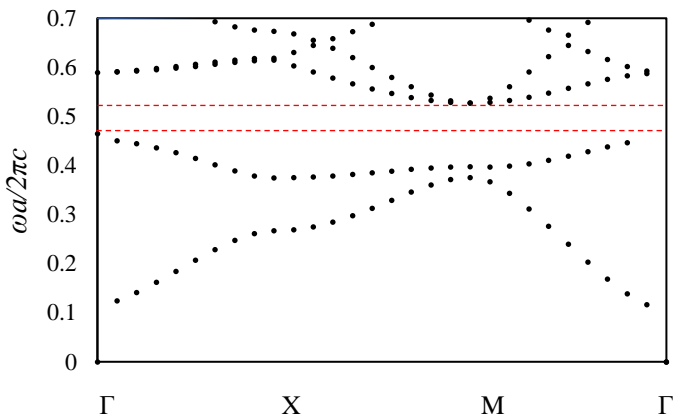
Geometry of Unit-Cell



(b)

TE Dispersion Curve

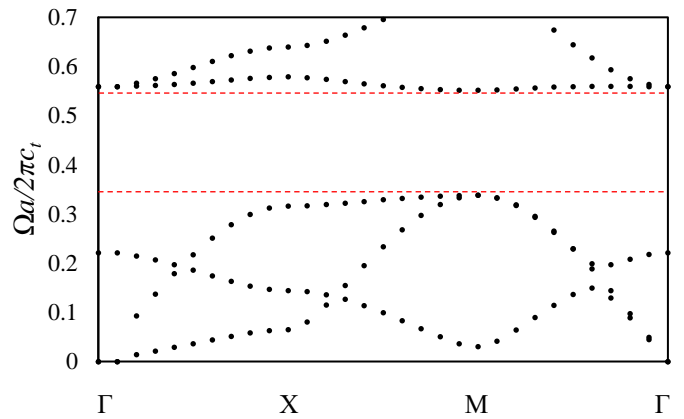
Dispersion diagram of photonic crystal along the high-symmetry axis  $\Gamma X$ ,  $XM$ ,  $M \Gamma$  of the first Brillouin Zone.



(c)

TM Dispersion Curve

Dispersion diagram of photonic crystal along the high-symmetry axis  $\Gamma X$ ,  $XM$ , and  $\Gamma M$  of the first Brillouin zone.



(d)

Phononic Dispersion Curve

Dispersion diagram of phononic crystal along the high-symmetry axis  $\Gamma X$ ,  $XM$ , and  $\Gamma M$  of the first Brillouin zone.

Figure 11: Representation of the Geometry, TE, TM, and Phononic Unit-Cell Dispersion Curve

Dispersion diagram of photonic and phononic crystals along the high-symmetry axis  $\Gamma X$ ,  $XM$ ,  $M \Gamma$  of the first Brillouin zone.

### 3.6 Photonic Crystals Cavities

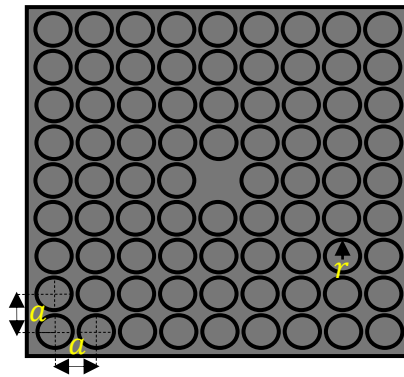


Figure 12: Sketch of a square 2-D photonic crystal  $L_1$  Nano-cavity.

The medium's reflectivity of the periodic media is used to confine the wave in a cavity. The cavity is formed by localized suppression of the periodicity (ex. modifying geometric parameters locally or omitting one or more inclusions). And this explains the term defect of the crystalline structure used to denote a cavity in photonic crystals, having for historical origin the introduction of defects in solid state crystals such as semiconductors. The periodic media reflectivity is effective only for the frequencies inside the bandgap. We seek to use a material with wide bandgap and design a cavity whose resonance frequency is located in the bandgap.

The discretization of the spectrum is explained by the fact that the confinement of the wave in a small space results in a standing wave characterized by a well-defined frequency. This can be easily admitted as a generalization of the 1-D Fabry-Perot resonator using an ideal mirror where a resonance mode can exist only if the half-wavelength in the cavity is a divider of its length. Otherwise, the interference will be destructive after a few back and forth in the cavity. These resonance peaks are repeated periodically in the frequency domain  $\omega_m = m \left( \frac{\pi c}{X_0} \right)$  where  $X_0$  is the cavity's optical length,  $c$  is the speed of light in vacuum and  $m$  an integer. In the case of dielectric mirrors only a few of these resonance frequencies will remain; those which correspond to the bandgap where the multilayers play the role of a mirror.



It is the idea of applying this principle to laser cavities that led Yablonovitch [19] to suggest the use of photonic crystals in order to favor a single mode of laser emission to the detriment of others. Thanks to the nanotechnology advancements, it is theoretically possible to design a three-dimensional artificial crystal so that the range of omnidirectional bandgap size only admits a single mode of resonance. The widening of the resonance peaks reflects the fact that the confinement is not perfect: the reflectivity of the dielectric mirrors does not reach 100%; there is leakage of energy to the outside. The study of resonance modes in cavities is largely based on the analogy with the damped harmonic oscillator. The notion of quality factor is recurrent during the characterization of the oscillators.

### 3.6.1 Cavity Confinement and Quality Factor

Confining light in a volume having a fraction of wavelength volume isn't easy and is subject to leakages due to insufficient confinement efficiency.

The quality factor ( $Q$ ) concept has been introduced in the study of damped harmonic oscillators, whatever their nature is (mechanical, electrical, electromagnetic cavities, etc.) and it is generally defined according to the relation [93]:

$$Q = \omega_0 \frac{U(t)}{\frac{dU(t)}{dt}} \quad \dots (40)$$

Where  $\omega_0$  represents the resonant angular frequency of this oscillator in the case of critical damping and stored energy  $U(t)$ . In the case of an ideal oscillator where no damping occurs, the energy is not dissipated:  $\frac{dU(t)}{dt} = 0$ ; the quality coefficient tends to infinity. The quality coefficient is the measure of an ideal oscillator which has conserved its stored energy.

The inverse of the quotient in equation (40) corresponds to the energy damping and known as the attenuation constant  $\alpha = |d[\ln(U(t)) / dt]|$ . So, another form of the quality factor is given by:

$$Q = \frac{\omega_0}{\alpha} \quad \dots (41)$$

The oscillator study in Fourier domain (frequency domain) shows that the spectrum of the dissipated power  $\frac{dU(t)}{dt}$  presents a narrower peak of resolution as the quality factor is high. The ratio between the mid height  $\Delta\omega$  and the angular frequency  $\omega_0$  is equal to the inverse of the quality factor. Thus the equation of the quality factor can be written as [93]:

$$Q = \frac{\omega_0}{\Delta\omega} \quad \dots (42)$$

Light can be stored for a long time in a small volume in an optical cavity, where the trapped field can reach very high levels of intensity. Thus, photonic crystal cavities with high  $Q$  factors and tight confinement of light in very small volumes are an ideal field for light-matter interaction. Equation (42) is the ratio between the resonant frequency and the full width at half maximum of the cavity. Moreover, it represents the lifetime of a trapped particle inside the cavity and defines the time scale in which optical processes can work.

### 3.6.2 Concept of Supercell

The numerical modeling of a localized cavity in an overall ideal periodic crystal is not easy. A useful tool generally used is the Supercell Technique. It consists of extending the calculation domain to include an equal number of unit-cells on each part of the cavity: the latter being fixed at its center. The numerical solution of the wave equation, subject to the Bloch-Floquet condition, is calculated all over the Supercell domain. So doing, implies that the physical

problem under consideration has changed: it is the Supercell domain as a whole that is periodically repeated identical to it-self. This virtually introduces unwanted periodical defects which can introduce errors due to the coupling of the cavity modes with those of the artifact cavities. The solution is to increase the number of unit-cells included in the Supercell. So doing, we expand the distance between the cavities and reduce the overlap of the confined modes. But increasing the supercell dimensions demands more calculation time. So, the key is to find the good tradeoff between the computation time and the isolation of the virtual cavities.

On the other hand, the supercell method introduces band folding in the band structure. Fortunately, the band folding does not affect the bandgaps and so the cavity modes may be easily obtained. This is because the folding only concerns the already existing propagating bands correctly obtained by the unit-cell technique.

In our test case, we analyse the behaviour of wave's confinement in  $L_1$  cavities using a  $9 \times 9$  supercell. This constitutes a good compromise between precision and computer time saving. This also ensures sufficient decoupling between neighboring virtual cavities.

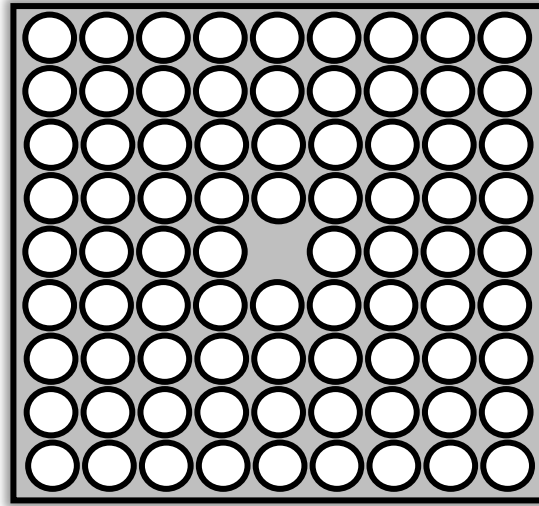
The edges of the bandgap obtained here are the same as the ones obtained in the absence of the cavity. Additional cavity modes: they appear within the gap and are characterized by frequencies almost independent of the wave vector  $k$  (i.e. quasi horizontal lines and qualified for this reason as “flat modes”). As illustrated in Figure 13, the frequency of the resonance modes is invariant as a function of the wave vector according to  $\Gamma X$ .

Figure 13 (a) represents the geometry of the supercell. Figure 13 (b & c) show the dispersion patterns of an optical supercell in TE and TM polarizations respectively accompanied by cavity mode profiles. The profiles of the associated cavity modes are shown on the right-hand side. The optical cavity modes are represented as a function of the electric

field and the magnetic field outside the plane. The study of the square lattice confirms the choice of TM polarization for silicon. This exhibits better confined cavity modes than those for the TE polarization. As can be seen, three modes are for TE, two of them being degenerated (having the same eigenfrequency and mode profiles with related symmetry properties). Five modes are found for TM, with two degenerated couples.

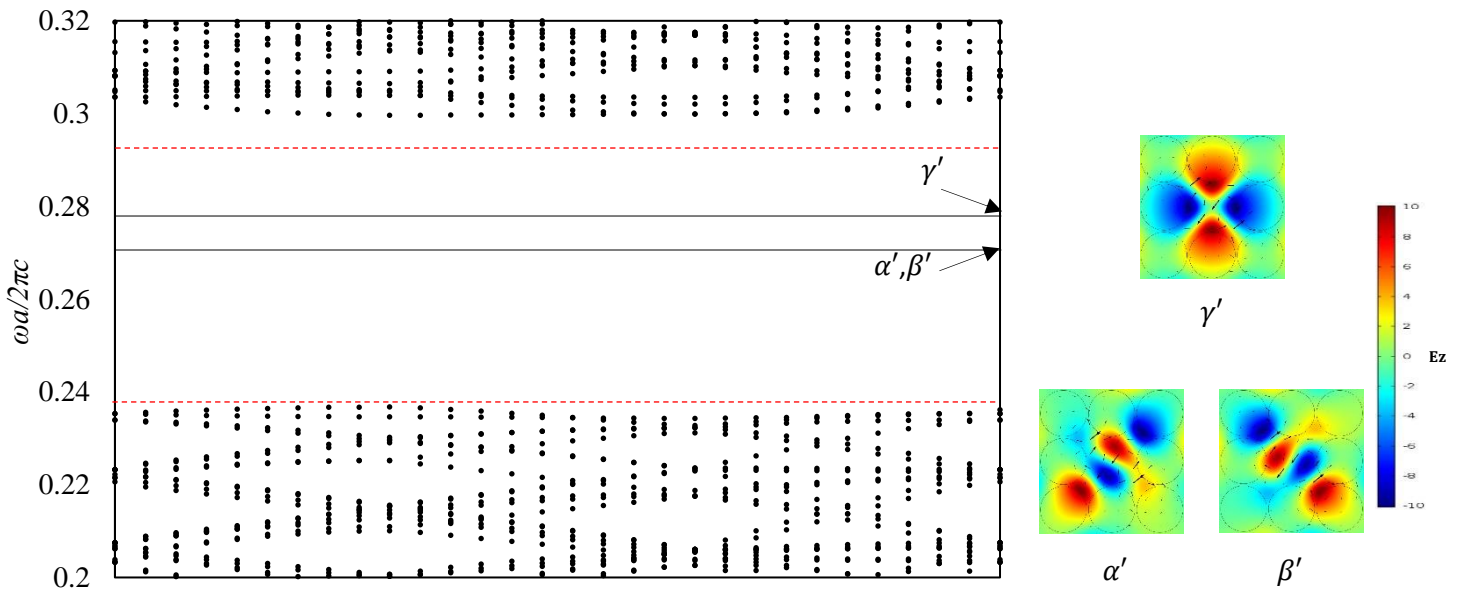
Figure 13 (d) shows the dispersion diagram of an acoustic supercell. The profiles of the associated cavity modes are shown on the right-hand side also. The six acoustic cavity modes found are represented as a function of the total displacement in the plane. The arrows indicate the direction of the acoustic displacement.

The modes presented in Figure 13 constitute the set of the eigenmodes of the unperturbed problem. They are used at the beginning of the perturbation method procedure. The photonic modes are perturbed by the phononic modes and their evolution is the end result of the perturbation method developed in Chapter IV.



(a)

Geometry of the Supercell

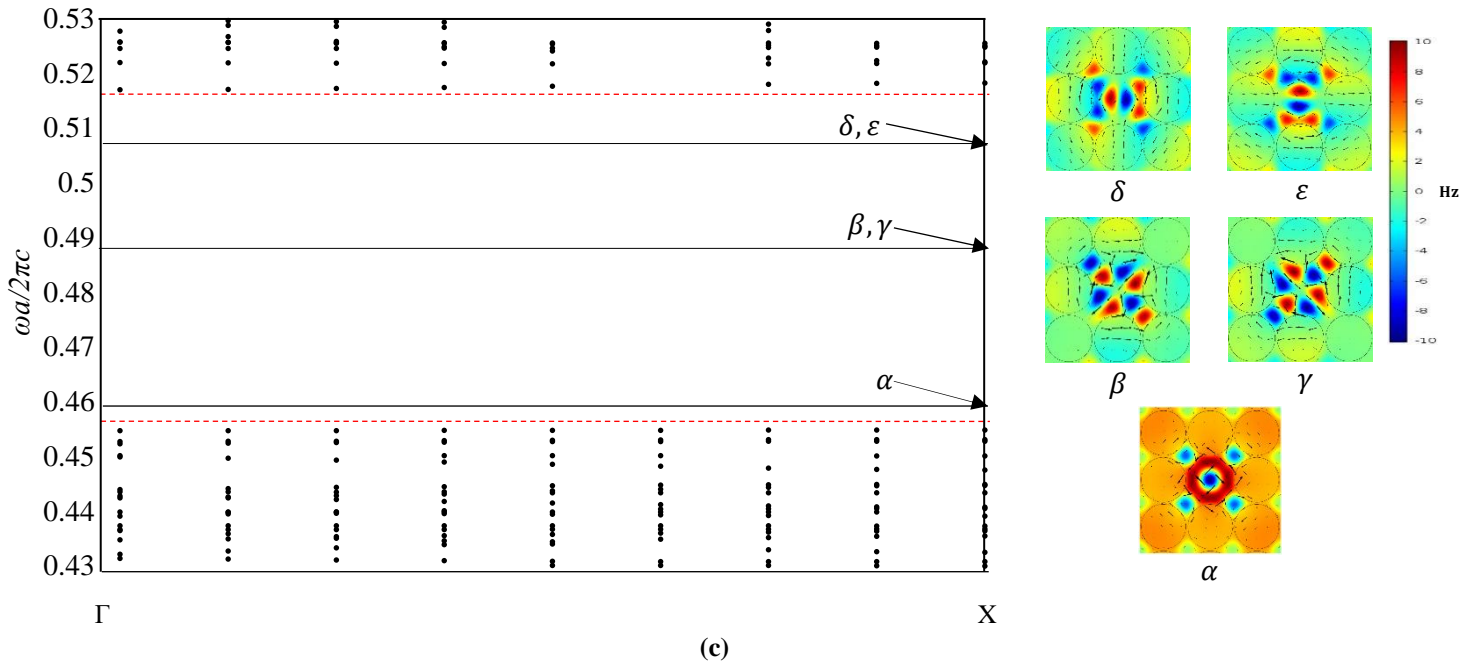


(b)

TE Cavity Eigenfrequencies

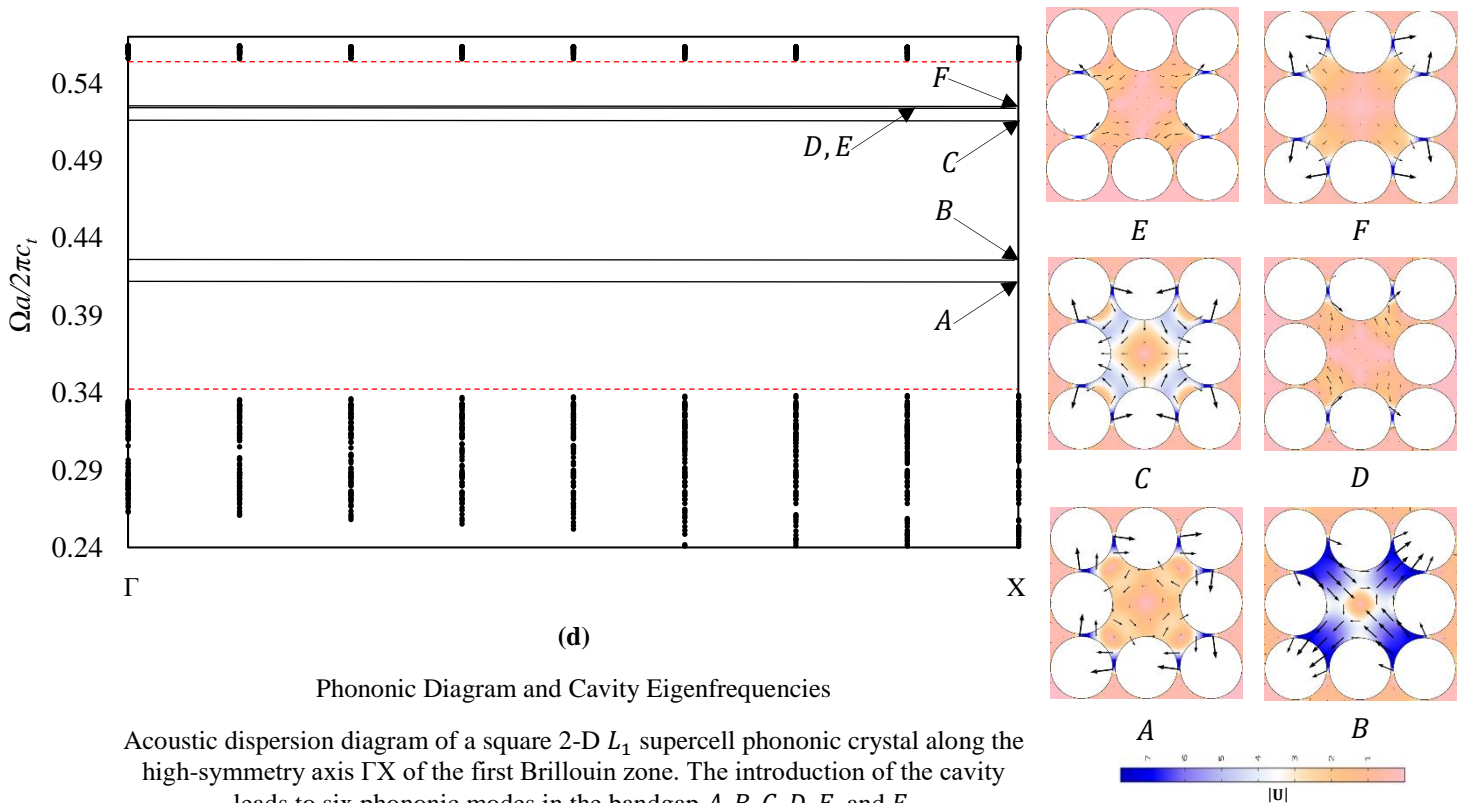
Transverse Electric (TE) Photonic Diagram and Cavity Eigenfrequencies

TE dispersion diagram of a square 2-D  $L_1$  supercell photonic crystal along the high-symmetry axis  $\Gamma X$  of the first Brillouin zone. The introduction of the cavity leads to three TE photonic modes in the bandgap  $\alpha', \beta'$  and  $\gamma'$ .



Transverse Magnetic (TM) Photonic Diagram and Cavity Eigenfrequencies

TM dispersion diagram of a square 2-D  $L_1$  supercell photonic crystal along the high-symmetry axis  $\Gamma X$  of the first Brillouin zone. The introduction of the cavity leads to five TM photonic modes in the bandgap  $\alpha, \beta, \gamma, \delta$ , and  $\epsilon$ .



Phononic Diagram and Cavity Eigenfrequencies

Acoustic dispersion diagram of a square 2-D  $L_1$  supercell phononic crystal along the high-symmetry axis  $\Gamma X$  of the first Brillouin zone. The introduction of the cavity leads to six phononic modes in the bandgap  $A, B, C, D, E$ , and  $F$ .

Figure 13: Representation of the Geometry, TE, TM, and Phononic Supercell Dispersion Diagram  
Dispersion diagram of Photonic and Phononic Crystals Along the high-symmetry axis  $\Gamma X$  of the first Brillouin zone.

### 3.7 Mechanisms Behind Photon-Phonon Interaction

The classical photon phonon interaction concerns a volume acoustic wave diffracting an optical wave, which classifies in two main diffraction patterns; the Râman-Nath diffraction and the Bragg diffraction. The optical properties of a material in such devices are periodically modified by the acoustic wave. This periodic modification is called a “Bragg grating”, with a period equivalent to the acoustic wavelength; this periodic structure is responsible of the diffraction of the optical wave.

The modulation of the optical properties due to the acousto-optical interaction in a confined medium is somehow different. The acoustic wave modifies the optical properties of the periodic dielectric medium, there are two mechanisms responsible of the modification of the refractive index. The first aspect is the classical modulation of the refractive index (or equivalently dielectric permittivity  $n = \sqrt{\epsilon_r}$ ), and the second effect is due to the boundary shifting mechanism [94]. For the first one, the photo-elastic effect, the refractive index changes as a function of the acoustic deformations, characterized by the strain tensor elements, applied to the material. The second one is due to the index modification induced by the acoustic wave deformations which modify the boundaries of the solid and thus the optical structures. Some authors call this phenomenon opto-mechanical effect.

The total acousto-optical coupling in periodic structures results in modulations of the optical field, as a combination of the two effects. A complete study of the coupling coefficients is given in Chapter IV.

### 3.7.1 Photo-Elastic Effect

In the photo-elastic effect, the refractive index changes are due to strain in the material. In the devices considered here, the strain is created by a given acoustic mode field distribution. The modulation of impermeittivity  $\Delta\eta_{ij}$  is related to the acoustic strain  $S_{kl}$  by Pockels tensor  $p_{ijkl}$ .

$$\Delta\eta_{ij} = p_{ijkl}S_{kl} \quad \dots (43)$$

The impermeittivity is defined as the inverse of permittivity i.e.:  $\varepsilon_{ij}\eta_{jk} = \delta_{ik}$  where  $\delta_{ik}$  is the Kronecker symbol. The photo-elastic effect is expressed by:

$$\Delta\varepsilon_{il} = -\varepsilon_{ij}p_{jkmn}\varepsilon_{kl}S_{mn} \quad \dots (44)$$

In the special case of m3m cubic lattice (case of the Silicon used in Chapter IV), using the Voigt notation, the components  $p_{ijkl}$  of the fourth rank tensor can be written as:

$$\underline{\underline{p}} = \begin{bmatrix} p_{11} & p_{12} & p_{12} & 0 & 0 & 0 \\ p_{12} & p_{11} & p_{12} & 0 & 0 & 0 \\ p_{12} & p_{11} & p_{11} & 0 & 0 & 0 \\ 0 & 0 & 0 & p_{44} & 0 & 0 \\ 0 & 0 & 0 & 0 & p_{44} & 0 \\ 0 & 0 & 0 & 0 & 0 & p_{44} \end{bmatrix} \quad \dots (45)$$

### 3.7.2 Opto-Mechanical Effect

The opto-mechanical effect corresponds to the interface deformation caused by the acoustic shift  $u_i$ . The shifting of a boundary introduces a localized change of the refractive index. This effect can be easily illustrated in the one-dimensional case. As illustrated in Figure 14, where, low and high index materials are respectively situated on the left and on the right of the



boundary. A right-shifting of the boundary (Figure a on the left) will introduces variation of the index  $\Delta n = n_{final} - n_{initial}$  which is negative ( $\Delta n < 0$ ) and localized in the vicinity of the boundary and vanishes elsewhere. In case of a left shifting (Figure b on the right), the same phenomena cause a positive variation  $\Delta n > 0$ .

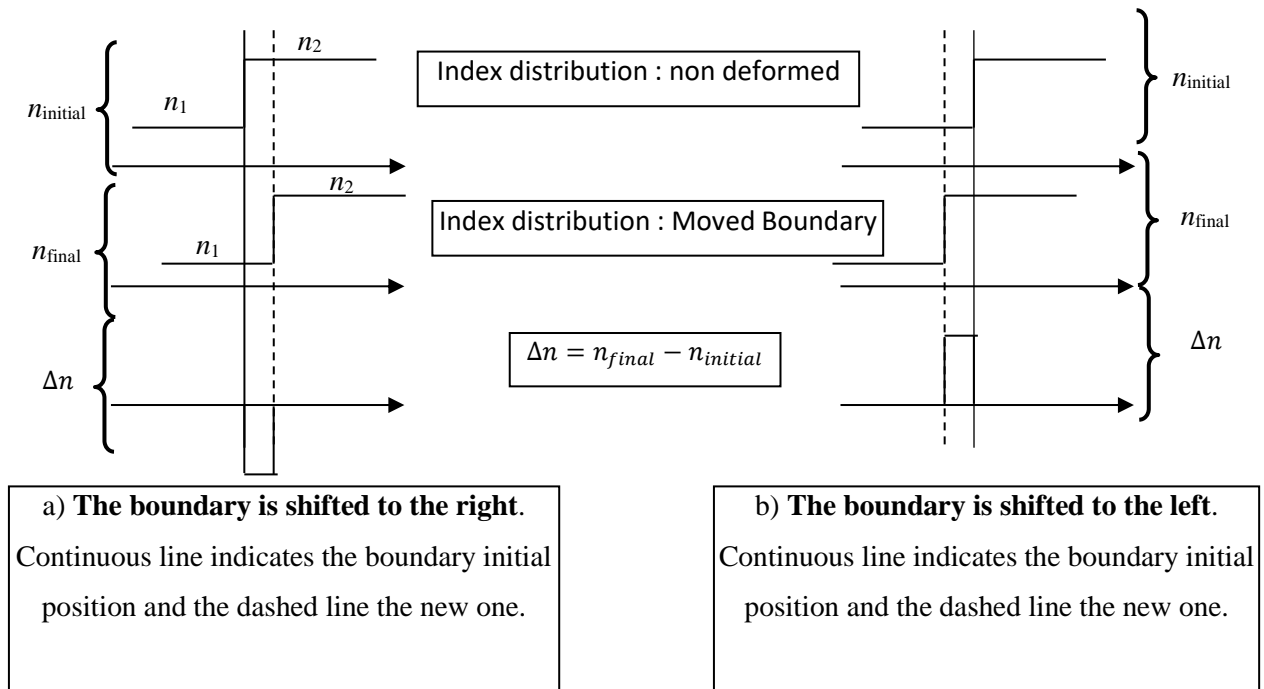


Figure 14: Illustration of the refractive index variation corresponding to an interface shifting caused by acoustic displacements.

The generalization to 2-D and 3-D, we use in the following chapter, have been established by Jonson et al. [94] in terms of permittivity variation instead of refractive index variation:

$$\Delta \varepsilon^{-1} = \varepsilon_{material}^{-1} - \varepsilon_{air}^{-1} \text{ and } \Delta \varepsilon = \varepsilon_{material} - \varepsilon_{air} \quad \dots (46)$$

where  $\varepsilon$  is the materials permittivity.

## 3.8 Conclusion

After an overview on the optic and acoustic wave propagation in homogeneous media, we highlighted the specificities of wave propagation in periodic media. Then, for both photonic and phononic domains, we applied the unit-cell and the supercell techniques to respectively determine the band structures and the cavity modes of the test case we used to illustrate the perturbation method in the following chapter. We also introduced the basis of the mechanisms responsible of the optical parameter variations induced by a cavity confined acoustic mode. This constitutes the perturbation of the medium responsible of the modulation of a cavity optical mode by an acoustic one; both confined in the same cavity.

## Chapter IV

# Evaluation of the Opto-Mechanical Coupling Strength

### 4.1 Introduction

This chapter, based on a work we published in [112], presents the potentialities of the perturbation method to provide physical interpretations of opto-mechanical coupling in a simultaneous photonic and phononic crystal cavity.

The field of opto-mechanical systems refers to devices meant for the coupling of mechanical oscillations to the optical waves. Cavity opto-mechanics promotes resonant enhancement and simultaneous confinement of photonic and phononic modes to a very small volume, leading to the possible strong coupling of mechanical and optical fields [95].

Photonic and phononic crystal cavities, also called phoXonic cavities, are promising systems compatible with photonic circuits approach. Silicon based, Indium Phosphide and Gallium Arsenide structures have been demonstrated [96] [97] [98]. Within the eigenfrequency bandgap, any structural defect can play the role of a confining cavity. Different cavities have been proposed: the  $L_n$  cavity formed by missing of  $n$ -aligned holes in a perfect crystal consisting of an array of holes in a bulk material [99], the modification of the radius of one or more holes or even the gradual modulation of neighboring holes [100].

Multimode cavity opto-mechanics finds applications in various systems such as sensing, or optical signal processing [94] [101] [102]. Linear and quadratic coupling strength in such systems are of particular interest, as many applications require a tight control of the opto-

mechanical behavior. For example, new functionalities such as measurement of position squared detuning of a cavity have been proposed [103] [104], which sensitivity benefits from the use of degenerated modes. Such cavities are good candidates for sensing purpose.

The advent of multi-physical software has led to a great advance in the development of finely tuned systems. Despite their high computing power, these software's suffer from the drawback of pure numerical methods: the lack to "inherently" provide physical interpretations. For example, the ability to predict, before the numerical results are obtained, the degeneracy lifting, the relative strength between 1<sup>st</sup> and 2<sup>nd</sup> order effects, and ultimately the aptitude to introduce design rules. The perturbation theory is an efficient approach that can be employed to fulfill this drawback without the expense of heavy computations [99] [100] [105] [106] [81] [107].

In this thesis we extend the perturbation formalism to the particular case of degenerated modes, up to the second order. We determine the opto-mechanical coupling coefficients in various cases, when the permittivity undergoes a quasi-static acoustic perturbation in phoXonic cavities. Then, we consider the very simple case of the  $L_1$  type cavity: consisting of one missing hole in a perfect rectangular phoXonic crystal.

Besides its simplicity, this structure provides interesting situations which permit to satisfactory illustrate the versatility of the perturbation method in analyzing the results. On the basis of our complete numeric approach [108] [109], we select two pertinent situations: one where the 1<sup>st</sup> order is relatively high so that any 2<sup>nd</sup> order behavior is not perceptible, resulting in a nearly first harmonic fluctuation of the modulation results. The second one, where the 2<sup>nd</sup> order effect is discernible: due to a specific symmetry of the permittivity perturbation, either the 1<sup>st</sup> order correction is identically zero (in the case of non-degenerated modes) or it exists but is too weak (in the case of degenerated modes). In the latter situation, the modulation results

exhibit purely second harmonic fluctuations or a mix of 1<sup>st</sup> and 2<sup>nd</sup> harmonics fluctuations respectively for non-degenerate and degenerate modes. The overall photonic eigenfrequencies modulations, obtained by the perturbation method, are in good agreement with a previous fully numeric approach [108] [109].

This chapter is structured as follows: in section 4.2, for completeness, we first detail the perturbative approach applied to the calculation of opto-mechanical coupling strength up to the second order. Then, we extend each order corrections to the case of degenerated modes. In section 4.3, we present briefly the design of the opto-mechanical cavity exploited to illustrate the versatility of the perturbation method. In section 4.4, we present the permittivity modulation induced by acoustical perturbation. In section 4.5, we apply the perturbative method to evaluate the opto-mechanical coupling coefficients. Then we exploit these opto-mechanical coupling factors in harmonic time series, giving back the dynamic behavior of the photonic modes. Finally, exploiting the results we show how it constitutes a useful tool that simplifies the analysis and interpretation of the results.

## 4.2 Perturbative Approach of Opto-Mechanical Coupling

The electric field formulation of the optical eigenproblem is well adapted for perturbative approach [105]. The spatial part of time harmonic modes field distribution verifies the optical wave equation:

$$\nabla \times \nabla \times \mathbf{E} = k_{0n}^{(0)2} \varepsilon \mathbf{E} \quad \dots (47)$$

The first step, before applying the acoustical perturbation procedure, is to determine the complete set of photonic crystal modes: their eigenfrequencies  $\omega_n^{(0)}$  and the associated eigenfunctions  $\mathbf{E}_n^{(0)}$  "the optical mode profiles" assumed to be discrete for localized modes.

Then, the aim of the perturbative approach is to find out the modifications  $(\Delta\omega_n, \Delta\mathbf{E}_n)$  that a given optical mode  $(\omega_n^{(0)}, \mathbf{E}_n^{(0)})$  experiences when an acoustic perturbation is applied. The  $n$  subscript labels the mode under consideration and the (0) superscript refers to the unperturbed situation: no applied acoustic mode in our case. The mode  $n$  (like any others) must satisfy the unperturbed wave equation:

$$\nabla \times \nabla \times \mathbf{E}_n^{(0)} = k_{0n}^{(0)2} \varepsilon^{(0)} \mathbf{E}_n^{(0)} \quad \dots (48)$$

Where,  $\varepsilon^{(0)}$  describes the spatial distribution of the relative permittivity over the entire nano-structured photonic crystal including cavity (our unperturbed system). For shortness, we use  $k_{0n}^{(0)} \equiv \omega_n^{(0)} \sqrt{\varepsilon_0 \mu_0} = \omega_n^{(0)} / c$  as the eigenvalue where  $\varepsilon_0, \mu_0$ , are respectively the vacuum permittivity and permeability, and  $c$  the free space light velocity.

Equation (47) constitutes a generalized Hermitian eigenproblem. Thus, the eigenvalues are real and the eigenfunctions (the mode profiles) are orthogonal to each other in the case of non-degenerate modes [105]. We assume hereafter that all the modes have been previously determined. We also assume that they have been normalized according to the normalization factor:  $\left[ \langle \mathbf{E}_n^{(0)} | \varepsilon^{(0)} | \mathbf{E}_n^{(0)} \rangle \right]^{-1/2}$ , and that the degenerated modes profiles have been beforehand also orthogonalized. Thus, these eigenfunctions  $\mathbf{E}_n^{(0)}$  constitutes a complete set of orthonormal basis functions  $\{ \mathbf{E}_n^{(0)} \}$  and any function can be developed as a linear combination of these basis functions. In particular, the function describing the perturbation  $\Delta\mathbf{E}_n$  of a mode profile can be expressed as a weighted sum (generally infinite) of the unperturbed mode eigenfunctions. Fortunately, in perturbation theory the weighting constants in these expansions sharply decrease as their eigenfrequencies move away from the eigenfrequency  $\omega_n^{(0)}$  of the mode we are dealing with. Usually, these linear combinations can be limited to a relatively small number

of terms. For completeness, we recall the derivation of the first and second order correction terms. For each order, the formalism is extended to include the case of degenerated modes.

### ***Rayleigh-Schrödinger Perturbation Method Applied to the Optical Wave Equation***

In the presence of an acoustic mode trapped in the cavity, the strength of the perturbation  $\Delta\varepsilon$  of the relative permittivity  $\varepsilon^{(0)}$  can be related to the sinusoidally varying acoustic displacement at a judiciously selected point: the point exhibiting the maximum amplitude displacement. Thus, the amplitude of the displacement is an obvious candidate for the perturbation parameter  $\lambda$ , over which we can develop power series for eigenfrequencies and eigenfunctions:

$$k_{0n} = k_{0n}^{(0)} + \lambda k_{0n}^{(1)} + \lambda^2 k_{0n}^{(2)} + \dots \quad \dots (49)$$

$$\mathbf{E}_n = \mathbf{E}_n^{(0)} + \lambda \mathbf{E}_n^{(1)} + \lambda^2 \mathbf{E}_n^{(2)} + \dots \quad \dots (50)$$

Often in real situations, the acoustic displacements are tiny. So, on the one hand, the relative permittivity variation  $\Delta\varepsilon$  is limited to the 1<sup>st</sup> order:  $\Delta\varepsilon = \varepsilon^{(0)} + \lambda\varepsilon^{(1)}$  whatever the mechanism responsible of this variation is: photo-elastic [110] [4], moving interface [94] or possibly piezoelectric if the material is concerned [5] [111]. On other hand, the power series (49) and (50), converge rapidly and generally, the first and possibly the second order terms are sufficient to give accurate results.

Inserting (49) and (50) and  $\varepsilon = \varepsilon^{(0)} + \Delta\varepsilon = \varepsilon^{(0)} + \lambda\varepsilon^{(1)}$  in equation (47) and noting that the obtained relations must be verified independently for the different orders terms in  $\lambda$ . Equation (47) splits in a system of equations: one for each order: O(0), O(1) and O(2). These equations write:

$$\left\{ \begin{array}{l} \text{O}(0): \nabla \times \nabla \times \mathbf{E}_n^{(0)} = k_{0n}^{(0)2} \varepsilon^{(0)} \mathbf{E}_n^{(0)} \\ \text{O}(1): \nabla \times \nabla \times \mathbf{E}_n^{(1)} = \left( k_{0n}^{(0)2} \varepsilon^{(1)} + 2k_{0n}^{(0)} k_{0n}^{(1)} \varepsilon^{(0)} \right) \mathbf{E}_n^{(0)} + k_{0n}^{(0)2} \varepsilon^{(0)} \mathbf{E}_n^{(1)} \\ \text{O}(2): \nabla \times \nabla \times \mathbf{E}_n^{(2)} = k_{0n}^{(0)2} \varepsilon^{(0)} \mathbf{E}_n^{(2)} + 2k_{0n}^{(0)} k_{0n}^{(1)} \varepsilon^{(0)} \mathbf{E}_n^{(1)} + \\ \quad + 2k_{0n}^{(0)} k_{0n}^{(2)} \varepsilon^{(0)} \mathbf{E}_n^{(0)} + 2k_{0n}^{(0)} k_{0n}^{(1)} \varepsilon^{(1)} \mathbf{E}_n^{(0)} + k_{0n}^{(1)2} \varepsilon^{(0)} \mathbf{E}_n^{(0)} + k_{0n}^{(0)2} \varepsilon^{(1)} \mathbf{E}_n^{(1)} \end{array} \right. \quad \dots (51)$$

In equation (51) we can expand  $\mathbf{E}_n^{(1)}$  and  $\mathbf{E}_n^{(2)}$  as linear combinations of the basis functions  $\{\mathbf{E}_m^{(0)}\}$ . Using the Dirac "bra-kets" notation these expansions write:

$$\left\{ \begin{array}{l} |\mathbf{E}_n^{(1)}\rangle = \sum_{m \neq n} \sum_{i=1}^{d_m} a_m |\mathbf{E}_{m,i}^{(0)}\rangle \\ |\mathbf{E}_n^{(2)}\rangle = \sum_{m \neq n} \sum_{i=1}^{d_m} b_m |\mathbf{E}_{m,i}^{(0)}\rangle \end{array} \right. \quad \dots (52)$$

Equation (52) takes into account the likely degeneracy of certain modes  $m$ , this is the reason of the added second subscript  $i$  in the basis eigenfunctions  $\mathbf{E}_{m,i}^{(0)}$  and the summation is carried out over  $i$  running from 1 to the degree of degeneracy  $d_m$  of the mode  $m$ . We assume that these degenerated modes have been already orthonormalized i.e.  $\langle \mathbf{E}_{m,i}^{(0)} | \varepsilon^{(0)} | \mathbf{E}_{m,j}^{(0)} \rangle = \delta_{ij}$ .

### ***First Order Correction of a Given Mode $n$***

Multiplying the equation O(1) of (51) by the bra  $\langle \mathbf{E}_l^{(0)} |$  and taking into account the equation O(0) of (51) which establishes the action of the operator  $\nabla \times \nabla \times (\cdot)$  on the basis functions, we obtain the 1<sup>st</sup> order corrections; for the eigenvalue  $k_{0n}^{(1)}$  if  $l = n$  and the coefficients  $a_m$  of the expansion series (52) of  $\mathbf{E}_n^{(1)}$  if  $l = m \neq n$ .

In the case where the mode  $n$  is non-degenerated, we straightforwardly obtain:

$$2 \frac{k_{0n}^{(1)}}{k_{0n}^{(0)}} = 2 \frac{\omega_n^{(1)}}{\omega_n^{(0)}} = -\langle \mathbf{E}_n^{(0)} | \varepsilon^{(1)} | \mathbf{E}_n^{(0)} \rangle + \text{O}(2) \quad \dots (53)$$



And

$$\left| \mathbf{E}_n^{(1)} \right\rangle = k_{0n}^{(0)2} \sum_{m \neq n} \sum_{i=1}^{d_m} \frac{\langle \mathbf{E}_{m,i}^{(0)} | \varepsilon^{(1)} | \mathbf{E}_n^{(0)} \rangle}{k_{0m}^{(0)2} - k_{0n}^{(0)2}} \left| \mathbf{E}_{m,i}^{(0)} \right\rangle \quad \dots (54)$$

In the case where the mode  $n$  presents a 2-fold degeneracy, it is well known that any linear combination  $\mathbf{E}_n^{(0)} = c_1 \mathbf{E}_{n,1}^{(0)} + c_2 \mathbf{E}_{n,2}^{(0)}$  of the two degenerated modes sharing the same eigenfrequency  $\omega_n^{(0)}$  is also an eigenfunction of the unperturbed optical system with the same eigenfrequency  $\omega_n^{(0)}$ .

Substituting this linear combination in the 1<sup>st</sup> order equation [O(1) of (51)] and next multiplying as we do for the non-degenerated case but this time successively by the two degenerated bras  $\langle \mathbf{E}_{n,i}^{(0)} |$ ;  $i = 1,2$ , we transform the coupled linear differential equation eigenproblem into an eigenproblem of a system of linear equations where the unknowns are coefficients  $c_1$  and  $c_2$ . This system writes:

$$\begin{pmatrix} \Gamma_{11} & \Gamma_{12} \\ \Gamma_{21} & \Gamma_{22} \end{pmatrix} \begin{pmatrix} c_1 \\ c_2 \end{pmatrix} = -2 \frac{k_{0n}^{(1)}}{k_{0n}^{(0)}} \begin{pmatrix} c_1 \\ c_2 \end{pmatrix}; \Gamma_{ij} \equiv \langle \mathbf{E}_{n,i}^{(0)} | \varepsilon^{(1)} | \mathbf{E}_{n,j}^{(0)} \rangle \quad \dots (55)$$

Thus, the solution gives the two eigenvectors of (55)  $\begin{pmatrix} c_1^\pm \\ c_2^\pm \end{pmatrix}$  i.e. the two possible sets of the unknown expansion coefficients  $\begin{pmatrix} c_1 \\ c_2 \end{pmatrix}$  while, the condition of existence of these solutions gives the couple of the 1<sup>st</sup> order corrections of the eigenfrequencies  $\omega_n^{(1)+}$  and  $\omega_n^{(1)-}$ :

$$2 \frac{k_{0n}^{(1)\pm}}{k_{0n}^{(0)}} = 2 \frac{\omega_n^{(1)\pm}}{\omega_n^{(0)}} = -\frac{\Gamma_{11} + \Gamma_{22}}{2} \pm \frac{1}{2} \sqrt{(\Gamma_{11} - \Gamma_{22})^2 + 4\Gamma_{12}\Gamma_{21}} \quad \dots (56)$$

In general, unless the expression under the square root vanishes, the degeneracy is lifted. The corresponding zero-order eigenfunctions are no more arbitrary but imposed by the

eigenvectors defined by the calculated coefficients  $\begin{pmatrix} c_1^\pm \\ c_2^\pm \end{pmatrix}$  of the actual linear

combinations  $\mathbf{E}_n^{(0)\pm} = c_1^\pm \mathbf{E}_{n,1}^{(0)} + c_2^\pm \mathbf{E}_{n,2}^{(0)}$ . In case of real  $\varepsilon^{(1)}$  these eigenfunctions can be set in the orthonormalized explicit form as [106]:

$$\begin{cases} \left| \mathbf{E}_n^{(0)+} \right\rangle = \sin \frac{\theta}{2} e^{j \frac{\phi_{12}}{2}} \left| \mathbf{E}_{n,1}^{(0)} \right\rangle - \cos \frac{\theta}{2} e^{-j \frac{\phi_{12}}{2}} \left| \mathbf{E}_{n,2}^{(0)} \right\rangle \\ \left| \mathbf{E}_n^{(0)-} \right\rangle = \cos \frac{\theta}{2} e^{j \frac{\phi_{12}}{2}} \left| \mathbf{E}_{n,1}^{(0)} \right\rangle + \sin \frac{\theta}{2} e^{-j \frac{\phi_{12}}{2}} \left| \mathbf{E}_{n,2}^{(0)} \right\rangle \end{cases} \quad \dots (57)$$

Where,  $\tan \theta \equiv \frac{2|\Gamma_{12}|}{\Gamma_{11} - \Gamma_{22}}$ ;  $0 < \theta < \pi$  and  $\phi_{12} \equiv \text{Arg}\{\Gamma_{12}\}$ .

These solutions  $\mathbf{E}_n^{(0)+}, \mathbf{E}_n^{(0)-}$  of the generalized hermitian eigenproblem verify the orthogonality relation:

$$\begin{cases} \left\langle \mathbf{E}_n^{(0)\pm} \left| \varepsilon^{(1)} \right| \mathbf{E}_n^{(0)\pm} \right\rangle = -2 \frac{k_{on}^{(1)\pm}}{k_{on}^{(0)}} ; \text{ auto product} \\ \left\langle \mathbf{E}_n^{(0)\pm} \left| \varepsilon^{(1)} \right| \mathbf{E}_n^{(0)\mp} \right\rangle = 0 ; \text{ cross product} \end{cases} \quad \dots (58)$$

On the other hand,  $\mathbf{E}_n^{(0)+}$  and  $\mathbf{E}_n^{(0)-}$  are also eigensolutions of the zero-order equation [O(0) of (51)] and are assumed to be beforehand orthonormalized with respect to the scalar product  $\left\langle \mathbf{E}_n^{(0)\pm} \left| \varepsilon^{(0)} \right| \mathbf{E}_n^{(0)\pm} \right\rangle$ . In other words, their expressions (57) verify the condition:  $c_1^{\pm*} c_1^\pm + c_2^{\pm*} c_2^\pm = 1$ .

In the same way as we have derived equation (54), we multiply the equation O(1) of (51) by the bra  $\langle \mathbf{E}_l^{(0)} |$  where  $l = m \neq n$  gives the expansion coefficients of both the two new 1<sup>st</sup> order corrections  $\left| \mathbf{E}_n^{(1)+} \right\rangle$  and  $\left| \mathbf{E}_n^{(1)-} \right\rangle$  of the eigenfunctions  $\left| \mathbf{E}_n^{(0)\pm} \right\rangle$  we can write:

$$\left| \mathbf{E}_n^{(1)\pm} \right\rangle = k_{on}^{(0)2} \sum_{m \neq n} \sum_{i=1}^{d_m} \frac{\langle \mathbf{E}_{m,i}^{(0)} | \varepsilon^{(1)} | \mathbf{E}_n^{(0)\pm} \rangle}{k_{om}^{(0)2} - k_{on}^{(0)2}} \left| \mathbf{E}_{m,i}^{(0)} \right\rangle \quad \dots (59)$$

The case where the degeneracy is not lifted is a very special case. Indeed, the expression under the square root of (56) vanishes if at the same time the diagonal matrix elements are equal  $\Gamma_{11} = \Gamma_{22}$  and the off-diagonal vanish:  $\Gamma_{12} = \Gamma_{21} = 0$ . In these circumstances, equation (55) reduces to:

$$\begin{pmatrix} \Gamma_{11} & 0 \\ 0 & \Gamma_{11} \end{pmatrix} \begin{pmatrix} c_1 \\ c_2 \end{pmatrix} = -2 \frac{k_{on}^{(1)}}{k_{on}^{(0)}} \begin{pmatrix} c_1 \\ c_2 \end{pmatrix}$$

Thus, the system of equations uncouples the two modes  $\mathbf{E}_{n1}^{(0)}$  and  $\mathbf{E}_{n2}^{(0)}$ . They remain degenerated and experience both the same 1<sup>st</sup> order correction of their eigenfrequency:

$$2 \frac{k_{on}^{(1)}}{k_{on}^{(0)}} = 2 \frac{\omega_n^{(1)}}{\omega_n^{(0)}} = -\Gamma_{11} = -\Gamma_{22} \quad \dots (60)$$

The 1<sup>st</sup> order corrections ( $\mathbf{E}_{n1}^{(1)}$  and  $\mathbf{E}_{n2}^{(1)}$ ) of the two degenerated eigenfunctions  $\left| \mathbf{E}_{n1}^{(0)} \right\rangle$  and  $\left| \mathbf{E}_{n2}^{(0)} \right\rangle$

write:

$$\begin{cases} \left| \mathbf{E}_{n1}^{(1)} \right\rangle = k_{on}^{(0)2} \sum_{m \neq n} \sum_{i=1}^{d_m} \frac{\langle \mathbf{E}_{m,i}^{(0)} | \varepsilon^{(1)} | \mathbf{E}_{n1}^{(0)} \rangle}{k_{om}^{(0)2} - k_{on}^{(0)2}} \left| \mathbf{E}_{m,i}^{(0)} \right\rangle \\ \left| \mathbf{E}_{n2}^{(1)} \right\rangle = k_{on}^{(0)2} \sum_{m \neq n} \sum_{i=1}^{d_m} \frac{\langle \mathbf{E}_{m,i}^{(0)} | \varepsilon^{(1)} | \mathbf{E}_{n2}^{(0)} \rangle}{k_{om}^{(0)2} - k_{on}^{(0)2}} \left| \mathbf{E}_{m,i}^{(0)} \right\rangle \end{cases} \quad \dots (61)$$

### ***Second Order Correction of the Eigenvalue***

In order to obtain the 2<sup>nd</sup> order correction  $k_{on}^{(2)}$  for the eigenvalue, we follow the same procedure as we do for the 1<sup>st</sup> order but, this time, multiplying the second order equation [O(2) of (51)] by the bra  $\langle \mathbf{E}_l^{(0)} |$ ;  $l = n$ .

### *Case of Non-Degenerated Mode n*

This procedure straightforwardly gives:

$$2 \frac{k_{0n}^{(2)}}{k_{0n}^{(0)}} = 3 \left( \frac{k_{0n}^{(1)}}{k_{0n}^{(0)}} \right)^2 - \left\langle \mathbf{E}_n^{(0)} \left| \varepsilon^{(1)} \right| \mathbf{E}_n^{(1)} \right\rangle + O(3) \quad \dots (62)$$

In case of real  $\varepsilon^{(1)}$  the latter equation reduces to:

$$2 \frac{k_{0n}^{(2)}}{k_{0n}^{(0)}} = 3 \left( \frac{k_{0n}^{(1)}}{k_{0n}^{(0)}} \right)^2 - k_{0n}^{(0)2} \sum_{m \neq n} \sum_{i=1}^{d_m} \frac{\left| \left\langle \mathbf{E}_{m,i}^{(0)} \left| \varepsilon^{(1)} \right| \mathbf{E}_n^{(0)} \right\rangle \right|^2}{k_{0m}^{(0)2} - k_{0n}^{(0)2}} + O(3) \quad \dots (63)$$

### *Case of 2-Fold Degenerated Mode n*

First, when the degeneracy is lifted at the first order, these modes can be treated in higher orders as non-degenerated ones provided, we adopt the framework of the normalized eigenbasis  $\left\{ \left| \mathbf{E}_n^{(0)\pm} \right\rangle \right\}$  (57).

Indeed, owing to (58) the corresponding matrix diagonalizes and equation (55) writes:

$$\begin{pmatrix} -2 \frac{k_{0n}^{(1)+}}{k_{0n}^{(0)}} & 0 \\ 0 & -2 \frac{k_{0n}^{(1)-}}{k_{0n}^{(0)}} \end{pmatrix} \begin{pmatrix} c'_1 \\ c'_2 \end{pmatrix} = -2 \frac{k_{0n}^{(1)}}{k_{0n}^{(0)}} \begin{pmatrix} c'_1 \\ c'_2 \end{pmatrix} \quad \dots (64)$$

The counterpart of equation (62), giving one of the eigenvalues, writes:

$$2 \frac{k_{0n}^{(2)+}}{k_{0n}^{(0)}} = + 3 \left( \frac{k_{0n}^{(1)+}}{k_{0n}^{(0)}} \right)^2 - \left\langle \mathbf{E}_n^{(0)+} \left| \varepsilon^{(1)} \right| \mathbf{E}_n^{(1)+} \right\rangle + O_3 \quad \dots (65)$$

The other eigenvalue is obtained by replacing the superscript + by a superscript -. Finally, the 2<sup>nd</sup> order correction of the eigenvalue is given by relations similar to (62,63) using the appropriate eigenbasis functions and the corresponding eigenvalues.

Second, if the degeneracy is not lifted in the 1<sup>st</sup> order, strictly speaking, we have to examine the eventual lift of the degeneracy during the 2<sup>nd</sup> order treatment. However, equation (60) tells us that the 1<sup>st</sup> order correction is non-negligible:  $\Gamma_{11} = \Gamma_{22} \neq 0$  and thus shields the eventual 2<sup>nd</sup> order correction according to power series (49).

Furthermore, usually the dielectric constant dependence is restricted to the 1<sup>st</sup> order whatever the concerned mechanism is (i.e. higher orders are not taken into account:  $\varepsilon^{(2)} \equiv 0$ ): this also justifies the fact that the second order can be neglected in this case.

### 4.3 Opto-Mechanical Cavity Characteristics

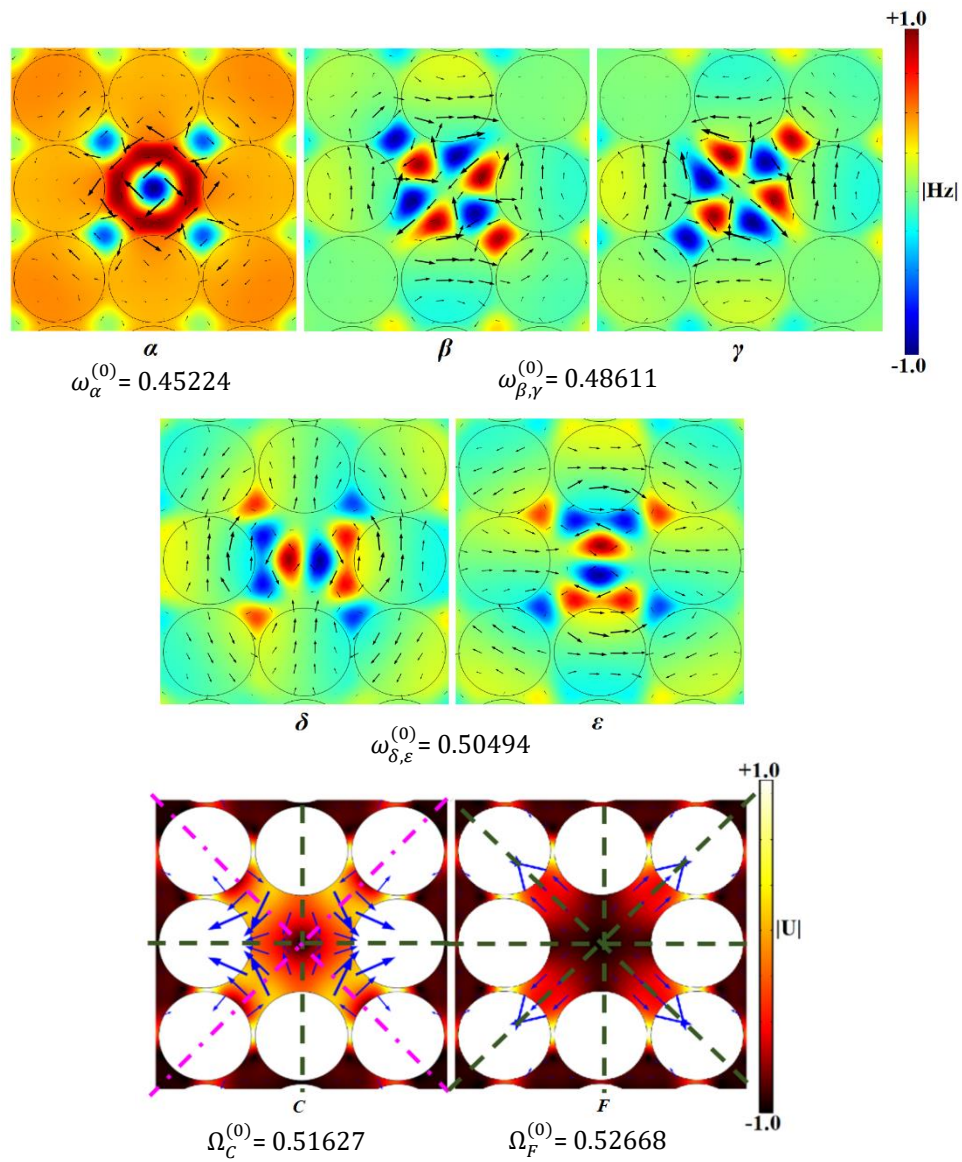
To evaluate the benefits of the developed expressions for degenerated modes, we apply them to a  $L_I$  system previously investigated with a complete numeric method [108] [109]. We recall here briefly the main characteristics of the test structure. It is assumed to be a square lattice periodic pattern of circular air holes drilled in a silicon substrate. A single missing hole constitutes the  $L_I$  cavity. The period is  $a = 650$  nm and the relative radius value,  $r/a$ , is 0.48. The cavity modes are determined using commercial Multiphysics Finite Element Method software. The  $L_I$  cavity is implemented using the supercell technique limited to 9×9 unit-cell which appeared to be a good compromise between precision and time saving [108].

Figure 15 depicts the photonic and phononic modes profiles exploited in section 4.5. In our perturbative treatment, the optical modes profiles stand for the unperturbed modes (i.e. in the

absence of the acoustic perturbation) while, the acoustic modes are responsible of the permittivity variations (i.e. the perturbation of the optical system).

The eigenfrequencies of both types of modes are also specified in Figure 15 as well as the bandgap edges. These modes combinations have been selected because they display pertinent modulation behaviors which highlight interesting aspects of the perturbation method capabilities.

More precisely, Figure 15 represent the TM (i.e. in-plane electric fields) optical modes profiles confined in the 1<sup>st</sup> bandgap of the photonic crystal as well as the acoustic displacement profiles of the two selected cavity modes used to modulate the optical mode eigenfrequency. The acoustic mode *F* is a breathing mode, while the acoustic mode *C* is periodically elongated in *x*-direction and contracted in the *y*-direction in one half of the acoustic cycle then, the situation is reversed in the 2<sup>nd</sup> half cycle.



**Figure 15:** Modes profiles of the elastic and electromagnetic fields in the  $(x, y)$  plane. TM photonic modes profiles  $H_z$  ( $\alpha, \beta, \gamma, \delta$ , and  $\epsilon$ ) the arrows indicate the polarization vector (electric field); Phononic modes profiles of the modes  $C$  and  $F$  the colored scale stands for the displacement magnitude  $|\vec{U}|$  the arrows specify the displacement vector field. The values of the normalized angular eigenfrequencies are given under the corresponding cavity mode profiles.

## 4.4 Permittivity Modulation Induced by Acoustical Perturbation

All the relations presented in section 4.2 are expressed in terms of the relative permittivity variations without any reference to the mechanism responsible of this variation. So, the expressions of the coupling terms: equations (53,56) for 1<sup>st</sup> order and (62,63) for the 2<sup>nd</sup> order are of general character whatever the effect modulating the relative permittivity is. The relative permittivity variation  $\Delta\epsilon$  is intended to be induced by the acoustic modes vibrations. Silicon being a non-piezoelectric crystal, thus  $\Delta\epsilon$  variation emanates from the conjunction of two effects [101]: The photo-elastic effect and the one resulting from the shifting of the interface [94] delimiting the two different dielectrics.

For the former effect, the components of the permittivity tensor  $\Delta\epsilon$  in terms of strain write [4] [5] [111]:

$$\Delta\epsilon_{il} = -\epsilon_{ij}p_{jkmn}\epsilon_{kl}S_{mn} \quad \dots (66)$$

Where, the  $p_{jkmn}$ ,  $\epsilon_{ij}$  and  $S_{mn}$  respectively stand for the materials photo-elastic coefficients, the permittivity and the strain tensor components.

In the case of silicon which belongs to the cubic  $m\bar{3}m$  class of symmetry, first the unperturbed crystal is optically isotropic, and second only 3 between the 12 non-trivial photo-elastic coefficients are independent. These non-trivial coefficients are, using Voigt notations:  $p_{33} = p_{22} = p_{11}$ ,  $p_{13} = p_{31} = p_{23} = p_{32} = p_{21} = p_{12}$  and  $p_{66} = p_{55} = p_{44}$ . Table 4 gives the photo-elastic coefficients for silicon used in our calculations.



	$p_{11}$	$p_{12}$	$p_{44}$
<i>Si</i> (1150 nm)	-0.1	0.01	-0.051

**Table 4:** Photo-elastic coefficients for *Si* [4] [5].

According to these symmetry considerations, the equation (66) also expressed in Voigt notation reduces to:

$$\Delta\varepsilon_i = -\varepsilon_r^2 p_{ij} S_j ; 1 \leq i, j \leq 6 \quad \dots (67)$$

Where  $\varepsilon_r$  is the bulk silicon relative permittivity.

Also, considering the in-plane propagation i.e.  $\partial/\partial z = 0$  of acoustic modes with in-plane polarization i.e. displacements  $u_z = 0$ , the variations of the components of the permittivity tensors further reduce to [81] [107] [110]:

$$\begin{cases} \Delta\varepsilon_1 \equiv \Delta\varepsilon_{xx} = -\varepsilon_r^2 (p_{11} S_1 + p_{12} S_2) \\ \Delta\varepsilon_2 \equiv \Delta\varepsilon_{yy} = -\varepsilon_r^2 (p_{11} S_2 + p_{12} S_1) \\ \Delta\varepsilon_3 \equiv \Delta\varepsilon_{zz} = -\varepsilon_r^2 p_{12} (S_1 + S_2) \\ \Delta\varepsilon_6 \equiv \Delta\varepsilon_{xy} = \Delta\varepsilon_{yx} = -\varepsilon_r^2 p_{44} S_6 \end{cases} \quad \dots (68)$$

The other components vanish:  $\Delta\varepsilon_4 \equiv \Delta\varepsilon_{yz} = \Delta\varepsilon_{zy} = 0$  and  $\Delta\varepsilon_5 \equiv \Delta\varepsilon_{xz} = \Delta\varepsilon_{zx} = 0$ .

Concerning the moving interface effect, the displacements of the boundaries can be assimilated to an alternate transfer of materials across the interface from silicon to air in the 1<sup>st</sup> half of the acoustic cycle, the situation being inverted in the 2<sup>nd</sup> half.

According to the continuity conditions of electric field and electric displacement, Johnson and al. [94] showed that each of the electric field components,  $E_{\perp}$  normal and  $E_{//}$  parallel to

the interface, experiences dissimilar permittivity's. For the case of silicon/air interfaces of the photonic crystal considered here these dissimilar permittivity writes:

$$\begin{cases} \Delta\varepsilon_{Si,air//} = (\varepsilon_{Si} - \varepsilon_{air})(n_l \cdot U)\delta(n_l - n_l \cdot U) \\ \Delta\varepsilon_{Si,air\perp} = -(\varepsilon_{Si}^{-1} - \varepsilon_{air}^{-1})\varepsilon_{Si}^2(n_l \cdot U)\delta(n_l - n_l \cdot U) \end{cases} \dots (69)$$

Where,  $U$  is the acoustic mode displacement vector and  $n_l$  stands for the normal unit-vector defined through the entire  $Si/air$  layout interfaces. The inclusion of the Dirac-delta function  $\delta(n_l - n_l \cdot U)$  converts, in our 2-D system, the surface integrals of the scalar product

$$\left\langle E_n^{(0)} \left| \Delta\varepsilon \right| E_n^{(0)} \right\rangle \text{ into curvilinear ones similar to those of reference [94]: } \int U \cdot n \left( \Delta\varepsilon_{Si/air} \cdot \left| E_{//}^{(0)} \right|^2 - \Delta(\varepsilon_{Si/air}^{-1}) \left| \varepsilon_{Si/air} E_{\perp}^{(0)} \right|^2 \right) dl.$$

## 4.5 Potentialities of the Perturbation Approach

As compared to pure numerical methods, the perturbation theory not only save calculation time but also fulfils their principal lack: it constitute a tool for the analysis and/or the physical interpretations of obtained results: relative strength of 1<sup>st</sup> and 2<sup>nd</sup> order modulation, degeneracy lifting ..., and ultimately deducing design rules.

This section is devoted to the illustration of these capabilities. The obtained perturbation method results concerning relevant situations are presented and discussed following a detailed analysis based on symmetry considerations. Also, in order to lighten the presentation and focus on the method potentialities, only the photo-elastic effect is taken into account. That is, the permittivity modulation is determined using equation (68). The procedure is exactly the same for the moving boundary effect if equation (69) is used instead of (68).

## *Opto-mechanical 1<sup>st</sup> and 2<sup>nd</sup> Order Coupling Coefficients*

We consider two relevant examples of perturbations: The acoustic mode  $F$  for which the second order correction is too small that the modulation of the optical eigenfrequencies displays a 1<sup>st</sup> order behavior and the acoustic mode  $C$  where the second order exist; alone, in case of a non-degenerated optical mode and beside, a reduced 1<sup>st</sup> order in case of 2-fold degenerated modes.

The opto-mechanical coupling coefficients are calculated from the numerically simulated photonic and phononic modes profiles: for the 1<sup>st</sup> order using expressions (53) in case of non-degenerate optical modes or (56) in case of degenerated ones; and for the 2<sup>nd</sup> order, we use expressions (62) or (65) respectively for non-degenerated and degenerated optical modes. The obtained numerical values of the 1<sup>st</sup> and 2<sup>nd</sup> order coupling coefficients are presented in Table5.

<b><i>TM</i></b> <b><i>Photonic</i></b> <b><i>modes</i></b>	<b><i>Unperturbed</i></b>	<b><i>Phononic Modes</i></b>			
	<b><i>normalized</i></b>	<b><i>C</i></b>		<b><i>F</i></b>	
	<b><i>frequency</i></b>				
	$\frac{a\omega_n^{(0)}}{2\pi c}$	$\frac{\omega_n^{(1)}}{\omega_n^{(0)}}$	$\frac{\omega_n^{(2)}}{\omega_n^{(0)}}$	$\frac{\omega_n^{(1)}}{\omega_n^{(0)}}$	$\frac{\omega_n^{(2)}}{\omega_n^{(0)}}$
$(\alpha)$	0,45224	<<	$7.6587 \times 10^{-5}$	$-5.4322 \times 10^{-4}$	$5.0213 \times 10^{-7}$
$(\beta, \gamma)^+$	0,48611	$8.1301 \times 10^{-5}$	$-1.1715 \times 10^{-5}$	$-6.5473 \times 10^{-4}$	$9.6977 \times 10^{-8}$
$(\beta, \gamma)^-$	0,48611	$-8.1014 \times 10^{-5}$	$-1.1666 \times 10^{-5}$	$-6.6704 \times 10^{-4}$	$9.6135 \times 10^{-8}$
$(\delta, \epsilon)^+$	0,50494	$3.3338 \times 10^{-4}$	$1.2783 \times 10^{-5}$	$-4.8881 \times 10^{-4}$	$1.0726 \times 10^{-7}$
$(\delta, \epsilon)^-$	0,50494	$-3.3375 \times 10^{-4}$	$1.2847 \times 10^{-5}$	$-4.893 \times 10^{-4}$	$1.0826 \times 10^{-7}$

**Table 5:** Opto-mechanical coupling rate in between TM photonic Eigen-modes  $\alpha, \beta, \gamma, \delta,$  and  $\epsilon$  and phononic Eigen-modes  $C$  and  $F$  for first and second order perturbations. The symbol << means that the value is below the numerical errors.

Figure 16 gives the modes profiles of the new eigenbasis  $\mathbf{E}_{\beta\gamma}^{(0)\pm}$  (labeled  $\{\mathbf{E}_n^{(0)\pm}\}$  in section 4.2). And Table 6 presents the corresponding expansion coefficients  $\begin{pmatrix} c_1^\pm \\ c_2^\pm \end{pmatrix}$ .

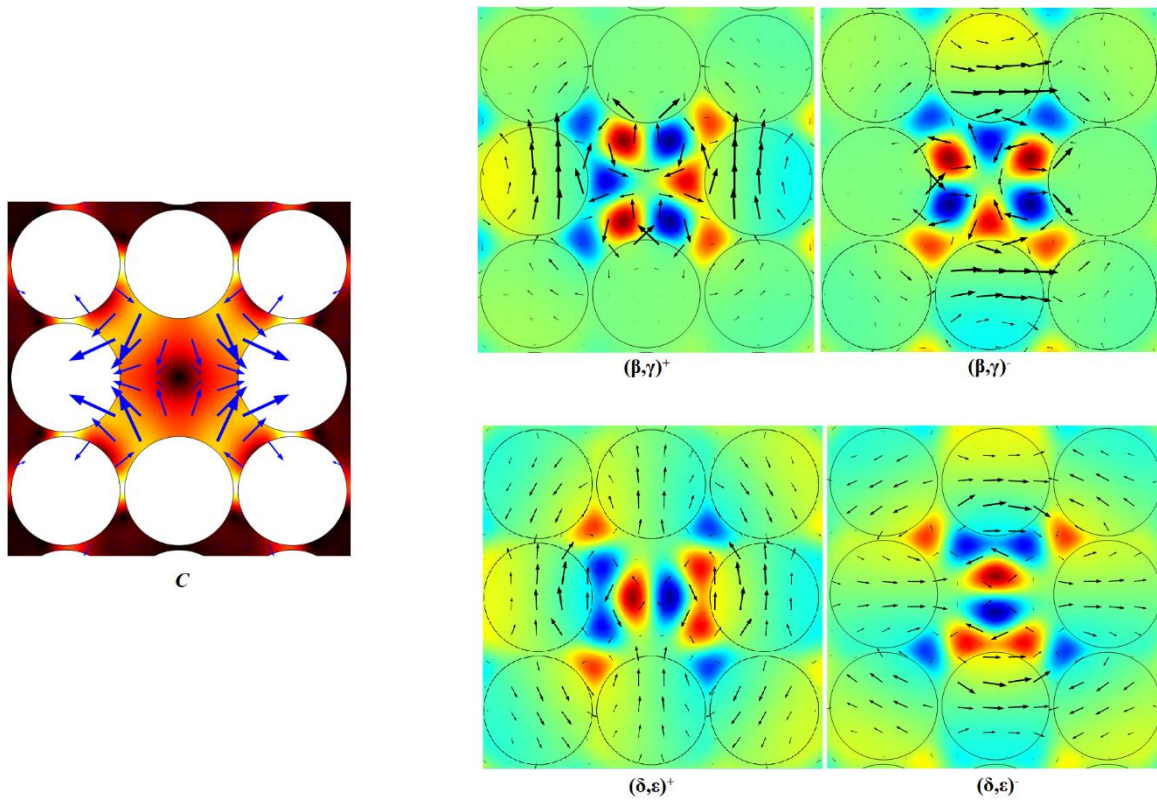


**Figure 16:** Profiles of the new modes obtained subsequently to degeneracy lifting, as a result of the perturbation introduced by the presence of the acoustic mode  $C$ , during the 1<sup>st</sup> order treatment. The corresponding new eigenfrequencies are presented in Figure 17.

	$\beta, \gamma$	$\delta, \varepsilon$
	<b>Phononic Mode C</b>	<b>Phononic Mode C</b>
	$c_2^+ = 1.2485c_1^+$	$c_2^+ = -0.0685c_1^+$
$c_{1N}^+$	0.6252	0.9977
$c_{2N}^+$	0.7805	-0.0683
	$c_2^- = -0.801c_1^-$	$c_2^- = 14.6003c_1^-$
$c_{1N}^-$	0.7805	0.0683
$c_{2N}^-$	-0.6252	0.9977

**Table 6:** Coefficients  $c_1^\pm$  and  $c_2^\pm$  for the new zero-order modes (after the degeneracy have been lifted) for TM degenerated photonic eigenmodes  $\beta$  &  $\gamma, \delta$  and  $\varepsilon$  with phononic perturbation induced by the eigenmode  $C$ .

Inserting these coupling coefficients  $k_{0n}^{(1)}$  and  $k_{0n}^{(2)}$  in equation (49) and remembering that the perturbation parameter  $\lambda$  stands for a sinusoidal time varying amplitude of the acoustic standing mode, we retrieve the dynamic of the photonic mode properties under perturbation. These modulations results are presented on (Figure 17 and 18). In the case of applied acoustic mode  $F$ , all the optical modes: the non-degenerated mode  $\alpha$ , and the two couples of degenerated modes  $(\beta, \gamma)$  and  $(\delta, \varepsilon)$ , exhibit first harmonic fluctuations at the acoustic angular frequency  $\Omega$ . Furthermore, the degeneracy of the modes  $(\beta, \gamma)$  and  $(\delta, \varepsilon)$  is not lifted. However, in the presence of the acoustic mode  $C$ , the modulation of the non-degenerated mode  $\alpha$  exhibits purely second harmonic fluctuations at the acoustic angular frequency  $2\Omega$ . Whereas concerning the degenerated modes  $(\beta, \gamma)$  and  $(\delta, \varepsilon)$  their degeneracy is lifted and the modulation of the optical frequency displays distorted sinusoids (more pronounced for  $\beta, \gamma$  modes) indicating the presence of higher harmonics beside the fundamental ones.

Those behaviors are consistent with what we found with a numeric approach [108] [109] [75].

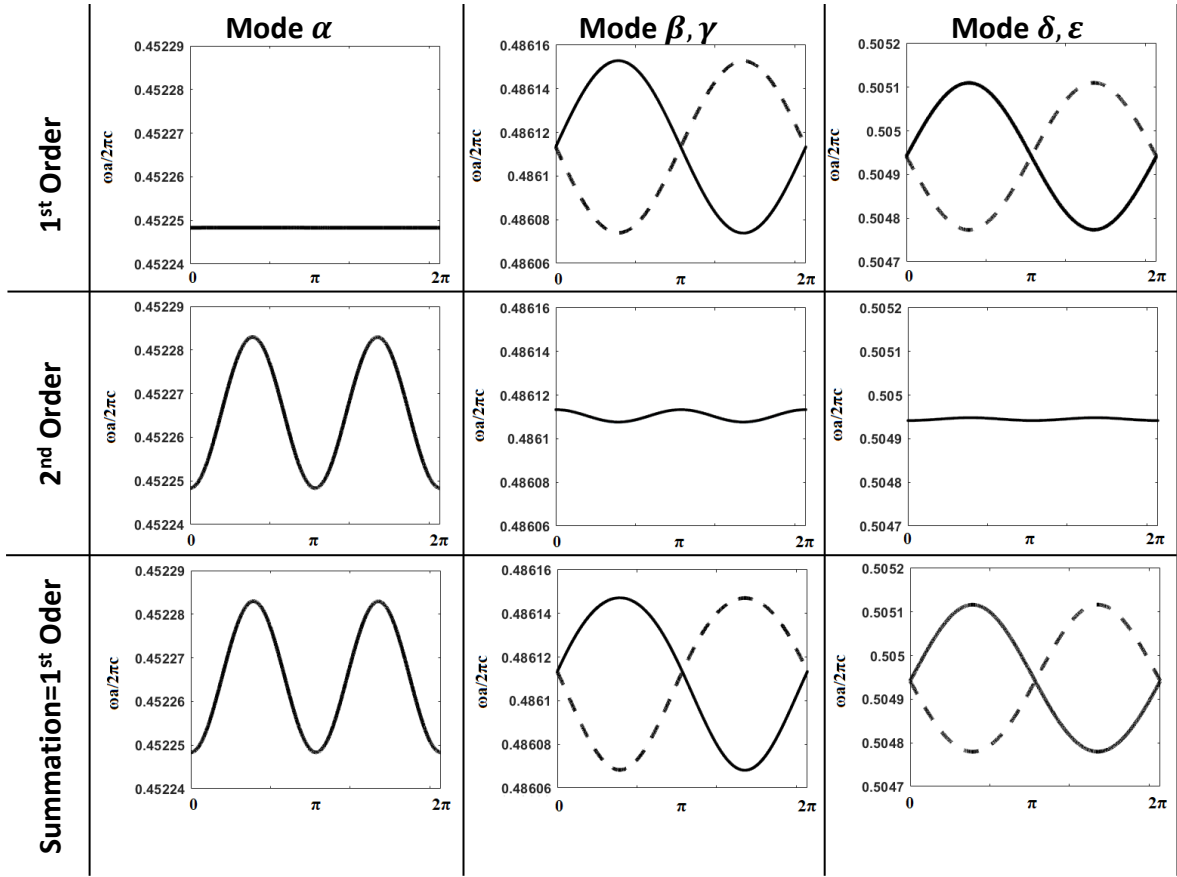


**Figure 17:** Modulation of the 5 photonic modes eigenfrequencies induced by the acoustic mode  $C$  during one acoustic cycle:  $0 \leq \Omega t \leq 2\pi$ . First and second rows give respectively the 1<sup>st</sup> and 2<sup>nd</sup> order corrections, the 3<sup>rd</sup> row represents the 1<sup>st</sup> and 2<sup>nd</sup> order combined effects. The singlet mode  $\alpha$  is disposed in the 1<sup>st</sup> column and the two doublet modes ( $\beta, \gamma$ ) and ( $\delta, \epsilon$ ) are piled in the 2<sup>nd</sup> and 3<sup>rd</sup> columns respectively. Each one of the dot dashed and the continuous lines stands for one of the split angular frequencies of the new doublet modes after degeneracy is lifted.

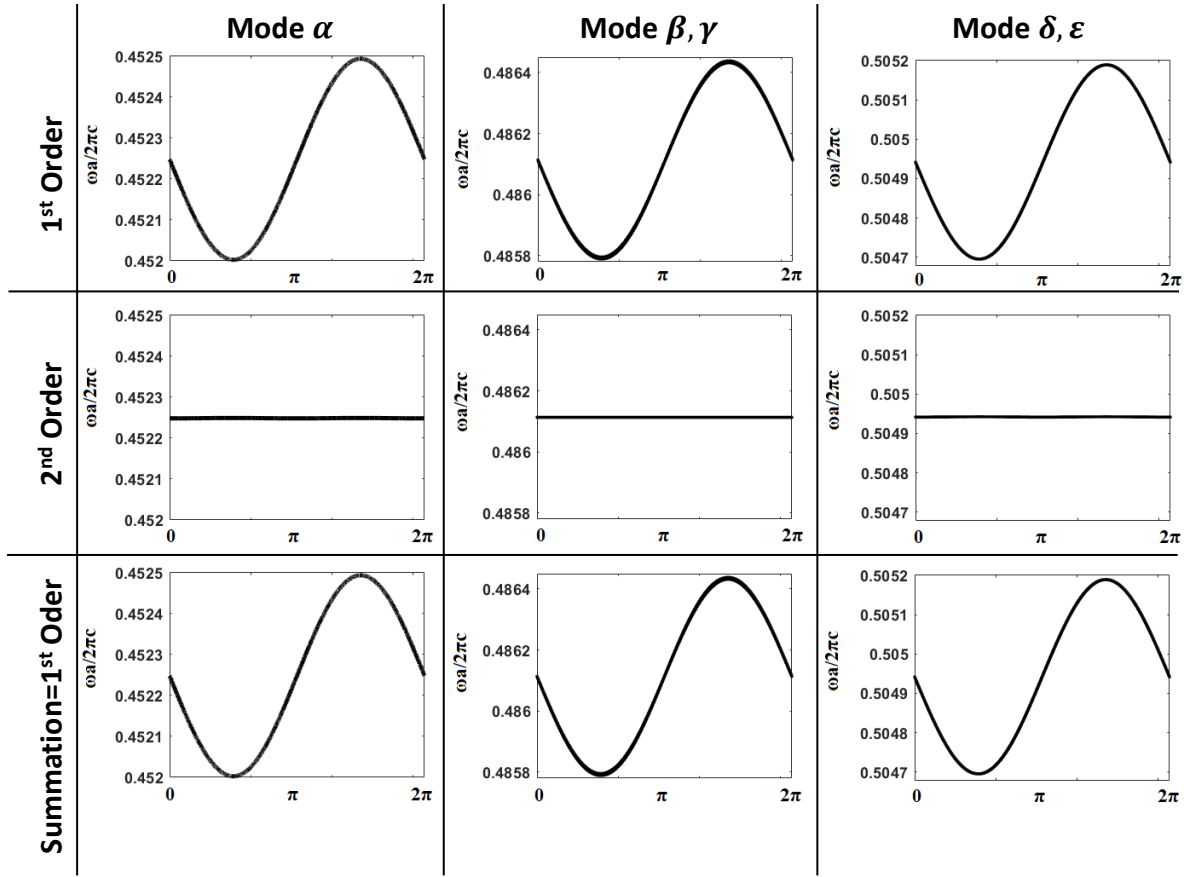


**Figure 18:** Modulation of the 5 photonic cavity modes eigenfrequencies induced by the acoustic mode  $F$  during one acoustic cycle:  $0 \leq \Omega t \leq 2\pi$ . First and second rows give respectively the 1<sup>st</sup> and 2<sup>nd</sup> order corrections the 3<sup>rd</sup> row represents the 1<sup>st</sup> and 2<sup>nd</sup> order combined effects. The singlet mode  $\alpha$  is disposed in the 1<sup>st</sup> column and the two doublet modes  $(\beta, \gamma)$  and  $(\delta, \epsilon)$  are piled in the 2<sup>nd</sup> and 3<sup>rd</sup> columns respectively. The breathing mode  $F$  does not introduce degeneracy lifting.

## Discussion

### Acoustic Mode $F$ Induced Perturbation

The mode  $F$  contains 4 symmetric planes intersecting at an angle of  $\pi/4$  (brown dashed line in Figure 15). The line of intersection coincides with the  $z$ -axis centered at the missing hole.

In addition, the mode  $F$  being a breathing mode, the overall symmetry of the cavity will not be altered during an acoustic cycle. And so is for the symmetries of the relative permittivities  $\varepsilon^{(1)}$  and  $\varepsilon^{(0)}$ .

#### *i) Considering the Non-Degenerate Mode $\alpha$*

The first order correction given by equation (59):  $\left\langle \mathbf{E}_\alpha^{(0)} \middle| \varepsilon^{(1)} \middle| \mathbf{E}_\alpha^{(0)} \right\rangle \equiv \int d^2r \left| \mathbf{E}_\alpha^{(0)} \right|^2 \varepsilon^{(1)}$  does not vanish. Indeed,  $\varepsilon^{(1)}$  is an even function so, the surface integral is "**a priori**" non-zero. But since  $\varepsilon^{(1)}$  and  $\varepsilon^{(0)}$  display the same symmetry and that  $\left\langle \mathbf{E}_\alpha^{(0)} \middle| \varepsilon^{(0)} \middle| \mathbf{E}_\alpha^{(0)} \right\rangle$  is known to be non-zero (As established during the zero-order eigenfrequency  $\omega_\alpha^{(0)}$  calculation), we can thus assert that the first order correction exists, and so, according to the perturbation theory, the 2<sup>nd</sup> order correction is expected to be relatively small with respect to the 1<sup>st</sup> order one. More details about the relative smallness of the second order (applicable to both non-degenerated and degenerated modes) are given at the end of subsection **ii** just below.

#### *ii) In Case of the 2-Fold Degenerated Modes $(\beta, \gamma)$ or $(\delta, \varepsilon)$*

As said before, the subset basis functions pertaining to the degenerated modes are orthonormalized in order to satisfy the condition:

$$\left\langle \mathbf{E}_{n,i}^{(0)} \middle| \varepsilon^{(0)} \middle| \mathbf{E}_{n,j}^{(0)} \right\rangle = \delta_{ij} \quad \dots (70)$$

Where the double subscript  $(n, i)$  is used in place of the single one (for example  $\beta \equiv n, 1$  and  $\gamma \equiv n, 2$ ), the second subscripts  $(i, j = 1, 2)$  distinguish between the two degenerated



profiles sharing the same eigenfrequency  $\omega_n^{(0)}$  designated by the first index  $n$  and  $\delta_{ij}$  is the Kronecker's delta.

Using again the fact that  $\varepsilon^{(1)}$  and  $\varepsilon^{(0)}$  share the same symmetry properties, we can assert that these modes remain orthogonal with respect to  $\varepsilon^{(1)}$  but not necessarily orthonormal. So, we can write:

$$\Gamma_{ij} \equiv \left\langle \mathbf{E}_{n,i}^{(0)} \middle| \varepsilon^{(1)} \middle| \mathbf{E}_{n,j}^{(0)} \right\rangle = \Gamma_{11} \delta_{ij} \quad \dots (71)$$

That is,  $\Gamma_{ij} = 0$  if  $i \neq j$  and,  $\Gamma_{11} = \Gamma_{22}$  if  $i = j$ . Indeed, in equation (71),  $\varepsilon^{(1)}$  leads to equal values for  $\left\langle \mathbf{E}_{n,1}^{(0)} \middle| \varepsilon^{(1)} \middle| \mathbf{E}_{n,1}^{(0)} \right\rangle$  and  $\left\langle \mathbf{E}_{n,2}^{(0)} \middle| \varepsilon^{(1)} \middle| \mathbf{E}_{n,2}^{(0)} \right\rangle$  in the same way as  $\varepsilon^{(0)}$  leads to the same value "unity" in equation (70) in case of ( $i = j$ ). Finally, equation (56) reduces to:

$$\frac{\omega_{0n}^{(1)+}}{\omega_{0n}^{(0)}} = \frac{\omega_{0n}^{(1)-}}{\omega_{0n}^{(0)}} = -\frac{1}{2} \Gamma_{11} = -\frac{1}{2} \left\langle \mathbf{E}_{n,i}^{(0)} \middle| \varepsilon^{(1)} \middle| \mathbf{E}_{n,i}^{(0)} \right\rangle \quad \dots (72)$$

We conclude that the degeneracy is not lifted i.e.  $\omega_{0n}^{(1)+} = \omega_{0n}^{(1)-}$  and as for non-degenerated modes, the 1<sup>st</sup> order correction does not vanish and so it will be the dominant correction.

### ***On the Negligibly Small Value of the 2<sup>nd</sup> Order Correction in the Particular Case of***

#### ***Mode F***

It is easy to show that the scalar product in the right-hand side of equation (62) in case of a non-degenerated mode (or (65) for a degenerated one) vanishes identically. Indeed, as stated in equation (52 or 59)  $\left| \mathbf{E}_n^{(1)} \right\rangle$  develops on all the basis functions  $\left| \mathbf{E}_{m,i}^{(0)} \right\rangle$  except  $m = n$ . Once more, recalling the similitude of the symmetry properties of  $\varepsilon^{(1)}$  and  $\varepsilon^{(0)}$  we can assert that  $\left\langle \mathbf{E}_n^{(0)} \middle| \varepsilon^{(1)} \middle| \mathbf{E}_{m,i}^{(0)} \right\rangle = 0; m \neq n$ , as it did for the orthonormal basis  $\left\{ \left| \mathbf{E}_n^{(0)} \right\rangle \right\}$  in the unperturbed case i.e.  $\left\langle \mathbf{E}_n^{(0)} \middle| \varepsilon^{(0)} \middle| \mathbf{E}_{m,i}^{(0)} \right\rangle = 0; m \neq n$ . Finally, in both cases of degenerated and non-

degenerated optical modes, the 2<sup>nd</sup> order correction is negligible with respect to the 1<sup>st</sup> order

since it is proportional to its square:  $\frac{k_{0n}^{(2)}}{k_{0n}^{(0)}} = +\frac{3}{2} \left( \frac{k_{0n}^{(1)}}{k_{0n}^{(0)}} \right)^2$ .

### ***Acoustic Mode C Induced Perturbation***

As shown on Figure 15, the acoustic **mode C** also contains 4 planes intersecting at the  $z$ -axis but this time two of them become anti-symmetric planes: the 2 diagonal ones (pink dash-dotted line in Figure 15). It is easy using equation (68) to deduce that these symmetry relations are inherited by the permittivity variation  $\Delta\varepsilon = \lambda\varepsilon^{(1)}$  : thus  $\varepsilon^{(1)}$  is an odd function in a new frame corresponding to a rotation of  $\pi/4$  around the  $z$ -axis.

#### ***i) Considering the Non-Degenerated TM Mode $\alpha$***

The parity of the function  $\varepsilon^{(1)}$  as described above enables us to assert that the first order correction given by equation (53) vanishes identically since the surface integral of an odd function (in the appropriate frame) is zero:

$$\left\langle \mathbf{E}_\alpha^{(0)} \left| \varepsilon^{(1)} \right| \mathbf{E}_\alpha^{(0)} \right\rangle \equiv \int d^2r \left| \mathbf{E}_\alpha^{(0)} \right|^2 \varepsilon^{(1)} = 0 \quad \dots (73)$$

That is, the first order correction:  $\lambda k_{0n}^{(1)}$  is zero. Thus, the power series expansion (49) shows quadratic variation with respect to the perturbation parameter  $\lambda$  since now  $\lambda^2 k_{0n}^{(2)}$  is the most significant term of the series.

Finally, recalling that  $\lambda$  is chosen as the sinusoidally varying acoustic displacement (at a given point of the structure, as explained in section 4.2), it is straightforward to justify using the trigonometric identity  $\sin^2\theta = (1 - \cos 2\theta)/2$  that the modulation shows purely 2<sup>nd</sup> harmonic response  $2\Omega$ , twice the acoustic frequency.

#### ***ii) In Case of the 2-Fold Degenerated Modes ( $\beta, \gamma$ ) or ( $\delta, \varepsilon$ )***

Again, the parity of  $\varepsilon^{(1)}$  function, which this time is odd, enables us to assert that the main part of the 1<sup>st</sup> order correction i.e. "the diagonal terms" vanishes. Indeed:

$$\Gamma_{11} = \Gamma_{22} \equiv \left\langle \mathbf{E}_{n,1}^{(0)} \left| \varepsilon^{(1)} \right| \mathbf{E}_{n,1}^{(0)} \right\rangle = \left\langle \mathbf{E}_{n,2}^{(0)} \left| \varepsilon^{(1)} \right| \mathbf{E}_{n,2}^{(0)} \right\rangle = 0 \quad \dots (74)$$

But, as can be seen in equation (56) the off-diagonal terms  $\Gamma_{12}$  and  $\Gamma_{21}$  also contribute to the 1<sup>st</sup> order correction. For instance, in case of silicon,  $\varepsilon^{(1)}$  is real so, we have:

$$\Gamma_{21} = \Gamma_{12}^*; \quad \dots (75)$$

There is no objective reason justifying that  $\Gamma_{12}$  vanishes in the presence of the odd parity of  $\varepsilon^{(1)}$ . Indeed, in the unperturbed case, the orthonormalisation of the basis tells us that the scalar product:  $\left\langle \mathbf{E}_{n,i}^{(0)} \left| \varepsilon^{(0)} \right| \mathbf{E}_{n,j}^{(0)} \right\rangle = 0$ . Now, when the perturbation  $\varepsilon^{(1)}$  is applied, the symmetry is somewhat disturbed and one can reasonably expect that  $\Gamma_{12} \equiv \left\langle \mathbf{E}_{n,1}^{(0)} \left| \varepsilon^{(1)} \right| \mathbf{E}_{n,2}^{(0)} \right\rangle$  will be different from zero, even though very small. We can write:

$$|\Gamma_{21}|^2 = |\Gamma_{12}|^2 \equiv \left| \left\langle \mathbf{E}_{n,1}^{(0)} \left| \varepsilon^{(1)} \right| \mathbf{E}_{n,2}^{(0)} \right\rangle \right|^2 \neq 0 \quad \dots (76)$$

As a consequence, the 1<sup>st</sup> order corrections exist but are relatively small (the initial unperturbed degenerated modes being orthogonal). These corrections write:

$$\frac{\omega_{0n}^{(1)\pm}}{\omega_{0n}^{(0)}} = \pm \frac{1}{2} |\Gamma_{12}| \quad \dots (77)$$

This explains why, the degeneracy is lifted at the first order but the remaining off-diagonal term  $|\Gamma_{12}|$  is too weak to completely screens the 2<sup>nd</sup> order correction. Thus, the 1<sup>st</sup> and 2<sup>nd</sup> order correction terms coexist. The end result is that the modulation of the optical resonant frequency  $\omega_{0n}^{(1)}$ , during an acoustic cycle, look like a warped sinusoid. This is the signature of the superposition of both the acoustic fundamental angular frequency  $\Omega$  fluctuation (1<sup>st</sup> order correction) and its 2<sup>nd</sup> harmonic  $2\Omega$  (2<sup>nd</sup> order correction).

The results produced by the analytical approach formalized by the second order correction applied to degenerated modes discussed here are in good agreement with the results from the full numeric approach [108] [109] [75]. But the proposed approach goes further as it provides

a useful tool for the interpretation of the modulation behaviors and for the design of devices relying on degenerated modes.

## 4.6 Conclusion

Analytical expressions for the first and second order perturbation corrections for degenerated and non-degenerated photonic modes have been derived. Then, considering the amplitude of the acoustic mode as the perturbation parameter, we retrieve the dynamic of the photonic mode. Next, using the simplest cavity example of a missing hole in a rectangular phoXonic crystal, we undergo a complete discussion about the relative strength of the first and second order corrections, and the degeneracy lifting. This discussion, associating perturbation theory with symmetry criteria, illustrates the capabilities of the method, to facilitate result interpretations and prefigure to be a useful tool for the design of opto-mechanical devices.

# General Conclusion

This thesis concerns a theoretical study of the interaction between confined photonic and phononic modes. It is based on the frame of the second order perturbation theory.

After an overview of the state of art of the photonic, phononic, and phoXonic crystals, we present a complete recall of the mathematical concepts needed for the description of a crystal in the real and reciprocal domain. Then, beginning with the wave structure in homogeneous media, we extend the presentation to identify the specificities of wave propagation in one- and two-dimensional periodic media. Next, we introduced the mathematical tools necessary for the description of photon / phonon coupling mechanisms. Also, all the parameters necessary for understanding and designing structures with confined phoXonic modes were stated. The existence of phoXonic structures have been validated by the identification of several phononic and photonic modes confined in the same  $L_1$  cavity formed by a unique missing hole. Finally, we developed a semi-analytical method to analyze the opto-mechanical coupling efficiency in these artificial periodic structures. Work has been done on two-dimensional (2-D) structures.

The complete derivation details of the perturbative approach applied to the calculation of opto-mechanical coupling coefficients up to the second order have been presented. Then, we extended the method to the case of degenerated modes for both first and second order.

We illustrated the method on the  $L_1$  point defect cavity. For our test case we used a 2-D square lattice periodic pattern of circular air holes drilled in a silicon substrate. The chosen period is  $a = 650 \text{ nm}$  and the relative radius value is  $r/a = 0.48$ , as it promotes bandgaps corresponding to the optical telecommunication range and to the ultrasonic bands. The unperturbed cavity modes are determined using a commercial Multiphysics Finite Element

Method software where the  $L_1$  cavity is implemented using the supercell technique limited to  $9 \times 9$  unit-cell, which appeared to be a good compromise between precision and time saving. We subsequently exploit the perturbative obtained opto-mechanical coupling factors in harmonic time series, to reconstruct the dynamic behavior of the photonic modes.

Then, based on symmetry criteria, the perturbation theory enabled us to explain why and how the choice of a given acoustic mode can drastically change the modulation behavior of the optical mode. For example, we define the symmetry criteria leading to the extinction of the first-order response and thus revealing of the second-order one. Or, in case of degenerated optical modes, the conditions which lead to the degeneracy lifting, as well as the events which lead to a warped sinusoidal response.

To conclude, we showed up usefulness of the perturbation method, associated with symmetry criteria, as tool to simplify the analysis and the interpretation of the results, and ultimately to predict the behavior of the structure. So, it prefigures to be a useful tool for the design of opto-mechanical devices.

# Appendix A

## TM and TE Polarizations

### TM Polarization

The TM polarization for the geometry in Figure 10 is characterized with the magnetic field parallel to the hole's axis in the  $z$ -direction, thus the magnetic field components are ( $H_x = 0, H_y = 0, H_z$ ). The wave equation for the  $H_z$  field component is written as:

$$\frac{\partial}{\partial x} \left( \frac{1}{\epsilon_r(r)} \frac{\partial H_z}{\partial x} \right) + \frac{\partial}{\partial y} \left( \frac{1}{\epsilon_r(r)} \frac{\partial H_z}{\partial y} \right) = \frac{1}{c^2} \frac{\partial^2 H_z}{\partial t^2} \quad \dots \text{(A.1)}$$

Once we find the  $H_z$  component, then the ( $E_x, E_y$ ) equations can be solved using equations:

$$\frac{\partial H_z}{\partial y} = \epsilon_r(r) \frac{\partial E_x}{\partial t} \quad \dots \text{(A.2)}$$

$$-\frac{\partial H_z}{\partial x} = \epsilon_r(r) \frac{\partial E_y}{\partial t} \quad \dots \text{(A.3)}$$

### TE Polarization

The TE polarization for the geometry in Figure 10 is characterized with the electric field parallel to the hole's axis in the  $z$ -direction, thus the electric field components are ( $E_x = 0, E_y = 0, E_z$ ). The wave equation for the  $E_z$  field component is written as:

$$\frac{1}{\epsilon_r(r)} \left( \frac{\partial^2 E_z}{\partial x^2} + \frac{\partial^2 E_z}{\partial y^2} \right) = \frac{1}{c^2} \frac{\partial^2 E_z}{\partial t^2} \quad \dots \text{(A.4)}$$

Once we find the  $E_z$  component, then the ( $H_x, H_y$ ) equations can be solved using equations:

$$\frac{\partial E_z}{\partial y} = -\mu_0 \frac{\partial H_x}{\partial t} \quad \dots \text{(A.5)}$$

$$-\frac{\partial E_z}{\partial x} = -\mu_0 \frac{\partial H_y}{\partial t} \quad \dots \text{(A.6)}$$

## References

- [1] Photonic Crystals Group ICMC art and craft of nano-photonics materials. (2018, May 12). *Photonic band gap*. Retrieved from <https://www.icmm.csic.es/luxrerum/photonic-band-gap/>.
- [2] Hofmann, P. (2015). *Solid State Physics: An Introduction*. John Wiley & Sons.
- [3] Bragg, D. (2014). *Tiling Spaces: Quasicrystals & Geometry*. Department of Mathematics University of Leicester.
- [4] Yariv, A., & Yeh, P. (2003). *Optical waves in crystals: propagation and control of laser radiation*. Hoboken, N.J.: Wiley.
- [5] Royer, D., & Dieulesaint, E. (2000). *Elastic Waves in solids*. Springer.
- [6] Aspelmeyer, M., Kippenberg, T. J., & Marquardt, F. (2014). *Cavity optomechanics*. *Reviews of Modern Physics*, 86(4), 1391–1452. <https://doi.org/10.1103/RevModPhys.86.1391>
- [7] Malet, A. (1989). *Studies on James Gregorie (1638 - 1675)*.
- [8] Palmer, C. A., Loewen, E. G., Richardson Grating Laboratory., & Thermo RGL. (2002). *Diffraction grating handbook*. Rochester, N.Y: Thermo RGL.
- [9] Cope, T. D. (1932). The rittenhouse diffraction grating. *Journal of the Franklin Institute*, 214(1), 99–104. [https://doi.org/10.1016/S0016-0032\(32\)90007-6](https://doi.org/10.1016/S0016-0032(32)90007-6)



- [10] Maxwell, J. C. (1865). *VIII. A dynamical theory of the electromagnetic field*. 155. *Phil. Trans. R. Soc.*.
- [11] BRAGG, W. L., (1913). *The Dawn of X-ray Crystallography*. Proceedings of the Cambridge Philosophical Society, VOL. XVII. Part 1.
- [12] Fujita, S., & Ito, K. (2007). Bloch Theorem. In S. Fujita & K. Ito (Eds.), *Quantum Theory of Conducting Matter: Newtonian Equations of Motion for a Bloch Electron* (pp. 85–95). [https://doi.org/10.1007/978-0-387-74103-1\\_7](https://doi.org/10.1007/978-0-387-74103-1_7)
- [13] Dresselhaus, M. S., Dresselhaus, G., & Jorio, A. (2008). *Group Theory: Application to the Physics of Condensed Matter*. Retrieved from [//www.springer.com/fr/book/9783540328971](http://www.springer.com/fr/book/9783540328971)
- [14] Kuchment, P. A. (1993). *Floquet Theory for Partial Differential Equations*. Retrieved from [//www.springer.com/la/book/9783764329013](http://www.springer.com/la/book/9783764329013)
- [15] Photonics - Hardcover - Amnon Yariv; Pochi Yeh - Oxford University Press. (2006). Retrieved November 12, 2018, from <https://global.oup.com/ushe/product/photonics-9780195179460?cc=us&lang=en&>
- [16] Yariv, A. (2003). *Optical waves in crystals : propagation and control of laser radiation* /. *Yariv A and Yeh P 2003 Optical waves in crystals Wiley Interscience*. (n.d.).
- [17] Yeh, P., & Yariv, A. (1976). Bragg reflection waveguides. *Optics Communications*, 19(3), 427–430. [https://doi.org/10.1016/0030-4018\(76\)90115-2](https://doi.org/10.1016/0030-4018(76)90115-2)
- [18] Yeh, P., Yariv, A., & Hong, C.-S. (1977). Electromagnetic propagation in periodic

stratified media I General theory\*. *Journal of the Optical Society of America*, 67(4), 423.  
<https://doi.org/10.1364/JOSA.67.000423>

[19] Yablonovitch, Eli. (1987). Inhibited Spontaneous Emission in Solid-State Physics and Electronics. *Physical Review Letters*, 58(20), 2059–2062.  
<https://doi.org/10.1103/PhysRevLett.58.2059>

[20] John, S. (1987). Strong localization of photons in certain disordered dielectric superlattices. *Physical Review Letters*, 58(23), 2486–2489.  
<https://doi.org/10.1103/PhysRevLett.58.2486>

[21] Brillouin, L. (2003). *Wave Propagation in Periodic Structures* (2 edition). Mineola, N.Y: Dover Publications.

[22] Leung, K. M., & Liu, Y. F. (1990). *Photon Band Structures: The Plane-Wave Method*. Department of Physics, Polytechnic University, 333 Jay Street, Brooklyn, New York 11201

[23] Economou, EN., & Zdetsis, A. (1989). *Classical wave propagation in periodic structures. Physical Review. B, Condensed Matter*, 40(2), 1334–1337.

[24] Ho, K. M., Chan, C. T., & Soukoulis, C. M. (1990). Existence of a photonic gap in periodic dielectric structures. *Physical Review Letters*, 65(25), 3152–3155.  
<https://doi.org/10.1103/PhysRevLett.65.3152>

[25] Yablonovitch, E., Gmitter, T. J., & Leung, K. M. (1991). Photonic band structure: The face-centered-cubic case employing nonspherical atoms. *Physical Review Letters*, 67(17), 2295–2298. <https://doi.org/10.1103/PhysRevLett.67.2295>

- [26] Özbay, E., Abeyta, A., Tuttle, G., Tringides, M., Biswas, R., Chan, C. T., Soukoulis, C. M., & Ho, K. M. (1994). Measurement of a three-dimensional photonic band gap in a crystal structure made of dielectric rods. *Physical Review. B, Condensed Matter*, *50*(3), 1945–1948.
- [27] Gadot, F., Chelnokov, A., De Lustrac, A., Crozat, P., Lourtioz, J. M., Cassagne, D., & Jouanin, C. (1997). Experimental demonstration of complete photonic band gap in graphite structure. *Applied physics letters*, *71*(13), 1780-1782.].
- [28] Lourtioz, J. M., De Lustrac, A., Gadot, F., Rowson, S., Chelnokov, A., Brillat, T., ... & Lippens, D. (1999). Toward controllable photonic crystals for centimeter-and millimeter-wave devices. *Journal of Lightwave Technology*, *17*(11), 2025-2031.].
- [29] Astratov, V. N., Bogomolov, V. N., Kaplyanskii, A. A., Prokofiev, A. V., Samoilovich, L. A., Samoilovich, S. M., & Vlasov, Yu. A. (1995). Optical spectroscopy of opal matrices with CdS embedded in its pores: Quantum confinement and photonic band gap effects. *Il Nuovo Cimento D*, *17*(11), 1349–1354. <https://doi.org/10.1007/BF02457208>
- [30] Míguez, H., López, C., Meseguer, F., Blanco, A., Vázquez, L., Mayoral, R., ... Mifsud, A. (1997). Photonic crystal properties of packed submicrometric SiO<sub>2</sub> spheres. *Applied Physics Letters*, *71*(9), 1148–1150. <https://doi.org/10.1063/1.119849>
- [31] Wijnhoven, J. E. (1998). Preparation of Photonic Crystals Made of Air Spheres in Titania. *Science*, *281*(5378), 802–804. <https://doi.org/10.1126/science.281.5378.802>
- [32] García-Santamaría, F., Miyazaki, H. T., Urquía, A., Ibisate, M., Belmonte, M., Shinya, N., ... López, C. (2002). Nanorobotic Manipulation of Microspheres for On-Chip Diamond Architectures. *Advanced Materials*, *14*(16), 1144. <https://doi.org/10.1002/1521->

- [33] Gupta, A. (2014). A Review on Sonic Crystal, Its Applications and Numerical Analysis Techniques. *Acoustical Physics*, 60, 223–234. <https://doi.org/10.1134/S1063771014020080>
- [34] Khelif, A., Hsiao, F.-L., Benchabane, S., Choujaa, A., Aoubiza, B., & Laude, V. (2008). Ultrasonic and hypersonic phononic crystals. *Proc SPIE*. <https://doi.org/10.1117/12.778573>
- [35] Lemanov, V. V., & Smolenskiĭ, G. A. (1973). HYPERSONIC WAVES IN CRYSTALS. *Soviet Physics Uspekhi*, 15(6), 708. <https://doi.org/10.1070/PU1973v015n06ABEH005058>
- [36] Fahmy, A. h., & Adler, E. L. (1973). Propagation of acoustic surface waves in multilayers: A matrix description. *Applied Physics Letters*, 22(10), 495–497. <https://doi.org/10.1063/1.1654482>
- [37] Lakhtakia, A., Varadan, V. V., & Varadan, V. K. (1988). Reflection characteristics of an elastic slab containing a periodic array of circular elastic cylinders: P and SV wave analysis. *The Journal of the Acoustical Society of America*, 83(4), 1267–1275. <https://doi.org/10.1121/1.395982>
- [38] Liu, J., Ye, L., Weitz, D. A., & Sheng, P. (1990). Novel acoustic excitations in suspensions of hard-sphere colloids. *Physics Review Letters*, 65(20):2602-2605. <https://doi.org/10.1103/PhysRevLett.65.2602>
- [39] Ye, L., Liu, J., Sheng, P., & Weitz, D. A. (1993). Sound-propagation in suspensions of solid spheres. *Physical Review E*, 48, 2805-2815. Copy at <http://www.tinyurl.com/k3twu8l>
- [40] Jing, X., Sheng, P., & Zhou, M. (1991). Theory of acoustic excitations in colloidal

suspensions. *Physical Review Letters*, 66(9), 1240–1243.

<https://doi.org/10.1103/PhysRevLett.66.1240>

[41] Ruffa, A. A. (1992). Acoustic wave propagation through periodic bubbly liquids. *The Journal of the Acoustical Society of America*, 91(1), 1–11. <https://doi.org/10.1121/1.402755>

[42] Kushwaha, M., Halevi, P., Dobrzynski, L., & Djafari-Rouhani, B. (1993). Acoustic band structure of periodic elastic composites. *Physical Review Letters*, 71, 2022–2025. <https://doi.org/10.1103/PhysRevLett.71.2022>

[43] Gazalet, J., Dupont, S., Kastelik, J. C., ROLLAND, Q., & Djafari-Rouhani, B. (2013). A tutorial survey on waves propagating in periodic media : electronic, photonic and phononic crystals. Perception of Bloch theorem in both real and Fourier domains. *Wave Motion*, 50, 619–654. <https://doi.org/10.1016/j.wavemoti.2012.12.010>

[44] Kushwaha, M. S., & Halevi, P. (1994). Band-gap engineering in periodic elastic composites. *Applied Physics Letters*, 64, 1085–1087. <https://doi.org/10.1063/1.110940>

[45] Kushwaha, M., & Djafari-Rouhani, B. (1996). Complete acoustic stop bands for cubic arrays of spherical liquid balloons. *Journal of Applied Physics*. 80, 3191–3195. <https://doi.org/10.1063/1.363259>.

[46] Economou, E. N., & Sigalas, M. (1994). Stop bands for elastic waves in periodic composite materials. *The Journal of the Acoustical Society of America*, 95(4), 1734–1740. <https://doi.org/10.1121/1.408692>

[47] Sigalas, M., & Economou, E. N. (1993). Band structure of elastic waves in two dimensional systems. *Solid State Communications*, 86(3), 141–143.

[https://doi.org/10.1016/0038-1098\(93\)90888-T](https://doi.org/10.1016/0038-1098(93)90888-T)

[48] Sarah Benchabane. Guidage et filtrage des ondes dans les cristaux phononiques. Acoustique [physics.class-ph]. Université de Franche-Comté, 2006. Français. (tel-00140347)

[49] Matsuda, O., & Wright, O. B. (2002). Reflection and transmission of light in multilayers perturbed by picosecond strain pulse propagation. *Journal of the Optical Society of America B*, 19(12), 3028. <https://doi.org/10.1364/JOSAB.19.003028>

[50] Braginsky, V. B., Strigin, S. E., & Vyatchanin, S. P. (2001). Parametric Oscillatory Instability in Fabry-Perot (FP) Interferometer. *Physics Letters A*, 287(5–6), 331–338. [https://doi.org/10.1016/S0375-9601\(01\)00510-2](https://doi.org/10.1016/S0375-9601(01)00510-2)

[51] Trigo, M., Bruchhausen, A., Fainstein, A., Jusserand, B., & Thierry-Mieg, V. (2002). Confinement of Acoustical Vibrations in a Semiconductor Planar Phonon Cavity. *Physical Review Letters*, 89(22), 227402. <https://doi.org/10.1103/PhysRevLett.89.227402>

[52] Worlock, J. M., & Roukes, M. L. (2003). Applied physics: Son et lumière. *Nature*, 421, 802–803.

[53] Lacharmoise, P., Fainstein, A., Jusserand, B., & Thierry-Mieg, V. (2004). Optical cavity enhancement of light–sound interaction in acoustic phonon cavities. *Applied Physics Letters*, 84(17), 3274–3276. <https://doi.org/10.1063/1.1734686>

[54] Gérard, D., Laude, V., Sadani, B., Khelif, A., Van Labeke, D., & Guizal, B. (2007). Modulation of the extraordinary optical transmission by surface acoustic waves. *Physical Review B*, 76(23), 235427. <https://doi.org/10.1103/PhysRevB.76.235427>

- [55] Berstermann, T., Brüggemann, C., Bombeck, M., Akimov, A. V., Yakovlev, D. R., Kruse, C., ... Bayer, M. (2010). Optical bandpass switching by modulating a microcavity using ultrafast acoustics. *Physical Review B*, 81(8), 085316. <https://doi.org/10.1103/PhysRevB.81.085316>
- [56] Psarobas, I. E., Papanikolaou, N., Stefanou, N., Djafari-Rouhani, B., Bonello, B., & Laude, V. (2010). Enhanced acousto-optic interactions in a one-dimensional phoxonic cavity. *Physical Review B*, 82(17). <https://doi.org/10.1103/PhysRevB.82.174303>
- [57] Papanikolaou, N., Psarobas, I. E., Stefanou, N., Djafari-Rouhani, B., Bonello, B., & Laude, V. (2012). Light modulation in phoxonic nanocavities. *Microelectronic Engineering*, 90, 155–158. <https://doi.org/10.1016/j.mee.2011.04.069>
- [58] Lanzillotti-Kimura, N. D., Fainstein, A., Huynh, A., Perrin, B., Jusserand, B., Miard, A., & Lemaître, A. (2007). Coherent Generation of Acoustic Phonons in an Optical Microcavity. *Physical Review Letters*, 99(21), 217405. <https://doi.org/10.1103/PhysRevLett.99.217405>
- [59] Piliposian, G., Avetisyan, A., & Ghazaryan, K. (2012). Shear wave propagation in periodic phononic/photonic piezoelectric medium. *Wave Motion*, 49, 125–134. <https://doi.org/10.1016/j.wavemoti.2011.08.001>
- [60] Maldovan, M., & Thomas, E. L. (2006). Simultaneous complete elastic and electromagnetic band gaps in periodic structures. *Applied Physics B*, 83(4), 595. <https://doi.org/10.1007/s00340-006-2241-y>
- [61] Maldovan, M. & Thomas, E. L. Simultaneous localization of photons and phonons in two-dimensional periodic structures. *Appl. Phys. Lett.* 88, 251907.

<http://dx.doi.org/10.1063/1.2216885>

[62] Sadat-Saleh, S., Benchabane, S., Baida, F. I., Bernal, M.-P., & Laude, V. (2009). Tailoring simultaneous photonic and phononic band gaps. *Journal of Applied Physics*, *106*(7), 074912.

<https://doi.org/10.1063/1.3243276>

[63] Sadat-Saleh, S., Benchabane, S., Baida, F. I., Bernal, M. P., & Laude, V. (2009, September). Simultaneous photonic and phononic band gaps in a two-dimensional lithium niobate crystal. In *2009 IEEE International Ultrasonics Symposium*(pp. 1118-1121). IEEE.

[64] Bria, D., Assouar, M. B., Oudich, M., Pennec, Y., Vasseur, J., & Djafari-Rouhani, B. (2011). Opening of simultaneous photonic and phononic band gap in two-dimensional square lattice periodic structure. *Journal of Applied Physics*, *109*, 014507-1–6.

<https://doi.org/10.1063/1.3530682>

[65] Laude, V., Beugnot, J. C., Benchabane, S., Pennec, Y., Djafari-Rouhani, B., Papanikolaou, N., ... & Martinez, A. (2011). Simultaneous guidance of slow photons and slow acoustic phonons in silicon photonic crystal slabs. *Optics express*, *19*(10), 9690-9698.

[66] Rouhani, B. D., Pennec, Y., El Boudouti, E. H., Vasseur, J. O., El Hassouani, Y., Li, C., ... & Bria, D. (2011). Band gap engineering in simultaneous phononic and photonic crystal slabs. *Applied Physics A*, *103*(3), 735-739.

[67] El Hassouani, Y., Li, C., Pennec, Y., El Boudouti, E. H., Larabi, H., Akjouj, A., ... & Rouhani, B. D. (2010). Dual phononic and photonic band gaps in a periodic array of pillars deposited on a thin plate. *Physical Review B*, *82*(15), 155405.



- [68] Pennec, Y., Rouhani, B. D., El Boudouti, E. H., Li, C., El Hassouani, Y., Vasseur, J. O., ... & Martinez, A. C. (2011). Band gaps and waveguiding in phoxonic silicon crystal slabs. *Chinese Journal of Physics*, 49(1), 100-110.
- [69] Mohammadi, S., Eftekhar, A. A., Khelif, A., & Adibi, A. (2010). Simultaneous two-dimensional phononic and photonic band gaps in opto-mechanical crystal slabs. *Optics express*, 18(9), 9164-9172.
- [70] Burr, G. W., Diziain, S., & Bernal, M. P. (2008). The impact of finite-depth cylindrical and conical holes in lithium niobate photonic crystals. *Optics Express*, 16(9), 6302-6316.
- [71] Yulistira, D., Pennec, Y., Djafari Rouhani, B., Dupont, S., & Laude, V. (2012). Non-radiative complete surface acoustic wave bandgap for finite-depth holey phononic crystal in lithium niobate. *Applied Physics Letters*, 100(6), 061912.
- [72] Pennec, Y., Rouhani, B. D., Li, C., Escalante, J. M., Martínez, A., Benchabane, S., ... & Papanikolaou, N. (2011). Band gaps and cavity modes in dual phononic and photonic strip waveguides. *AIP advances*, 1(4), 041901.
- [73] Hsiao, F. L., Hsieh, C. Y., Hsieh, H. Y., & Chiu, C. C. (2012). High-efficiency acousto-optical interaction in phoxonic nanobeam waveguide. *Applied Physics Letters*, 100(17), 171103.
- [74] Ma, T. X., Wang, Y. S., & Zhang, C. (2014). Investigation of dual photonic and phononic bandgaps in two-dimensional phoxonic crystals with veins. *Optics Communications*, 312, 68-72.
- [75] "Rolland Q 2013 PhD thesis UVHC."

- [76] Safavi-Naeini, A. H., Hill, J. T., Meenehan, S., Chan, J., Gröblacher, S., & Painter, O. (2014). Two-dimensional phononic-photon band gap optomechanical crystal cavity. *Physical Review Letters*, *112*(15), 153603.
- [77] Rolland, Q., Oudich, M., El-Jallal, S., Dupont, S., Pennec, Y., Gazalet, J., ... & Djafari-Rouhani, B. (2012). Acousto-optic couplings in two-dimensional phoxonic crystal cavities. *Applied Physics Letters*, *101*(6), 061109.
- [78] Gazalet, J., Dupont, S., Kastelik, J. C., Rolland, Q., & Djafari-Rouhani, B. (2013). A tutorial survey on waves propagating in periodic media: Electronic, photonic and phononic crystals. Perception of the Bloch theorem in both real and Fourier domains. *Wave Motion*, *50*(3), 619-654.
- [79] Akahane, Y., Asano, T., Song, B. S., & Noda, S. (2003). High-Q photonic nanocavity in a two-dimensional photonic crystal. *nature*, *425*(6961), 944.
- [80] Yoshie, T., Vučković, J., Scherer, A., Chen, H., & Deppe, D. (2001). High quality two-dimensional photonic crystal slab cavities. *Applied Physics Letters*, *79*(26), 4289-4291.
- [81] Joannopoulos, J. D., Ed. (2008). Photonic crystals: molding the flow of light, 2nd ed. Princeton: Princeton University Press.
- [82] Li, Q., Chan, C. T., Ho, K. M., & Soukoulis, C. M. (1996). Wave propagation in nonlinear photonic band-gap materials. *Physical Review B*, *53*(23), 15577.
- [83] Kushwaha, M. S. (1996). Classical band structure of periodic elastic composites. *International Journal of Modern Physics B*, *10*(09), 977-1094.

- [84] Skorobogatiy, M., & Yang, J. (2009). *Fundamentals of Photonic Crystal Guiding*, 1 edition. Cambridge, UK ; New York: Cambridge University Press.
- [85] ONDES ELASTIQUES DANS LES SOLIDES. Tome 2, Génération, interaction acousto-optique, applications - AbeBooks - Daniel Royer; Eugène Dieulesaint: 2225834415.
- [86] *Eugène Dieulesaint et Daniel Royer : Ondes élastiques dans les solides : application au traitement du signal. Masson et Cie, 1974*
- [87] Safavi-Naeini, A. H., & Painter, O. (2014). Optomechanical crystal devices. In *Cavity Optomechanics* (pp. 195-231). Springer, Berlin, Heidelberg.
- [88] Azodi Aval, G. (2013). *Phononic Crystal Waveguiding in GaAs*(Doctoral dissertation).
- [89] Joannopoulos, J. D., Johnson, S. G., Winn, J. N., & Meade, R. D. (2008). *Molding the flow of light. Princeton Univ. Press, Princeton, NJ [ua]*.
- [90] Kalra, Y., & Sinha, R. K. (2006). Photonic band gap engineering in 2D photonic crystals. *Pramana*, 67(6), 1155-1164.
- [91] Hou, J., Citrin, D. S., Wu, H., Gao, D., Zhou, Z., & Chen, S. (2011). Slab-thickness dependence of photonic bandgap in photonic-crystal slabs. *IEEE Journal of Selected Topics in Quantum Electronics*, 18(6), 1636-1642.
- [92] Adawi, A. M., Chalcraft, A. R. A., Whittaker, D. M., & Lidzey, D. G. (2007). Refractive index dependence of L3 photonic crystal nano-cavities. *Optics Express*, 15(22), 14299-14305.
- [93] *Optoélectronique*. (2019). Retrieved from <https://www.dunod.com/sciences->

techniques/optoelectronique

[94] Johnson, S. G., Ibanescu, M., Skorobogatiy, M. A., Weisberg, O., Joannopoulos, J. D., & Fink, Y. (2002). Perturbation theory for Maxwell's equations with shifting material boundaries. *Physical review E*, *65*(6), 066611.

[95] Aspelmeyer, M., Kippenberg, T. J., & Marquardt, F. (2014). Cavity optomechanics. *Reviews of Modern Physics*, *86*(4), 1391.

[96] Makles, K., Antoni, T., Kuhn, A. G., Deléglise, S., Briant, T., Cohadon, P. F., ... & Dolique, V. (2015). 2D photonic-crystal optomechanical nanoresonator. *Optics letters*, *40*(2), 174-177.

[97] Mitchell, M., Hryciw, A. C., & Barclay, P. E. (2014). Cavity optomechanics in gallium phosphide microdisks. *Applied Physics Letters*, *104*(14), 141104.

[98] Eichenfield, M., Chan, J., Camacho, R. M., Vahala, K. J., & Painter, O. (2009). Optomechanical crystals. *Nature*, *462*(7269), 78.

[99] Okano, M., Yamada, T., Sugisaka, J., Yamamoto, N., Itoh, M., Sugaya, T., ... & Mori, M. (2010). Analysis of two-dimensional photonic crystal L-type cavities with low-refractive-index material cladding. *Journal of Optics*, *12*(7), 075101.

[100] Li, Y., Cui, K., Feng, X., Huang, Y., Huang, Z., Liu, F., & Zhang, W. (2015). Optomechanical crystal nanobeam cavity with high optomechanical coupling rate. *Journal of Optics*, *17*(4), 045001.

- [101] Kalae, M., Paraiso, T. K., Pfeifer, H., & Painter, O. (2016). Design of a quasi-2D photonic crystal optomechanical cavity with tunable, large x 2-coupling. *Optics express*, 24(19), 21308-21328.
- [102] Lee, D., Underwood, M., Mason, D., Shkarin, A. B., Hoch, S. W., & Harris, J. G. E. (2015). Multimode optomechanical dynamics in a cavity with avoided crossings. *Nature communications*, 6, 6232.
- [103] Bui, C. H., Zheng, J., Hoch, S. W., Lee, L. Y., Harris, J. G. E., & Wei Wong, C. (2012). High-reflectivity, high-Q micromechanical membranes via guided resonances for enhanced optomechanical coupling. *Applied Physics Letters*, 100(2), 021110.
- [104] Kaviani, H., Healey, C., Wu, M., Ghobadi, R., Hryciw, A., & Barclay, P. E. (2015). Nonlinear optomechanical paddle nanocavities. *Optica*, 2(3), 271-274.
- [105] Sankey, J. C., Jayich, A. M., Zwickl, B. M., Yang, C., & Harris, J. G. E. (2009). *Proceedings of the XXI International Conference on Atomic Physics*, World Scientific.
- [106] Karuza, M., Galassi, M., Biancofiore, C., Molinelli, C., Natali, R., Tombesi, P., ... & Vitali, D. (2012). Tunable linear and quadratic optomechanical coupling for a tilted membrane within an optical cavity: theory and experiment. *Journal of Optics*, 15(2), 025704.
- [107] Cohen-Tannoudji, C., Diu, B., & Laloe, F. (1977). *Quantum Mechanics* Wiley Interscience.
- [108] Rolland, Q., Oudich, M., El-Jallal, S., Dupont, S., Pennec, Y., Gazalet, J., ... & Djafari-Rouhani, B. (2012). Acousto-optic couplings in two-dimensional photonic crystal cavities. *Applied Physics Letters*, 101(6), 061109.

- [109] El-Jallal, S., Oudich, M., Pennec, Y., Djafari-Rouhani, B., Makhoute, A., Rolland, Q., ... & Gazalet, J. (2013). Optomechanical interactions in two-dimensional Si and GaAs photonic cavities. *Journal of Physics: Condensed Matter*, 26(1), 015005.
- [110] Zhao, Y., Qian, C., Qiu, K., Tang, J., Sun, Y., Jin, K., & Xu, X. (2016). Gain enhanced Fano resonance in a coupled photonic crystal cavity-waveguide structure. *Scientific reports*, 6, 33645.
- [111] Tsai, CS. (1990). *Acousto-Optics Interactions Devices and Applications* Springer-Verlag.
- [112] El Soussi, A., Gazalet, J., Dupont, S., & Kastelik, J. C. (2019). Evaluation of second order optomechanical coupling strength in photonic crystal cavities, case of degenerated modes. *Journal of Optics*.

## Résumé

Dans cette thèse, une étude des microstructures périodiques et de leurs applications à la modulation optique par ondes acoustiques est présentée. Plus spécifiquement, le sujet traite du couplage opto-mécanique dans les cavités des cristaux phoXoniques. Cette étude montre comment la théorie des perturbations fournit un outil efficace d'analyse et de prédiction du comportement de la modulation dans de telles structures. Cette méthode permet également d'économiser du temps de calcul en comparaison aux calculs numériques purs.

L'étude théorique de la propagation des ondes dans les milieux périodiques est d'abord introduite, puis les paramètres de l'existence simultanée des bandes interdites photoniques et phononiques sont déduites. Le développement d'une méthode semi-analytique ayant pour but d'analyser l'efficacité du couplage acousto-optique dans les structures périodiques artificielles est ensuite réalisé. La théorie des perturbations est développée jusqu'au 2<sup>ème</sup> ordre. Celle-ci, associée à des considérations de symétrie, est utilisée pour l'interprétation des résultats. Une illustration de la versatilité de la méthode, basée d'une cavité ponctuelle  $L_1$  sur substrat silicium, est présentée. Les résultats obtenus sont en accord avec ceux donnés par une méthode purement numérique.

Mots-Clés : Cristaux Photonique, Cristaux Phononique, Cavités, Couplage Acousto-Optique, Couplage Opto-Mécanique

## Abstract

In this thesis, a study of periodic microstructures and their applications to optical modulation by acoustical waves is presented. More specifically, it deals with opto-mechanical coupling in phoXonic crystal cavities. This study shows how the perturbation theory provides an efficient tool to analyse and predict the behaviour of modulation in such structures. Moreover, when compared to pure numerical ones, this method leads to calculation time saving.

The theory of periodic media is first introduced and then we derive the parameters for the simultaneous existence of photonic and phononic bandgaps. We end up by the development of a semi-analytical method to analyze acousto-optical coupling efficiency in artificial periodic structures. The perturbation theory is developed up to 2nd order and is used together with symmetry considerations for interpretations. An illustration of the versatility of the developed method is presented using an  $L_1$  point defect cavity on silicon substrate and validated with classical numerical results.

Key Words: Photonic Crystals, Phononic Crystals, Cavity, Acousto-Optical Coupling, Opto-Mechanical Coupling